ARMY RESEARCH LABORATORY

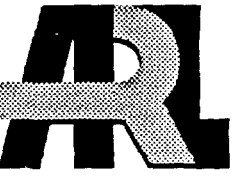

# Multipath-Induced, Low-Angle Tracking Error at 140 GHz

Suzanne R. Stratton
Donald G. Bauerle
H. Bruce Wallace



ARL-MR-140 June 1994

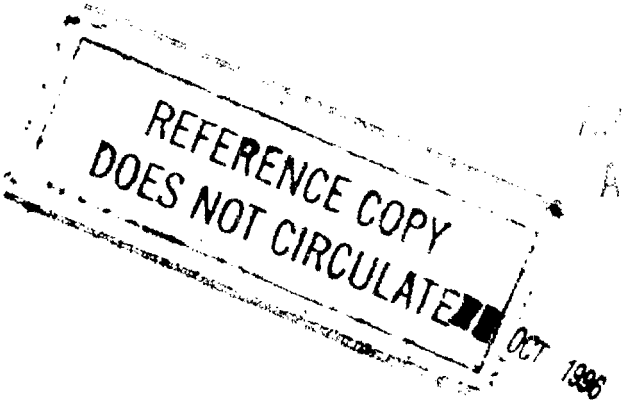

## NOTICES

Destroy this report when it is no longer needed. DO NOT return it to the originator.

Additional copies of this report may be obtained from the National Technical Information Service, U.S. Department of Commerce, 5285 Port Royal Road, Springfield, VA 22161.

The findings of this report are not to be construed as an official Department of the Army position, unless so designated by other authorized documents.

The use of trade names or manufacturers' names in this report does not constitute indorsement of any commercial product.

# REPORT DOCUMENTATION PAGE

Form Approved
OMB No. 0704-0188



| 1. AGENCY USE ONLY (Leave blank) | 2. REPORT DATE | 3. REPORT TYPE AND DATES COVERED |
|---|---|---|
| | June 1994 | Final, 3–19 September 1991 |

**4. TITLE AND SUBTITLE**
Mulitpath-Induced, Low-Angle Tracking Error at 140 GHz

**5. FUNDING NUMBERS**
PR: 1L161102AH43

**6. AUTHOR(S)**
Suzanne R. Stratton, Donald G. Bauerle, and H. Bruce Wallace

**7. PERFORMING ORGANIZATION NAME(S) AND ADDRESS(ES)**
U.S. Army Research Laboratory
ATTN: AMSRL-SS-SD
Aberdeen Proving Ground, MD 21005-5066

**8. PERFORMING ORGANIZATION REPORT NUMBER**

**9. SPONSORING / MONITORING AGENCY NAME(S) AND ADDRESS(ES)**
U.S. Army Research Laboratory
ATTN: AMSRL-OP-AP-L
Aberdeen Proving Ground, MD 21005-5066

**10. SPONSORING / MONITORING AGENCY REPORT NUMBER**
ARL-MR-140

**11. SUPPLEMENTARY NOTES**

**12a. DISTRIBUTION / AVAILABILITY STATEMENT**
Approved for public release; distribution is unlimited.

**12b. DISTRIBUTION CODE**

**13. ABSTRACT** *(Maximum 200 words)*

This report describes a measurement program to characterize multipath-induced errors which can affect missile guidance. Measurements of angular position errors were made using a 140-GHz amplitude monopulse radar and a vertical probe. Data was collected at ranges out to 4.8 km. The longest ranges give propagation geometries that are typical for a missile trajectory in close proximity to the earth. Angular positioning errors due to diffuse multipath, specular multipath, and atmospheric-induced noise were measured.

**14. SUBJECT TERMS**
missiles, monopulse radar, multipath, tracking

**15. NUMBER OF PAGES**
75

**16. PRICE CODE**

| 17. SECURITY CLASSIFICATION OF REPORT | 18. SECURITY CLASSIFICATION OF THIS PAGE | 19. SECURITY CLASSIFICATION OF ABSTRACT | 20. LIMITATION OF ABSTRACT |
|---|---|---|---|
| UNCLASSIFIED | UNCLASSIFIED | UNCLASSIFIED | SAR |

ACKNOWLEDGMENTS

The authors would like to thank Mr. Donald E. Testerman of the Sensors, Signatures, Signal, and Information Processing ($S^3I$) Directorate of the U.S. Army Research Laboratory (ARL) for fabricating and assembling parts of the experimental apparatus and assisting in the conduct of the experiment.

Victor Leitzke of Weapons Technology Directorate and Robert L. Bender of $S^3I$ Directorate reviewed this report and provided many thoughtful comments to the authors.

The authors would also like to thank Mike Christian of the U.S. Army Missile Command (MICOM) who was very helpful in providing the Redstone Arsenal meteorological data used in this report.

TABLE OF CONTENTS

INTENTIONALLY LEFT BLANK.

LIST OF FIGURES

INTENTIONALLY LEFT BLANK.

LIST OF TABLES

INTENTIONALLY LEFT BLANK.

## 1. INTRODUCTION

The U.S. Army's new generation of advanced radar-guided antiarmor munitions will be required to track low-angle targets on the battlefield. Such systems must deal with the potential problem of multipath propagation. The development of munitions flying at longer ranges in many different environments has created a need for more substantive data collected under a variety of conditions and over greater distances.

Various aspects of multipath propagation have been investigated over the years by the U.S. Army Ballistic Research Laboratory (BRL),* Aberdeen Proving Ground (APG), MD. Two earlier studies will be cited here for comparison with more recent results. One study (Kammerer and Richer 1964) at 68 GHz found that angular pointing errors of less than 1/10th of the beamwidth could be achieved with null-type conical scan pointing techniques. Another BRL investigation (Wallace 1979) at 140 GHz concluded that multipath effects are less serious when propagating over vegetated surfaces than over surfaces such as asphalt because the power of the undesired reflected signals will be reduced by absorption and the reflected signals diffused by a relatively rougher surface.

A more recent measurement program was conducted to collect data on millimeter wave (MMW) propagation over natural terrain with a variety of ground cover conditions (Stratton, Wallace, and Bauerle 1991). Measurements of tracking errors at 95 and 140 GHz were recorded with a conical scan antenna tracking a trihedral corner reflector that was moved through a continuous range of heights between 0.4 m and 3.6 m above the ground. Antenna diameters of 0.92 m (3 ft) and 0.61 m (2 ft) were used for propagation paths of 2,850.0 m and 838.4 m, respectively. The results indicated that tracking error is substantially higher when tracking over snow and ice than when tracking over grass.

This report describes the results of the most recent joint Army Research Laboratory (ARL) and Army Missile Command (MICOM) program to measure the effects of multipath interference on the guidance of a missile or projectile to a distant target. The radar instrumentation consisted of 95- and 140-GHz monopulse radars set up for simultaneous measurements. This report includes the results of the ARL 140-GHz measurements. Results of the 95-GHz measurements are available in Christian, Wintler, and Woods (1992).

---

* The U.S. Army Ballistic Research Laboratory was deactivated on 30 September 1992 and subsequently became a part of the U.S. Army Research Laboratory on 1 October 1992.

## 2. INSTRUMENTATION

The radar system used in this test is a 139.5-GHz amplitude monopulse system designed and fabricated at the former BRL. Figure 1 is a block diagram of the complete radio frequency (RF) and intermediate frequency (IF) sections of this radar. The monopulse antenna, comparator, and the local oscillator (LO) distribution network were built under contract by the TRG Division of Alpha Industries. (The antenna/comparator is a 0.61-m monopulse reflector-type antenna with amplitude sensing of the multiplicative and additive sensing functions of the comparator.) The operational frequency of this unit is 140 GHz ±600 MHz. Figure 2 is an antenna pattern in the vertical plane of this system measured at the operational frequency of 139.5 GHz.

The LO distribution network distributes the 138.5-GHz LO signal to each of three mixers with equal phase shift. A fourth mixer connected directly to the transmitting tube through a 30-dB directional coupler is used for automatic frequency control (AFC). The LO is a Hughes continuous wave (CW) IMPATT oscillator with an output power of +18 dBm. Each of the three receiver mixers operates with +5.5-dBm LO drive. The noise figure of each mixer with this level of drive is 6 dB.

The transmitter tube is a Varian Pulsed Extended Interaction Oscillator. The peak output power of this tube is 260 W. An external modulator built into the radar is set up for 100-ns pulses at a 20 KHz-repetition rate. Ferrite switches in synchronism with the transmitted pulses are used for receiver protection. Failure of any one or all of these switches will shut down the transmitter. AFC is implemented in the second conversion process. A 160-MHz discriminator samples the transmitter signal and, through the gated integrator, controls the frequency of the second 1,160-MHz LO. This tracks the received signals into the 20-MHz bandwidths of the 160-MHz (IF) amplifiers and monopulse processor.

The Monopulse Detector Subsystem is a complete unit that was purchased from RHG Electronics Laboratory. This device is a complete three-channel monopulse IF processing subsystem. The unit consists of an IF matrix, a detector matrix, and three matched limiter channels. This detector subsystem determines difference nulls by measuring the difference ($\Delta$) to sum ($\Sigma$) ratio. Each output error signal is proportional to this ratio and to the cosine of the phase angle between the $\Delta$ and $\Sigma$ signals. The output is of the form,

$$E_o = \frac{1.4\ (\Delta/\Sigma)\ \cos\ \phi}{\left(1 + 2\ (\Delta/\Sigma)\ \sin\ \phi + (\Delta/\Sigma)^2\right)^{1/2}} \ ,$$

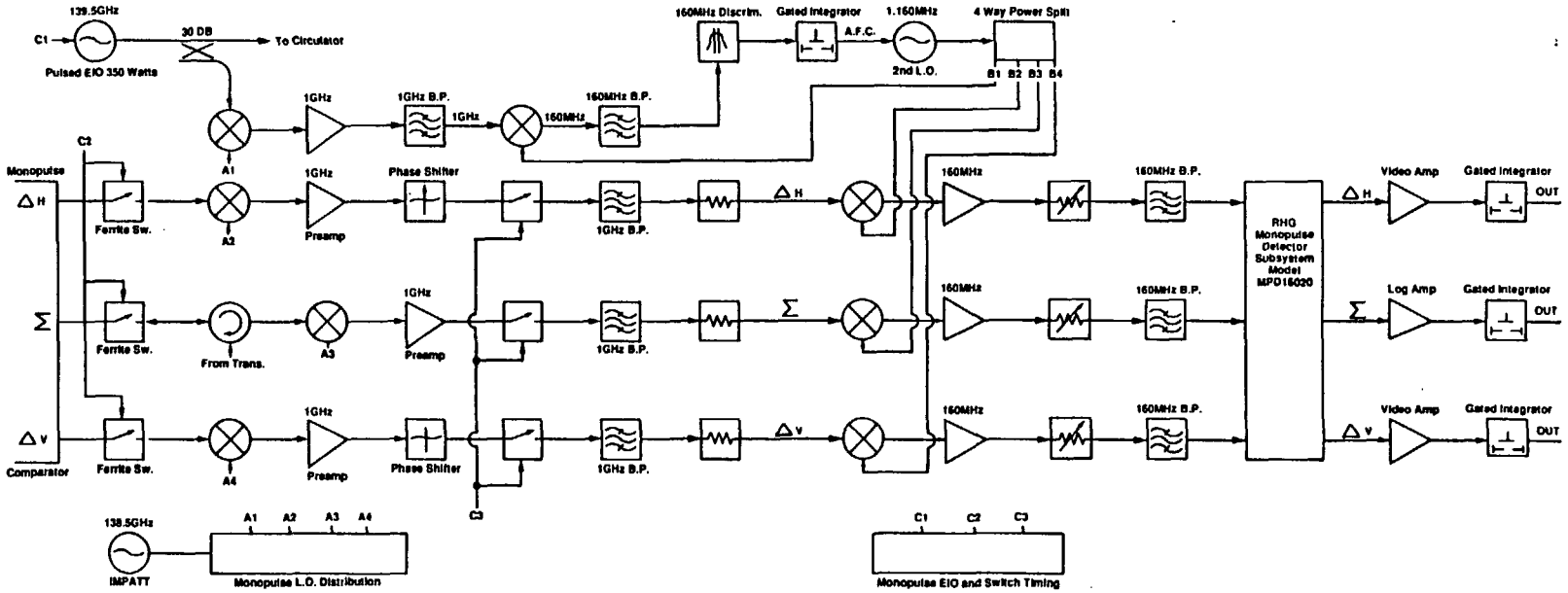


Figure 1. Block diagram of RF and IF sections.

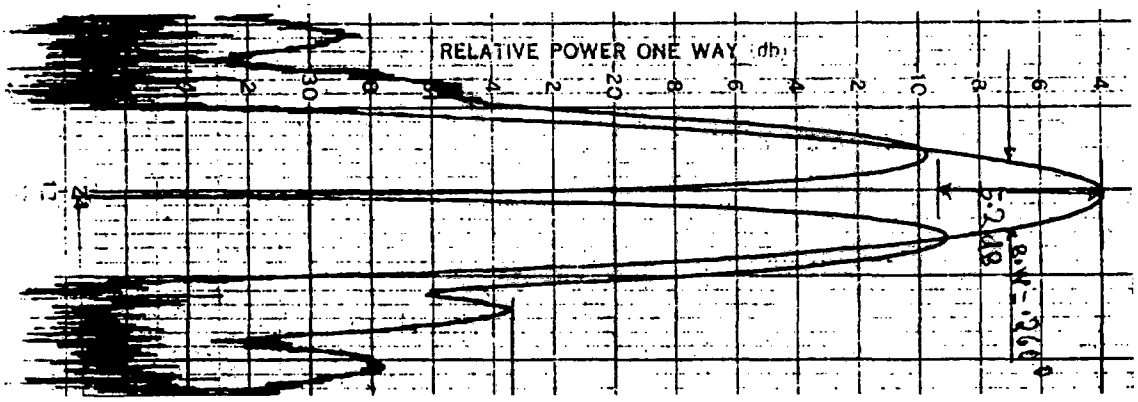


Figure 2. 140-GHz two-way antenna pattern, elevation plane.

where

$E_o$ = difference output voltage,

$\Delta/\Sigma$ = voltage ratio between $\Delta$ and $\Sigma$, and

$\phi$ = phase angle between $\Delta$ and $\Sigma$ .

The difference and sum channel outputs, still in the form of a 100-ns pulse, are passed on to the gated integrator modules (Evans Electronics Modules Model 4130A). Each unit is a fast, low-leakage integrator with an input-isolative gate that is opened under external control, which is a function of the range to the target. The output voltages of these devices closely approximates 1/RCx, the time integral of the input voltage, with integration proceeding only during the open gate intervals. The integral is held constant while the gate is closed. Figure 3 is an example of sum and vertical difference voltage outputs of the radar.

Initial alignment of the radar was accomplished with precise adjustments of the antenna, comparators, and phase shift adjustments in the first 1-GHz IF sections at the mixer outputs. Phase stability was maintained by temperature stabilizing all of the electronic components and the comparator.

The computer system used with this radar is a Hewlett-Packard (HP) Series 6900 Multiprogrammer with an HP 9000 CPU board and sufficient I/O cards for radar control functions and data input and output.

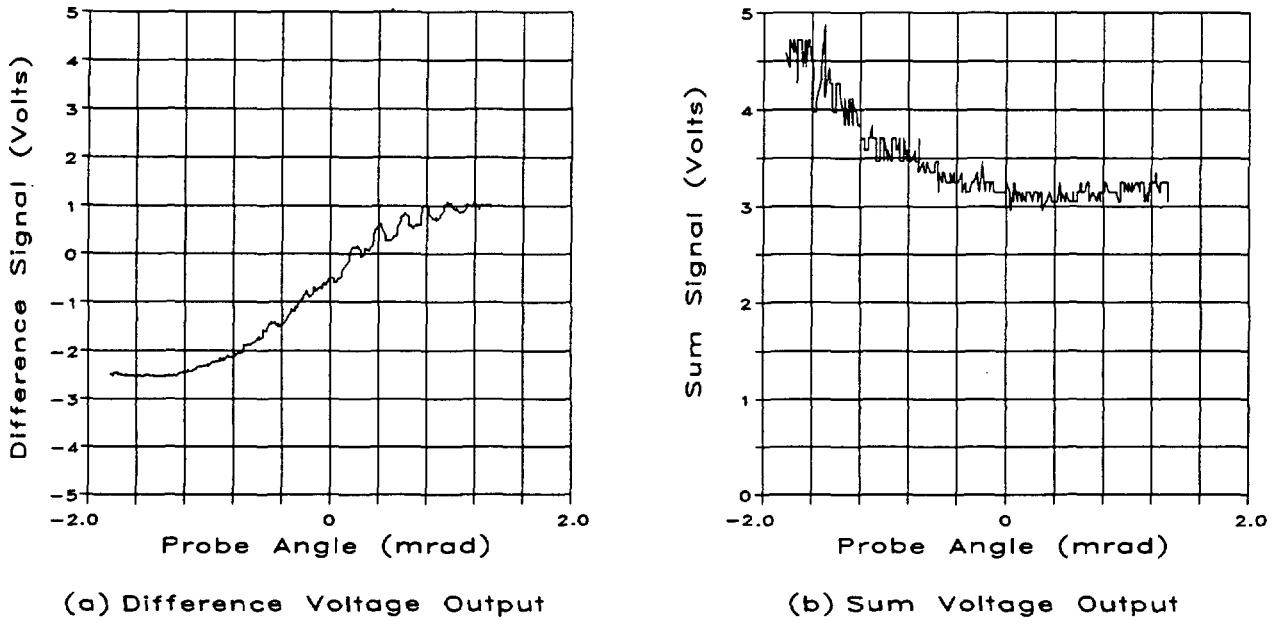


Figure 3. Typical measured vertical difference and sum outputs.

The vertical probe used for this test was designed and fabricated at the former BRL. The object of this device was to move a trihedral reflector through the fixed monopulse antenna beam at extended ranges from the radar. The probe shown in Figure 4 was mounted on a four-wheel trailer for ease of transportation and positioning. A radar reflector could be moved from near ground to a height of 5.36 m. The tower was constructed such that it had very low radar cross section. The vertical position of the reflector was continuously monitored and telemetered back to the transmitter trailer.

## 3. TEST SETUP AND TEST PROCEDURES

The radar was set up on an elevation over azimuth positioning mount located in the rear of an instrumentation trailer. The mount was attached to a special floor rack assembly that was detachable from the trailer and secured directly to the ground under the trailer. This was necessary to maintain the stability required for precise angular error measurements. The elevation axis of the positioning mount was instrumented for angle readout into the computer. The antenna was located 3 m above the ground for all the tests.

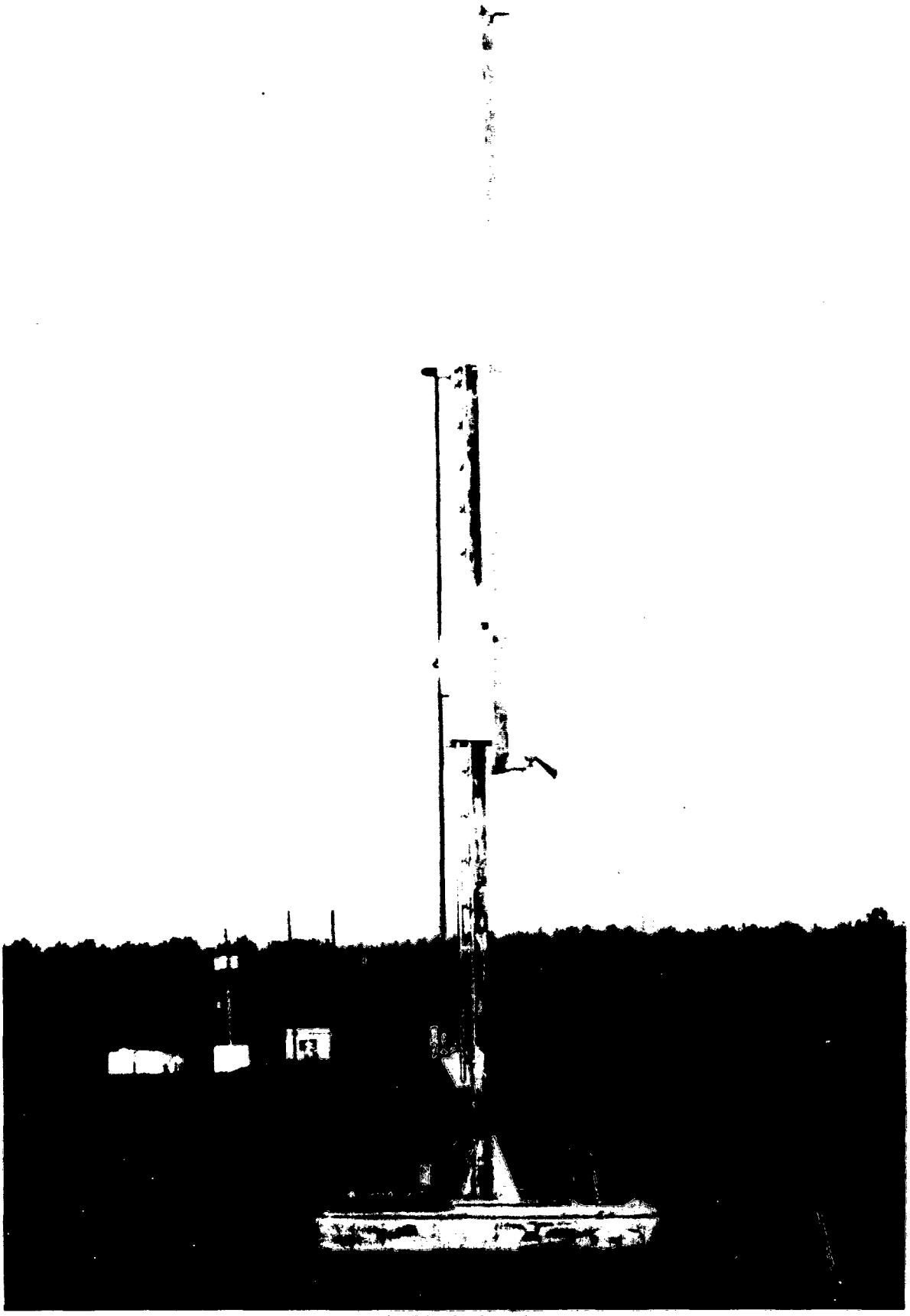

Figure 4. Vertical probe.

The site for this series of measurements was Test Area 3 at Redstone Arsenal, AL. These tests were designed to represent a radar locked on to a target at a range of 5 km and height above the ground of 1.5 m. The vertical probe was used to measure the effects multipath reflections would have on the guidance of a missile or projectile directed at the target.

A line of sight was set up between the radar and a target board at a range of 5 km. This line of sight was held constant, in both azimuth and elevation, for all but one of the measurements along the 5-km path. This optical boresight varied between 1 m and 3.6 m above the ground, depending on the terrain.

A calibrated corner reflector was set up at a range of 422 m at a height of 9 m. This point source was out of the antenna nearfield and high enough to ensure there were no multipath effects. The radar was boresighted with a television and Questar telephoto lens system. This high-resolution optical system was parallax aligned in the monopulse azimuth null plane and on the true elevation null. All subsequent multipath measurements were made relative to this optical boresight. The optics were boresighted to within 0.05 mrad of the true vertical null of the monopulse antenna. Figure 5 is a television still frame of a corner reflector at a range of 4 km.

Prior to each test, a series of calibration measurements was recorded using the calibration reflector. A complete vertical difference pattern was recorded. This was accomplished by sweeping the antenna beam, in the vertical plane, across the calibration reflector. One of these calibration patterns is shown in Figure 6. Long-term noise measurements of the vertical difference null signal were also recorded. This difference noise signal is calibrated in terms of angle offset from the zero null in the vertical difference channel. This angular variation is caused by receiver noise and atmospheric perturbations in the propagation path. Atmospheric noise was very low in the calibration measurements but was evident during subsequent long-range measurements.

The vertical probe was used for all the multipath measurements recorded during this series of tests. The probe was set up at various ranges out to 4.8 km in the direct line of sight to the target board. The boresighted optics were used to align the probe within the line of sight. Vertical error signals were recorded as the corner moved up through the antenna beam. Variations in these error signals are a measure of specular multipath. The measure of diffuse multipath error was the difference between the true optical calibration null and the apparent electrical null measured with the vertical probe. Long-term angular error noise was also recorded with the probe reflector adjusted to the electrical null of the antenna.

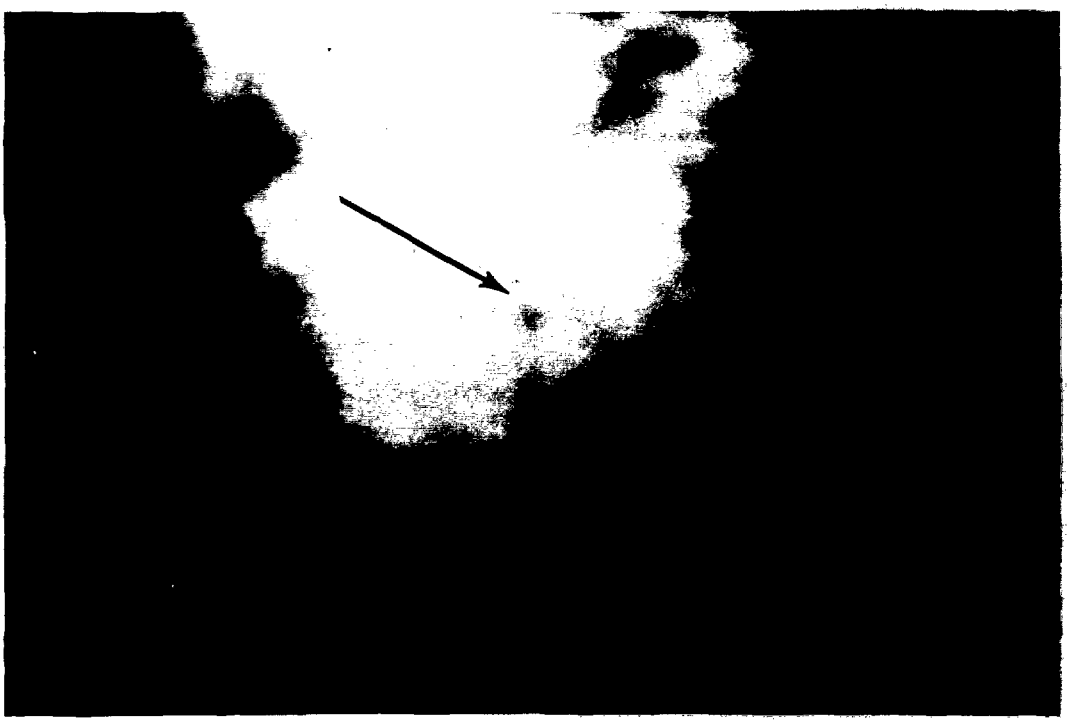

Figure 5. Television still frame of corner reflector at 4 km.

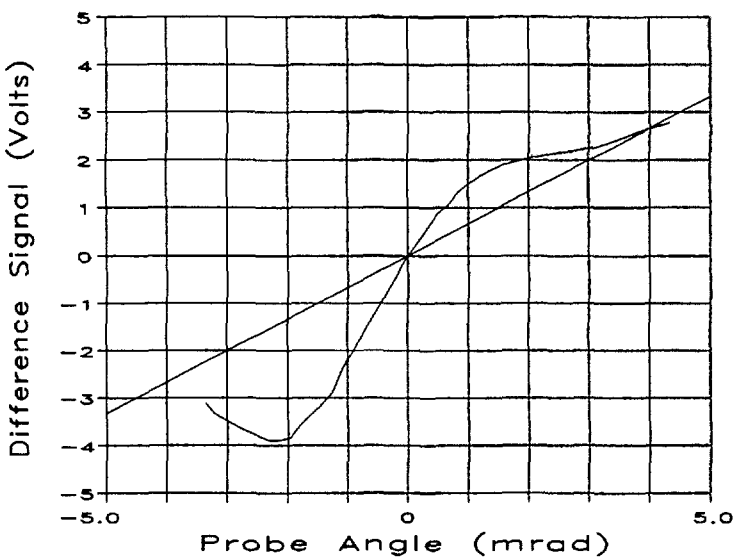


Figure 6. Typical calibration S-curve.

This noise was only recorded in the vertical error channel. The sum channel output was also recorded during each test. A corner reflector was set up approximately 20 m in front of the probe for each test. The sum range gate was alternately switched between this reflector and the probe to measure signal stability during each test. This precluded any errors associated with instabilities within the radar system or some momentary obstruction within the propagation path.

The test area, Redstone Arsenal Test Area 3, is a relatively flat field with a medium level of grass covering most of the propagation path. The terrain profile for part of the path is shown in Figure 7. Note that the vertical scale is significantly larger than the horizontal scale, to show that the profile is not perfectly flat. The profile was surveyed using a laser over the first 2,770 m of the propagation path. This short range was the limit of the laser system. The remaining 2,230 m of the path did not differ significantly in character from the measured path.


Figure 7. Terrain profile for the Redstone Arsenal Test Area 3.

Figure 8 is a photograph of the radar mounted in the trailer. The second antenna mounted on the tripod was the telemeter receiver used to transfer probe position data to the computer.

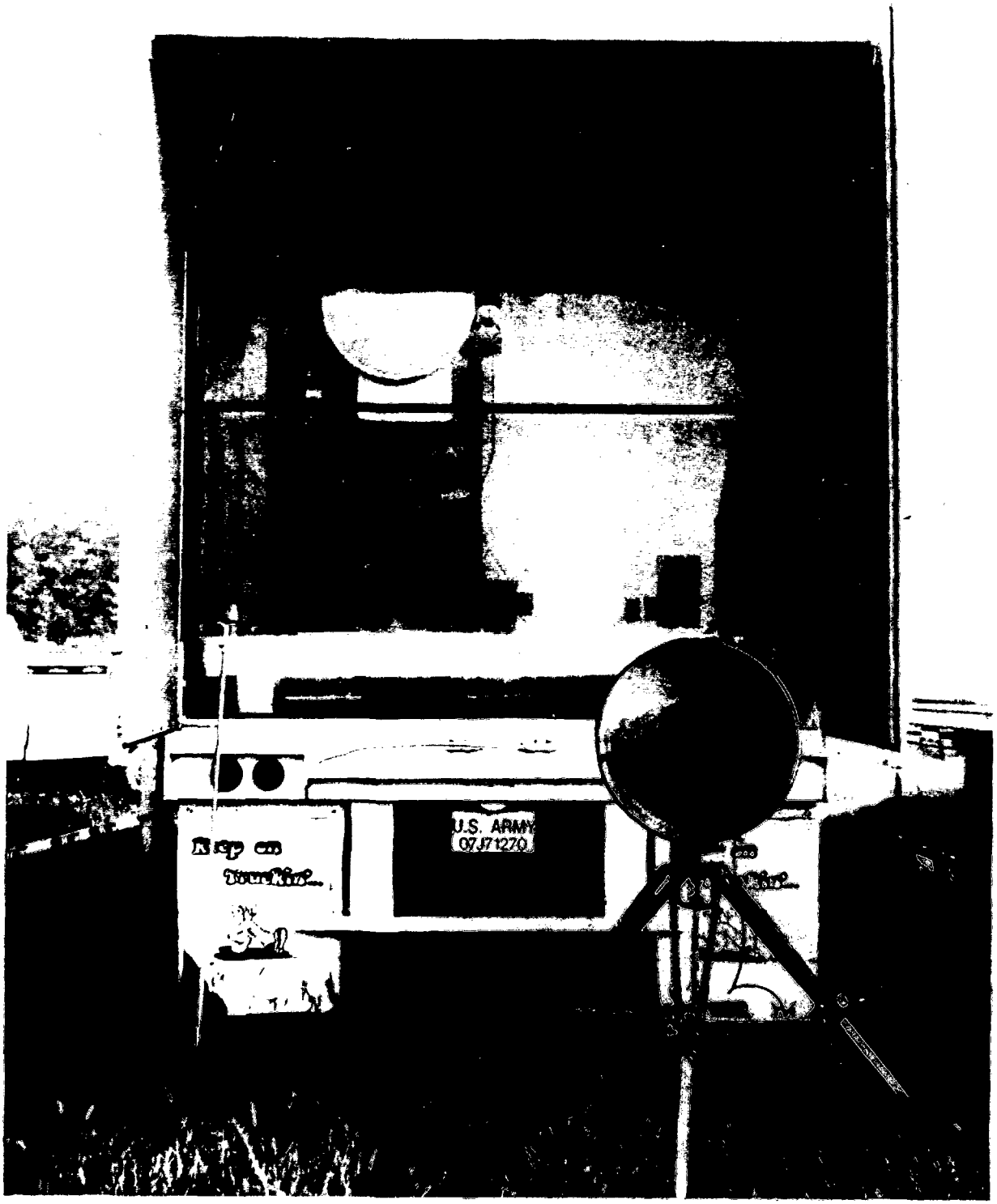


Figure 8. Monopulse antenna and instrumentation trailer.

## 4. DATA COLLECTED

Data was recorded on 11, 12, 13, 16, 17, and 18 September 1991. Measurements were made at six different ranges between 0.4 and 4.8 km. Additional measurements were made of static angular errors as a function of atmospheric weather conditions. A total of 18 usable measurements were made with the vertical probe. The total number of multipath tests was limited due to problems encountered with the 95-GHz monopulse radar system. The overall test plan called for simultaneous 95- and 140-GHz measurements. In one test, TR53, the optical boresight was raised 1.3 mrad above the normal optical boresight to determine if the multipath error would be reduced if there was a fixed vertical offset in the target track.

## 5. ANALYSIS OF MULTIPATH PROPAGATION DATA

Figure 9 shows typical difference and sum channel signals vs. probe position before calibration and filtering. Processing the raw error signal data was a three-step process that consisted of 1) converting angular vertical difference voltages to apparent angular difference in milliradians; 2) converting the probe position units to probe angle in milliradians; and 3) filtering the data with a smoothing algorithm.

The angular difference voltage was calibrated to give apparent angular difference by using information derived from the calibration S-curves recorded before each trial. The straight-line section in the middle of each S-curve was used to compute a slope. The slope is in units of volts/mrad, as can be seen in Figure 6. Digitized values of the angular difference voltage were scaled by this slope value, resulting in angular difference in milliradians.

Next, the position axis of the raw data was calibrated. The pulse-generated output from the vertical probe contained position information in terms of uncalibrated oscillator period "units," that changed linearly as the position along the probe pole changed. The maximum and minimum raw values were assumed to correspond to the highest and lowest positions of the probe in meters. The conversion to position in angle (with respect to the optical boresight) was accomplished by first converting the period value to probe distance from the boresight in meters using this linear relationship and then computing the angle by using the simple geometric relationship between the range and the probe height:

$$\text{angle (from boresight)} = \arctan\left[\frac{(\text{probe height}) \times (\text{datafreq} - \text{nullfreq})}{(\text{range to probe}) \times (\text{maxfreq} - \text{minfreq})}\right].$$

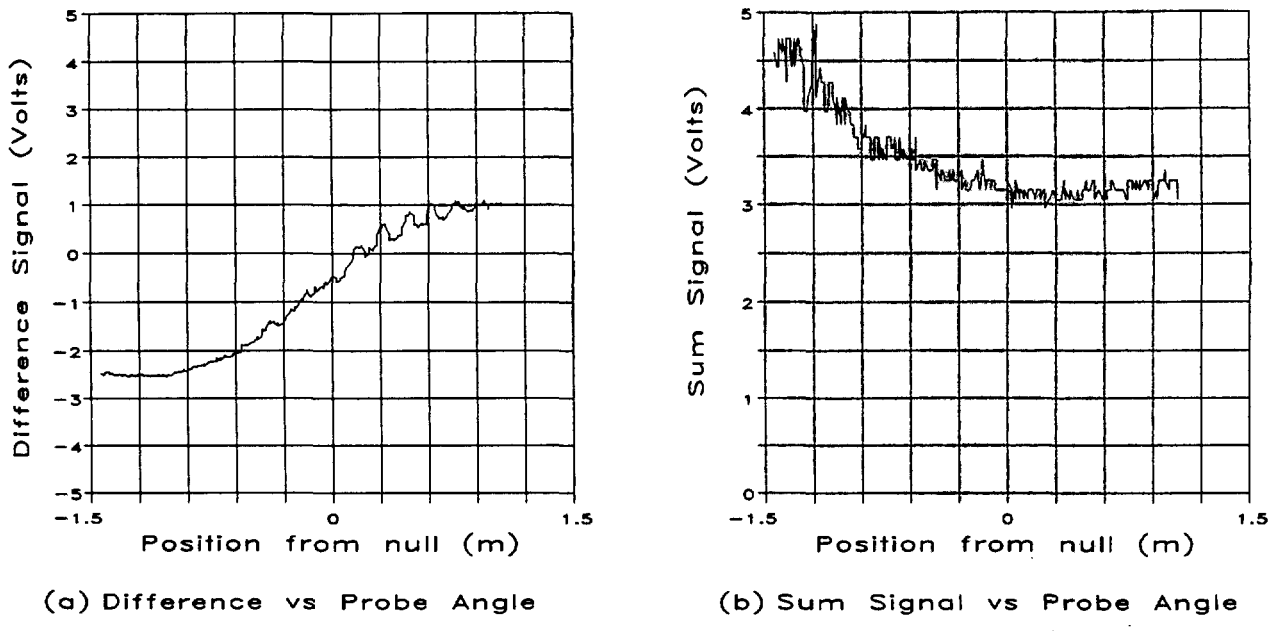


Figure 9. Typical difference and sum signals vs. probe position.

The last step in reducing the multipath probe data was smoothing to get rid of the noise that may have otherwise obscured the specular multipath variations. The bandwidth of the integrated signal was calculated to be 0.025 Hz by using the formula associated with the gated integrators (Evans Electronics),

$$\text{Noise factor} = \frac{(RC)}{n\,(t2-t1)} = 0.025 \text{ Hz} ,$$

where

R = integrator resistance = $10 \times 10^3$ Ohms

C = integrator capacitance = $10 \times 10^{-9}$ F

n = repitition rate = $20 \times 10^3$ Hz, and

t2 – t1 = integration time = 200 ns .

With a noise factor of 0.025 Hz, a smoothing constant can be determined using Shannon's Law of Sampling, (i.e., freq (sampling) $\geq 2 \times$ signal BW). The sampling rate used in this experiment was approximately 160 Hz; therefore, it was well within acceptable bounds to use a three-point moving average to smooth the data without introducing any aliasing effects. The resulting calibrated apparent angular error vs. true (or probe) angular error curves are shown in Appendix A (A-1 through A-18). Note that the x-axis scale is not constant over the entire set of data. The axis was expanded with increasing path length to allow the features of the difference curves to be seen more easily. At the longer distances, the length of the probe pole subtends a smaller angle than at the shorter distances, making for a smaller measured angular error curve.

The vertical difference-axis of the atmospheric noise plots shown in Appendix B (B-1 through B-20) was calibrated in the same way as the difference-axis of the plots in Appendix A. The difference data was calibrated with the S-curve taken closest in time to the noise run. The sum voltage was calibrated with the voltage calibration curve recorded on the day of the noise run. The points of the calibration curve were used as a lookup table to convert the sum voltages to decibels. Linear interpolation was used for voltage values that fell between points on the calibration curve.

## 6. MULTIPATH DIFFUSE AND SPECULAR ANGULAR VARIATIONS

Computations of all the probe measurements of diffuse and specular multipath vertical channel difference variations are shown in Table 1. All multipath tests were set up so the optical boresight, which was the center null of the antenna beam, was aligned with the boresight mark on the target board. The vertical probe was then set up along the propagation path within the optical boresight. The radar reflector was moved up the probe until it was aligned with the optical boresight. This point on the probe was noted as the zero null or crossover point of the antenna. The reflector was then lowered to the bottom of the vertical beam probe and slowly raised to the top, while sum and vertical difference channels were recorded. If there were no multipath effects, the zero crossover in the vertical difference channel would occur at the optical boresight level. Diffuse multipath causes the measured null or crossover to be biased below the optical boresight. The computed measure of diffuse multipath is noted in Table 1 as the mean difference calibrated in terms of angle.

Specular multipath would cause cyclical variations in the vertical difference channel output as the vertical probe reflector is moved through the antenna monopulse beam. The period of this variation is

Table 1. Mean and Standard Deviation of Angular Error for Path Lengths of 1, 2, 3, 4, and 5 km

| Target Reflector | | | | Calibration Reflector | | |
|---|---|---|---|---|---|---|
| Trial No. | Distance (km) | Mean (mrad) | Std. Dev. (mrad) | Trial No. | Mean (mrad) | Std. Dev. (mrad) |
| TR 24 | 0.8 | −0.14 | 0.36 | TR 22 | 0.00 | 0.05 |
| TR 25 | 0.8 | −0.07 | 0.43 | TR 22 | 0.00 | 0.05 |
| TR 29 | 0.8 | −0.06 | 0.25 | TR 27 | 0.02 | 0.03 |
| [1]TR 17 | 1.8 | −1.03 | 0.56 | TR 18 | −0.07 | 0.06 |
| TR 20 | 1.8 | 0.01 | 0.23 | TR 18 | −0.07 | 0.06 |
| [1]TR 21 | 1.8 | −0.52 | 0.54 | TR 18 | −0.07 | 0.06 |
| TR 53 | 1.8 | −0.13 | 0.15 | TR 51 | −0.02 | 0.06 |
| TR 54 | 1.8 | −0.12 | 0.23 | TR 51 | −0.02 | 0.06 |
| TR 3 | 2.8 | −0.18 | 0.38 | TR 5 | 0.01 | 0.03 |
| TR 6 | 2.8 | −0.07 | 0.32 | TR 5 | 0.01 | 0.03 |
| TR 11 | 2.8 | −0.45 | 0.48 | TR 9 | 0.01 | 0.03 |
| TR 14 | 2.8 | 0.08 | 0.16 | TR 9 | 0.01 | 0.03 |
| TR 32 | 2.8 | −0.05 | 0.15 | TR 30 | 0.00 | 0.03 |
| TR 36 | 2.8 | −0.38 | 0.39 | TR 34 | 0.06 | 0.03 |
| TR 44 | 2.8 | −0.04 | 0.15 | TR 37 | −0.06 | 0.02 |
| TR 47 | 2.8 | −0.41 | 0.26 | TR 48 | 0.10 | 0.09 |
| [2]TR 39 | 3.8 | — | 0.25 | TR 37 | −0.06 | 0.02 |
| [2]TR 42 | 4.8 | — | 0.13 | TR 37 | −0.06 | 0.02 |

[1] Data probably bad, probe sitting below optical boresight.
[2] Optical boresighting impossible at these lengths due to haze, so no mean error has been calculated.

a function of range to the probe (Barton and Ward 1984). The computed measure of specular multipath variations is noted in Table 1 as the standard deviation, calibrated in terms of angle. The data was filtered so that atmospheric angular variations were removed. This set of multipath data is shown in Appendix A.

Four separate plots are shown for each trial. Plot "a" (difference vs. probe angle) is the raw data (voltages) out of the vertical difference channel vs. the position of the vertical probe reflector in terms of angle—negative angle below the optical boresight and positive angle above the optical boresight. In Figure A-1, the specular and diffuse multipath-induced difference signals are apparent. Plot "b" (sum vs. angular probe position) shows the sum signal amplitude as a function of the vertical probe reflector position. This sum data is not filtered and shows the atmospheric signal amplitude variations. Plot "c" (difference voltage vs. vertical angle antenna mount position) is the raw data output (voltages) of the vertical difference channel when the monopulse antenna beam is swept vertically past the calibration

reflector. The calibration curve is used to calibrate the vertical difference channel in terms of angular difference. Plot "d" (apparent angle vs. probe angle) shows the calibrated multipath-induced vertical differences in terms of angle, plot "a," calibrated with plot "c," along with the theoretical straight-line difference curve that would have been achievable if there were no multipath errors. The mean difference from the theoretical straight line is the diffuse angular difference. The cyclical amplitude variations are the specular multipath differences.

At the longest ranges, 3.8 km and 4.8 km, haze conditions due to the hot, humid air limited the range of the optical boresight. Diffuse multipath at these ranges could not be measured with any degree of accuracy. Appendix C contains tabular data on water vapor values that were computed from meterological data measure during the testing.

For Trial 53, the optical boresight was raised 1.3 mrad in the vertical plane above the target board. This is approximately one-quarter of the sum of the antenna beam pattern beamwidth. This test was performed to measure the difference in multipath-induced errors if a slight bias in the vertical plane was applied to the tracking loop. Trials 53 and 54 were run for direct comparison at 1.8 km (Figures A-7 and A-8). There is a definite difference in the data sets. Trial 54, with boresight on the target board, shows both specular and diffuse multipath-induced errors. When the antenna beam was raised for Trial 53, there was no trace of specular multipath and the diffuse error at 0° probe angle is very small. In Trial 54, the lower optical boresight allows more of the antenna beam to intercept the ground, causing a stronger surface-reflected signal that can interfere with the direct radar-target-radar signal. The error is less in Trial 53 because the higher boresight implies less illumination of the ground, hence a weaker surface-reflected signal.

## 7. ATMOSPHERIC NOISE

The weather pattern during this series of tests consisted of extremely high temperatures with high levels of relative humidity. Large variations in difference channel and sum channel noise were noted throughout the course of this measurement program. It has been noted in other measurement programs (McMillan, Wiltse, and Snider 1979) that atmospheric noise and phase front distortions increase as the moisture content of the atmosphere increases. Water vapor is a continuously changing medium with areas of variable concentrations (scale sizes 10–100 m and strata of approximately 1 m). MMWs traveling through changing media are subject to random variations in both amplitude and phase (Deepak, Wilkerson, and Ruhnke 1980).

A series of measurements was made to ascertain the effects of this atmospheric noise on monopulse tracking accuracies. The antenna monopulse boresight was set up on the probe with the corner reflector set at the height of the target board boresight. Static measurements of the sum and vertical difference channels were recorded at all the measurement ranges out to 4.8 km, as a function of time. These static measurements were also recorded on the 0.4-km calibration reflector prior to or after each long-range measurement. Direct comparisons are shown in the data set which is in Appendix B.

Computations of all the static noise measurements are shown in Table 2. The vertical difference channel output was calibrated in terms of angular differences. The sum channel outputs are calibrated in terms of decibels. The measurements at 0.4 km of the calibration reflector are essentially system noise. This data is shown for comparison. The amplitude of the difference channel angular noise increases with range out to 2.8 km. The standard deviations of the data sets, shown in Table 2, characterize the relative magnitudes of the noise in terms of angular error. The number of measurements made at the longer ranges, 3.8 and 4.8 km, were not enough to indicate any further trend.

Phase front distortions and signal amplitude fluctuations could cause the angular difference fluctuations noted in both the vertical and horizontal difference channels. The RHG monopulse processor in this system employs hard limiters in the sum and delta processing channels. The return signal levels out to ranges of 3 km were of such amplitude to be hard limited; thus, signal amplitude fluctuations would not be a dominant factor in the processed difference channel outputs. The static angular variations measured out to 2.8 km in range are believed to be caused by phase front distortions. The sum channel outputs shown in Appendix B were not hard limited.

## 8. CONCLUSIONS

The measurements made during this test characterize errors that can affect the guidance of a missile or projectile to a distant target. Consider a missile that flies within a radar monopulse antenna beam. The monopulse radar tracking a target would measure the instantaneous position of the missile relative to the target, and guidance commands would be issued to the missile to correct its flight path to the target. There are three major sources of missile position error other than the tracking accuracies associated with the radar system: 1) atmospheric noise, 2) diffuse multipath, and 3) specular multipath.

Table 2. Mean and Standard Deviation of Angular Error for Noise Runs Over Path Lengths of 422 m, and 1, 2, 3, 4, and 5 km

| Trial No. | Distance (km) | Mean (mrad) | Std. Dev. (mrad) |
|---|---|---|---|
| TR 5 | 0.4 | 0.01 | 0.03 |
| TR 8 | 0.4 | –0.01 | 0.04 |
| TR 9 | 0.4 | 0.01 | 0.03 |
| TR 12 | 0.4 | 0.00 | 0.04 |
| TR 15 | 0.4 | 0.04 | 0.08 |
| TR 18 | 0.4 | –0.07 | 0.06 |
| TR 22 | 0.4 | 0.00 | 0.05 |
| TR 27 | 0.4 | 0.02 | 0.03 |
| TR 30 | 0.4 | 0.00 | 0.03 |
| TR 34 | 0.4 | 0.06 | 0.03 |
| TR 37 | 0.4 | –0.06 | 0.02 |
| TR 45 | 0.4 | –0.02 | 0.02 |
| TR 48 | 0.4 | 0.10 | 0.09 |
| TR 51 | 0.4 | –0.02 | 0.06 |
| TR 23 | 0.8 | –0.01 | 0.07 |
| TR 28 | 0.8 | –0.01 | 0.07 |
| TR 16 | 1.8 | 0.00 | 0.22 |
| TR 19 | 1.8 | 0.00 | 0.06 |
| TR 52 | 1.8 | –0.02 | 0.06 |
| TR 55 | 1.8 | 0.00 | 0.08 |
| TR 4 | 2.8 | 0.02 | 0.12 |
| TR 7 | 2.8 | 0.04 | 0.25 |
| TR 10 | 2.8 | –0.01 | 0.05 |
| TR 13 | 2.8 | –0.02 | 0.13 |
| TR 31 | 2.8 | –0.08 | 0.15 |
| TR 33 | 2.8 | 0.00 | 0.04 |
| TR 35 | 2.8 | –0.01 | 0.11 |
| TR 43 | 2.8 | 0.05 | 0.10 |
| TR 46 | 2.8 | 0.09 | 0.09 |
| TR 49 | 2.8 | 0.00 | 0.12 |
| TR 38 | 3.8 | –0.04 | 0.06 |
| TR 26 | 4.8 | –0.04 | 0.08 |
| TR 40 | 4.8 | 0.01 | 0.04 |
| TR 41 | 4.8 | 0.00 | 0.05 |

Atmospheric noise, which manifests itself in signal amplitude and phase front distortions, is a variable factor dependent on the water vapor continuum. In the damp atmosphere of summer, this angular variation was measured to be as great as ±0.15 mrad. Atmospheric noise can be reduced through closed loop bandwidth reduction when tracking a slow-moving distant target. Position tracking of a missile or projectile requires a very wide open loop bandwidth, which would include atmospheric noise.

Diffuse multipath error is variable depending on terrain features and surface moisture conditions. This source of error manifests itself in a negative bias error below the radar aimpoint. Diffuse errors measured during this test were as great as -0.45 mrad.

Specular multipath errors are also dependent on terrain and surface moisture conditions. The magnitude of this error increases as diffuse bias errors increase. Specular multipath is coherent in nature and will cycle with range. The error is impressed on the diffuse bias; thus, it will add to or subtract from the bias error. Specular multipath errors measured during this test had an average magnitude of 0.25 mrad.

Both diffuse and specular multipath errors can be reduced by introducing a small positive bias in the antenna boresight so that less of the beam intercepts the ground. This was shown to be the case in Trials 53 and 54. This simple method of reducing multipath error can be exploited to allow for more accurate tracking at low elevation angles.

## 9. REFERENCES


Barton, D., and H. Ward. Handbook of Radar Measurement. Englewood Cliffs, NJ, Pentice-Hall, 1984.

Christian, M. R., J. B. Winter, and T. D. Woods. "W Band Low Angle Multipath Measurements." Proceedings Precision Munitions Guidance Symposium, 1992.

Deepak, A., T. Wilkerson, and L. Ruhnke. Atmospheric Water Vapor. Academic Press, 1980.

Evans Electronics. "Gated Integrator Module - Model 4130A." Operator's Manual, Berkeley, CA.

Kammerer, J. E., and V. A. Richer. "4-mm Near-Earth Antenna Multipath Pointing Errors." BRL-MR-1559, U.S. Army Ballistic Research Laboratory, Aberdeen Proving Ground, MD, March 1964.

McMillan, R. W., J. C. Wiltse, and D. E. Snider. "Atmospheric Turbulence Effects on Millimeter Wave Propagation." IEEE EASCON 79 Conference Records, vol. 1, 1979.

Stratton, S. R., H. B. Wallace, and D. G. Bauerle. "Multipath Induce Tracking Errors at 95- and 140-GHz." BRL-MR-3947, U.S. Army Ballistic Research Laboratory, Aberdeen Proving Ground, MD, 1991.

Wallace, H. B. "140-GHz Propagation Measurements Over Varied Terrain Covers." IEEE EASCON-79 Conference Record, vol. 2, p. 256, 1979.

INTENTIONALLY LEFT BLANK.

# APPENDIX A:

# MULTIPATH MEASUREMENTS

INTENTIONALLY LEFT BLANK.

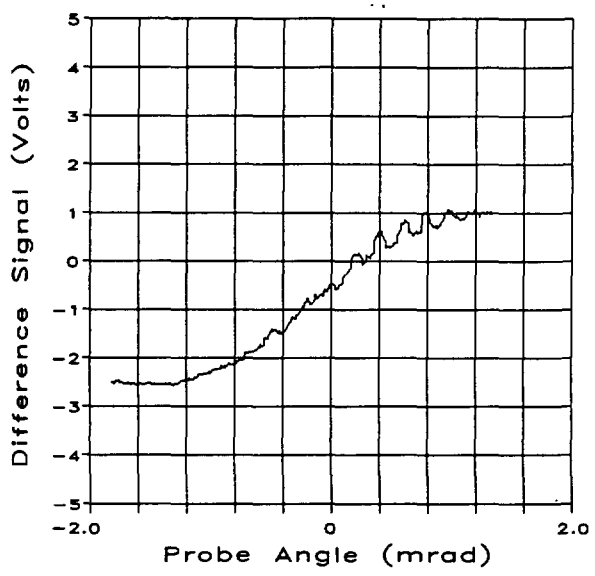


(a) Difference vs Probe Angle

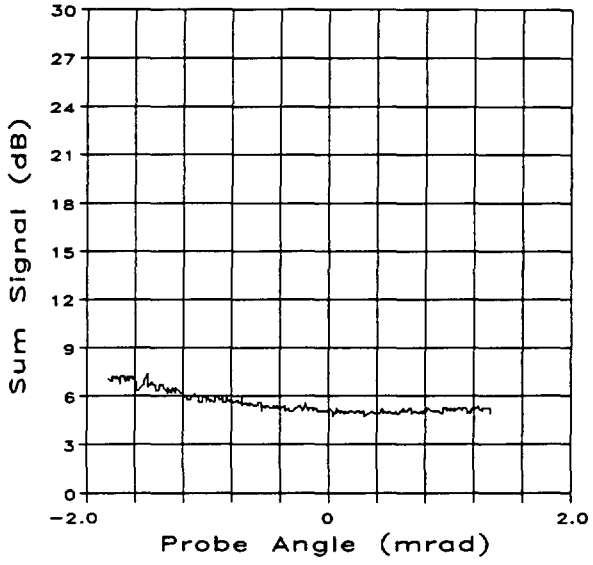


(b) Sum Signal vs Probe Angle

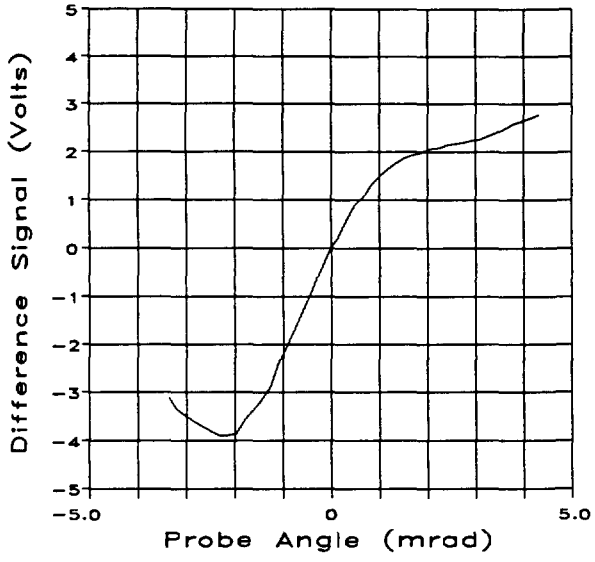


(c) Calibration Diff. vs Probe Angle

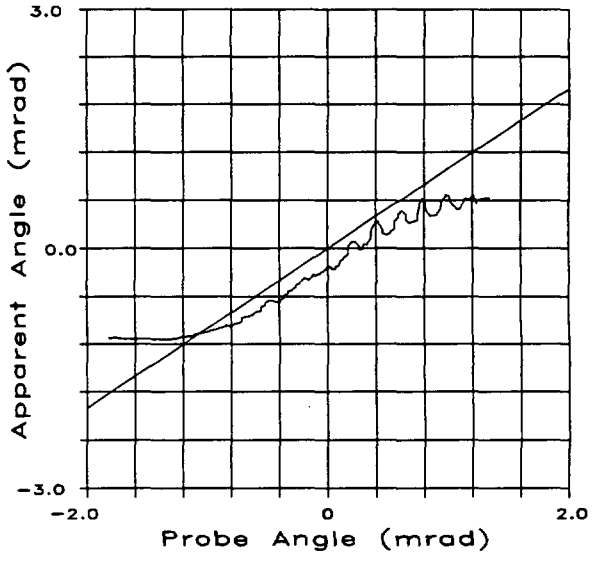


(d) Apparent Angle vs Probe Angle

Figure A-1. Trial 24, 0.8 km.

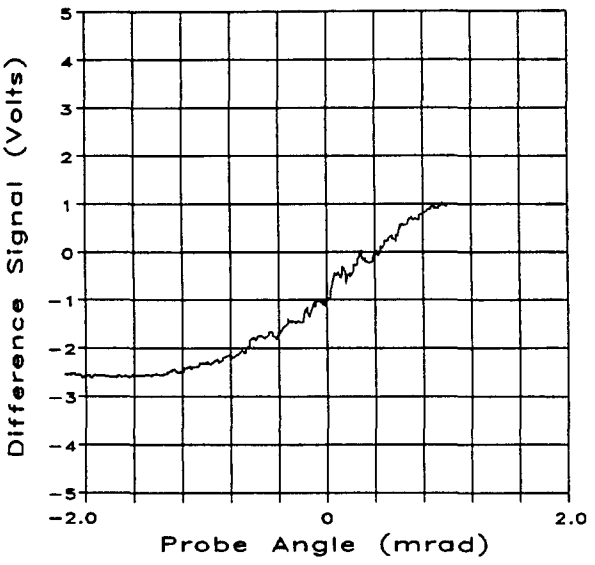


(a) Difference vs Probe Angle

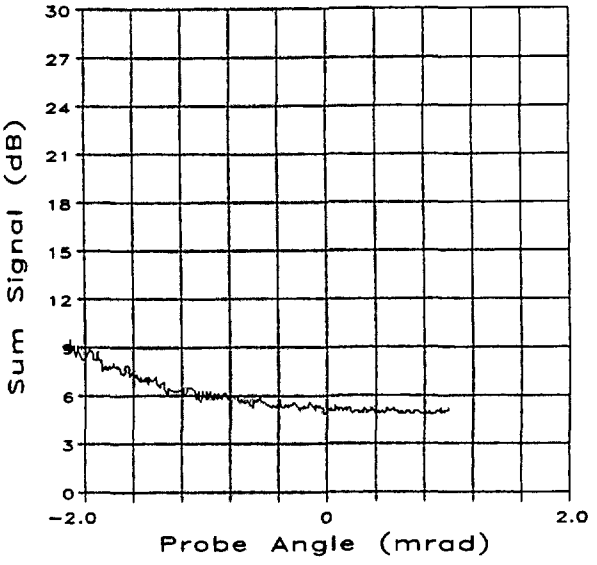


(b) Sum Signal vs Probe Angle

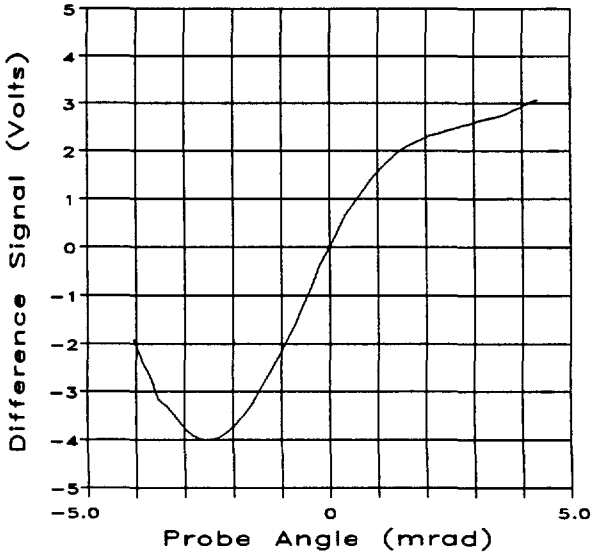


(c) Calibration Diff. vs Probe Angle

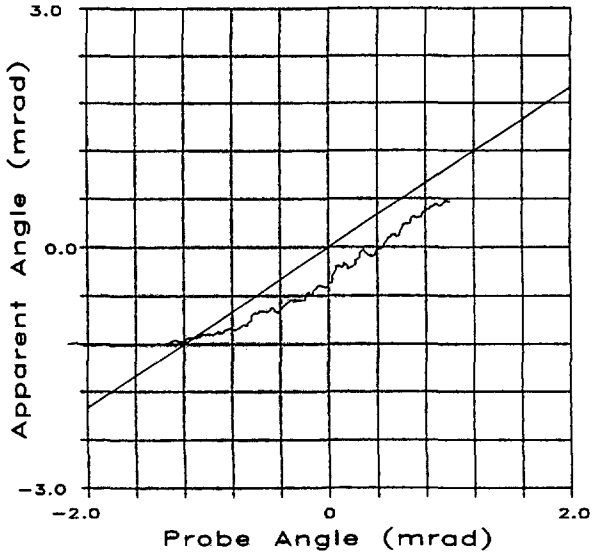


(d) Apparent Angle vs Probe Angle

Figure A-2. Trial 25, 0.8 km.

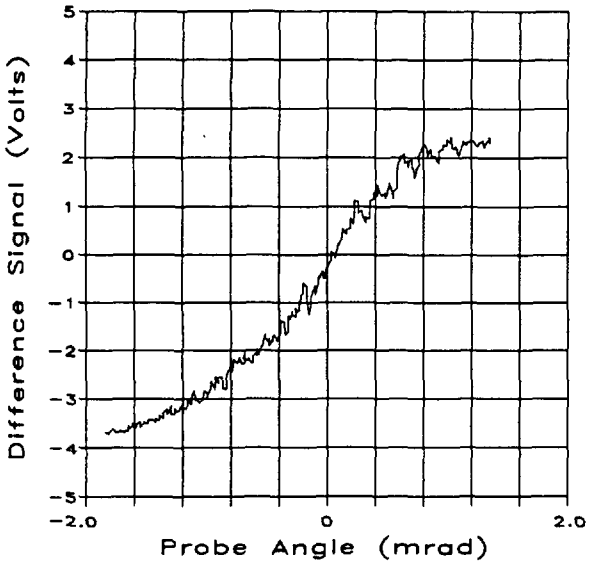


(a) Difference vs Probe Angle

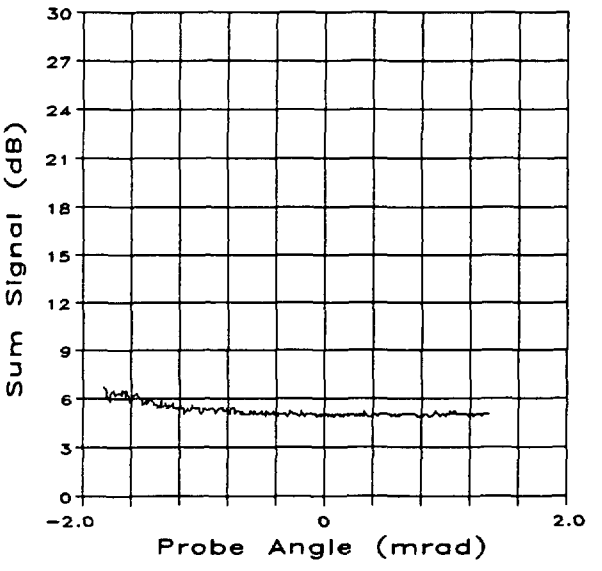


(b) Sum Signal vs Probe Angle

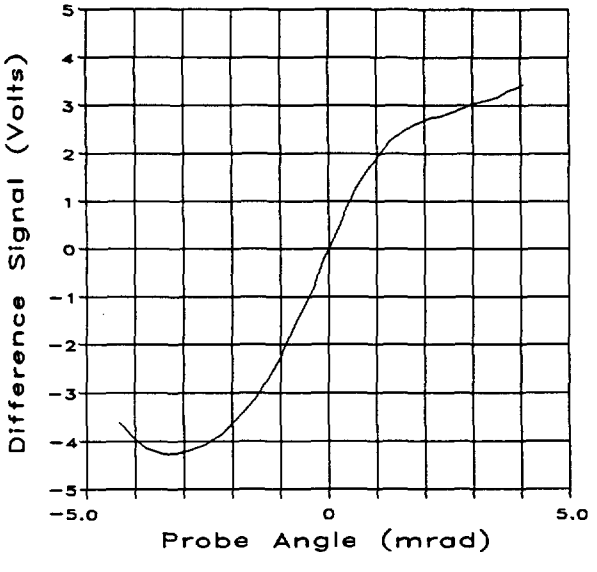


(c) Calibration Diff. vs Probe Angle

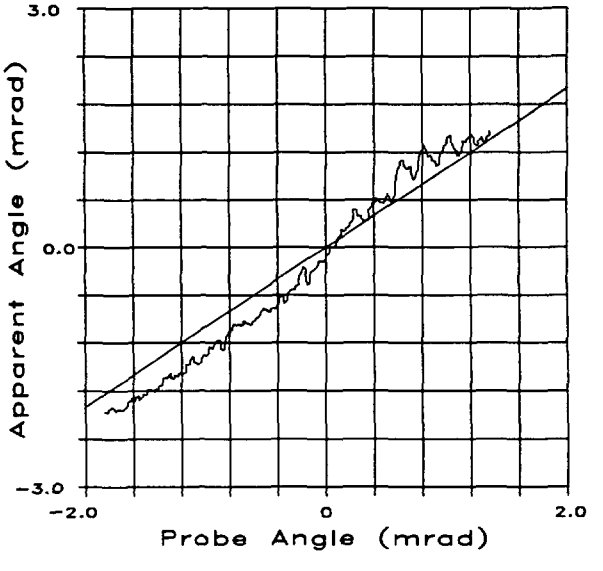


(d) Apparent Angle vs Probe Angle

Figure A-3. Trial 29, 0.8 km.

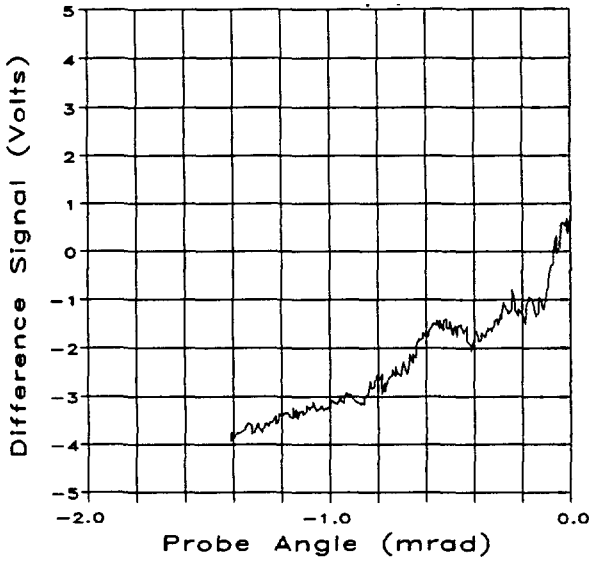


(a) Difference vs Probe Angle

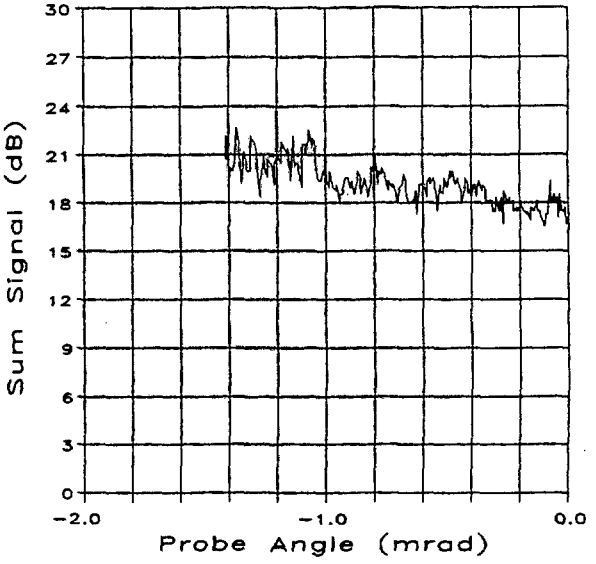


(b) Sum Signal vs Probe Angle

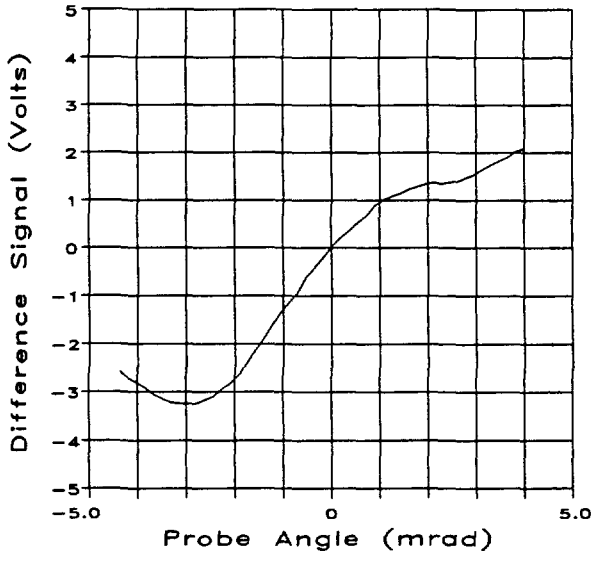


(c) Calibration Diff. vs Probe Angle

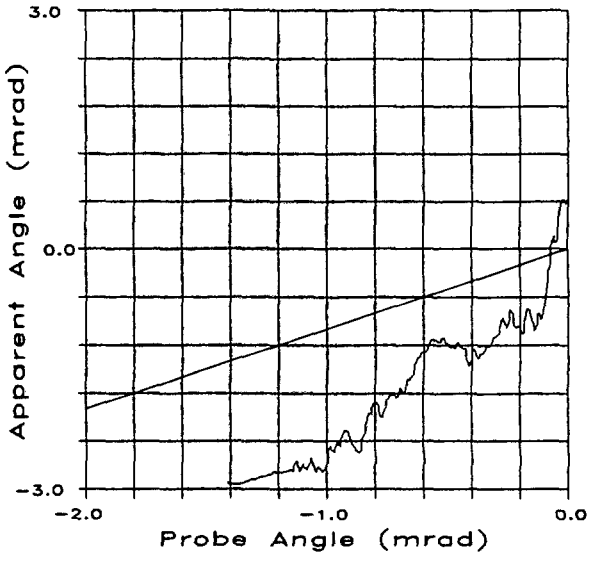


(d) Apparent Angle vs Probe Angle

Figure A-4. Trial 17, 1.8 km.

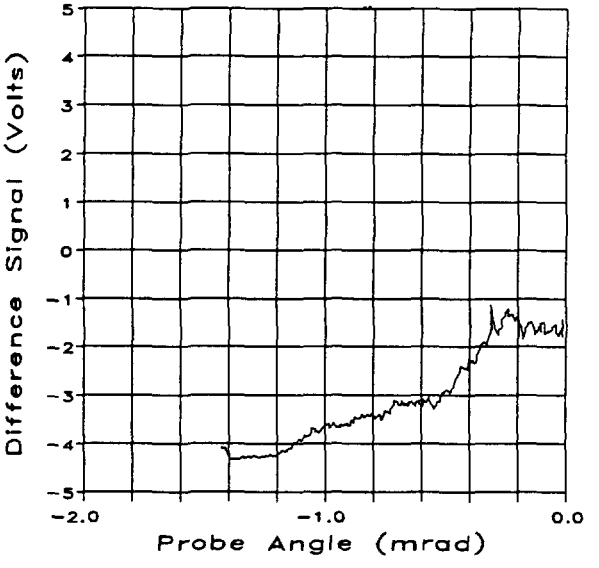


(a) Difference vs Probe Angle

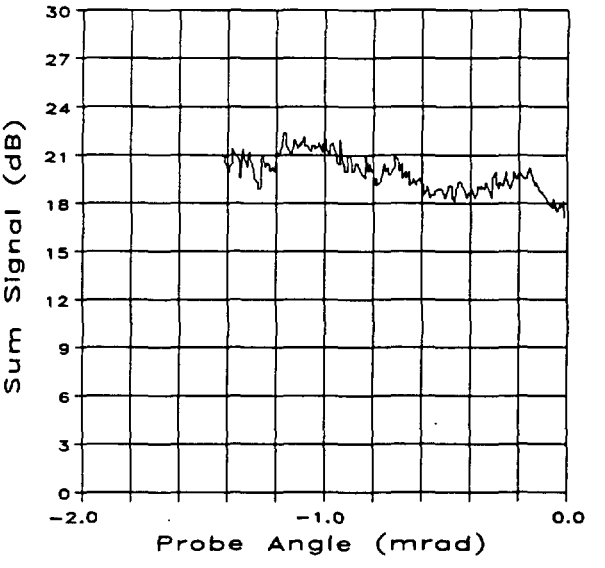


(b) Sum Signal vs Probe Angle

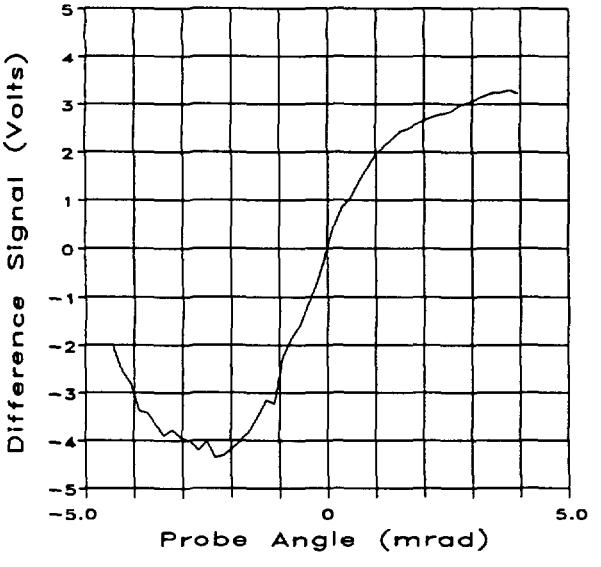


(c) Calibration Diff. vs Probe Angle

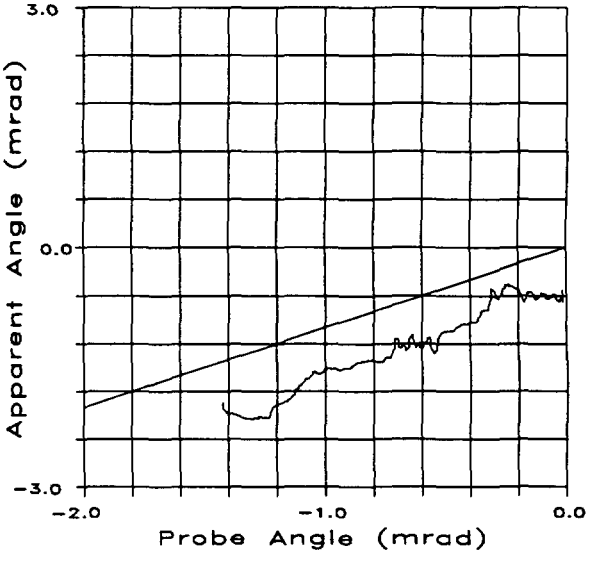


(d) Apparent Angle vs Probe Angle

Figure A-5. Trial 21, 1.8 km.

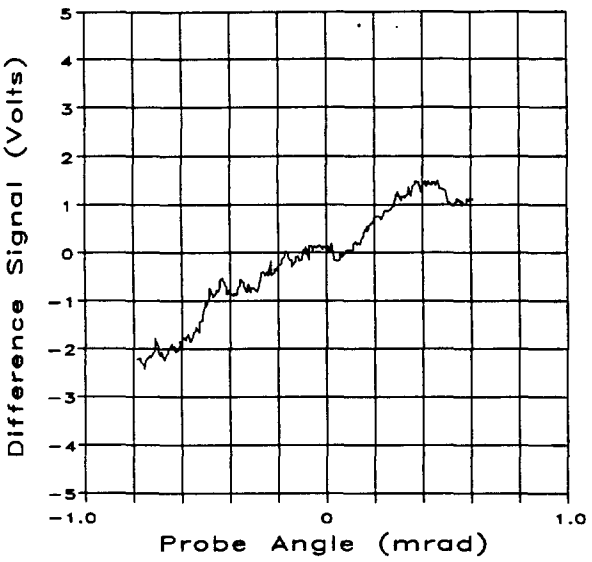


(a) Difference vs Probe Angle

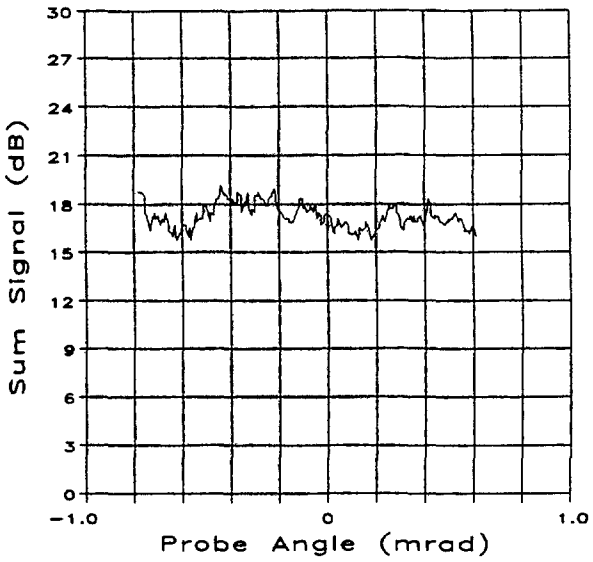


(b) Sum Signal vs Probe Angle

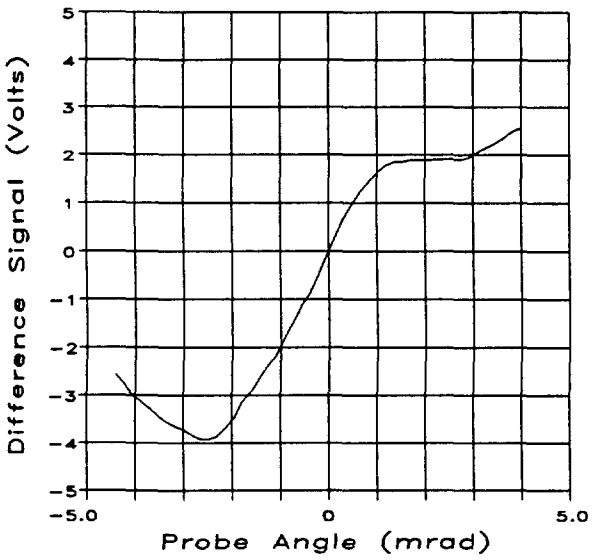


(c) Calibration Diff. vs Probe Angle

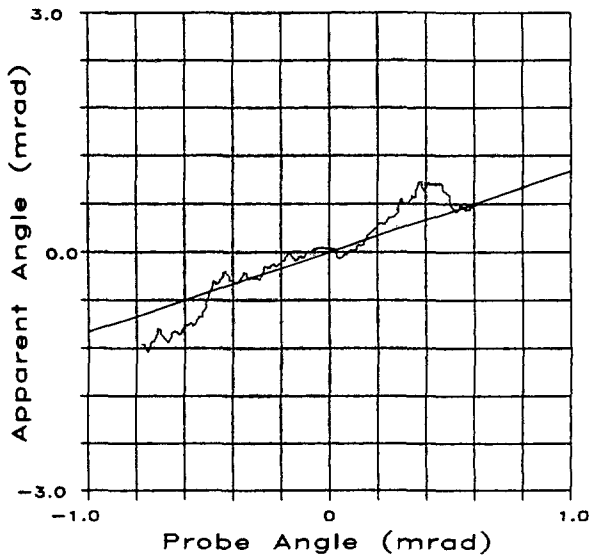


(d) Apparent Angle vs Probe Angle

Figure A-6. Trial 20, 1.8 km.

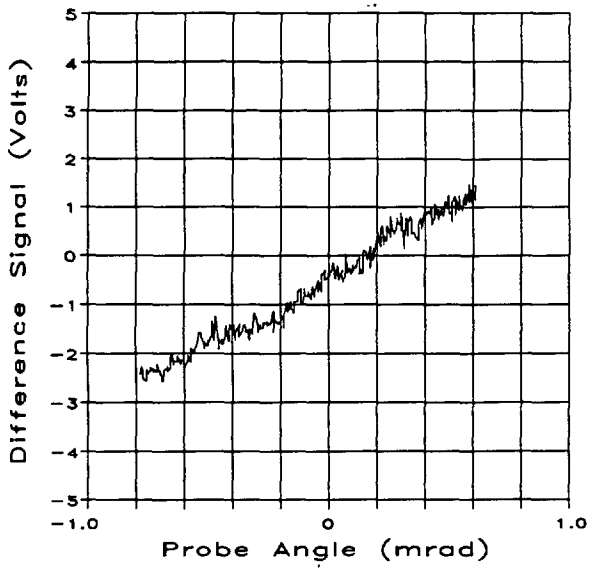


(a) Difference vs Probe Angle

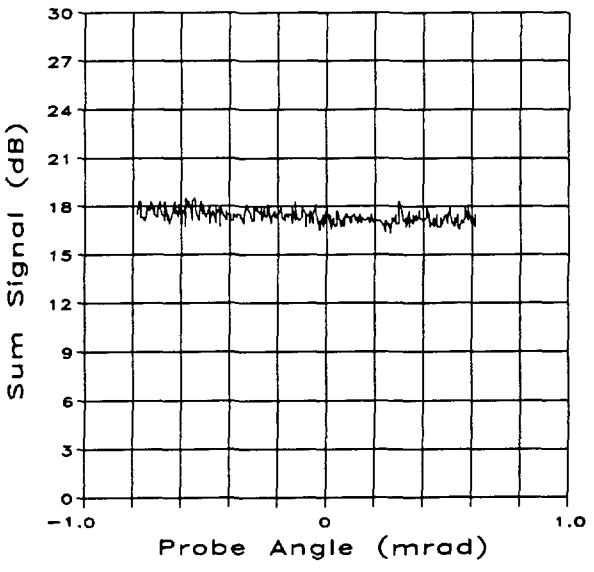


(b) Sum Signal vs Probe Angle

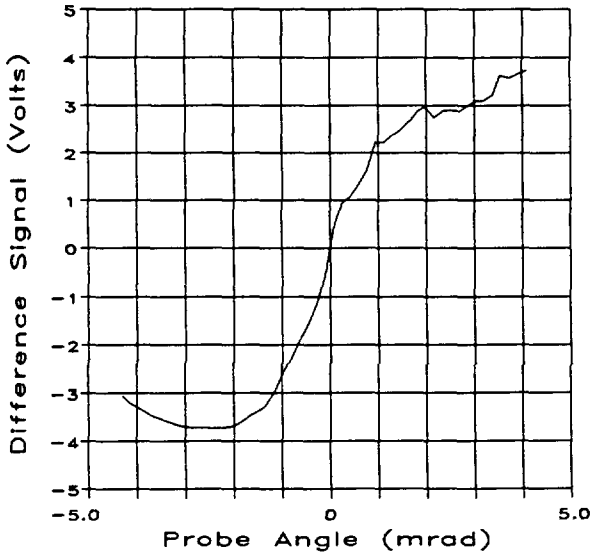


(c) Calibration Diff. vs Probe Angle

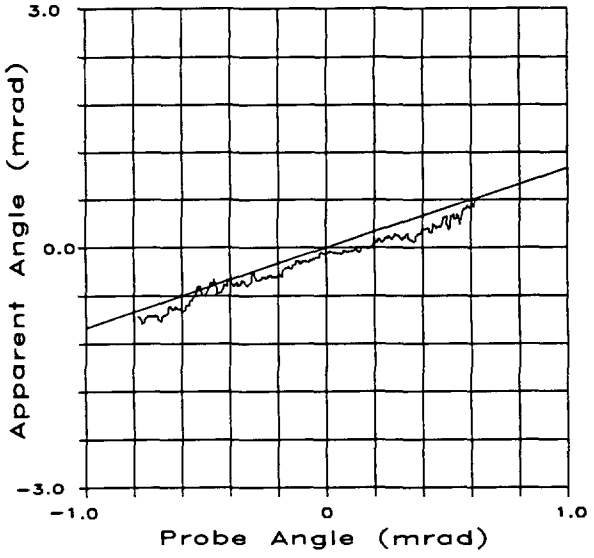


(d) Apparent Angle vs Probe Angle

Figure A-7. Trial 53, 1.8 km.

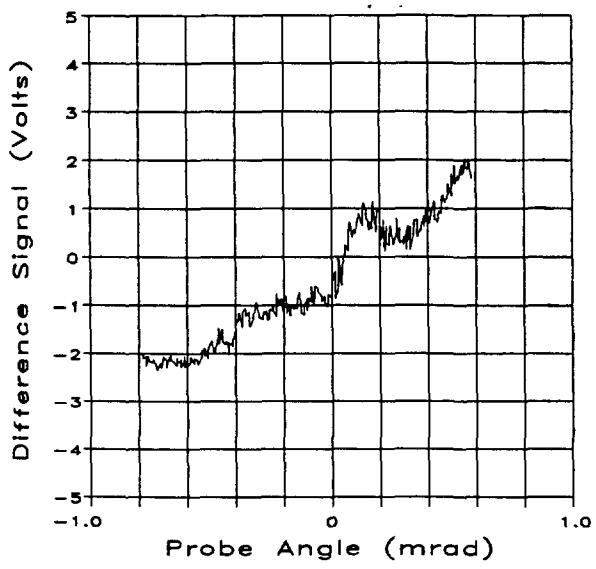


(a) Difference vs Probe Angle

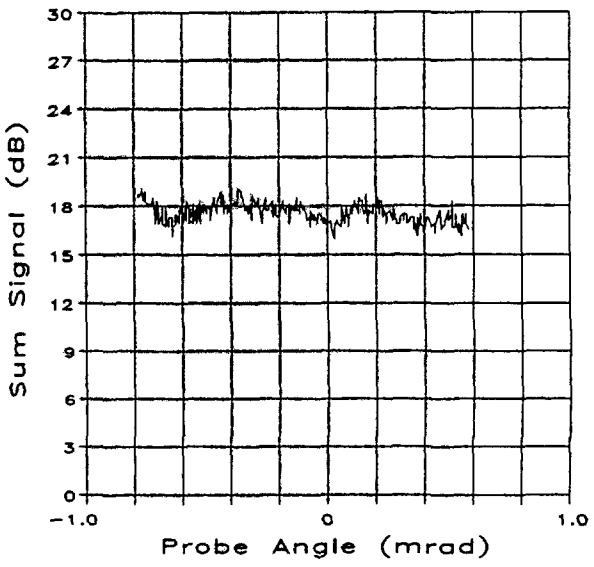


(b) Sum Signal vs Probe Angle

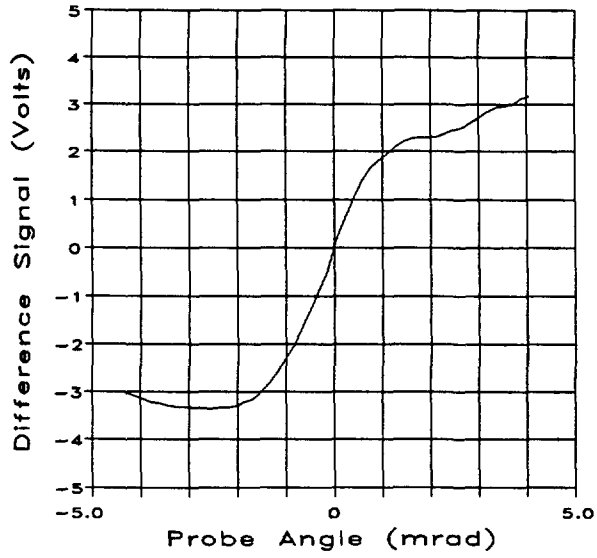


(c) Calibration Diff. vs Probe Angle

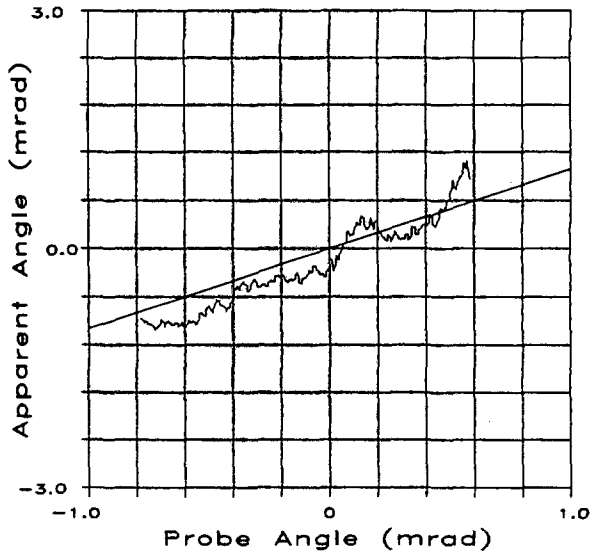


(d) Apparent Angle vs Probe Angle

Figure A-8. Trial 54, 1.8 km.

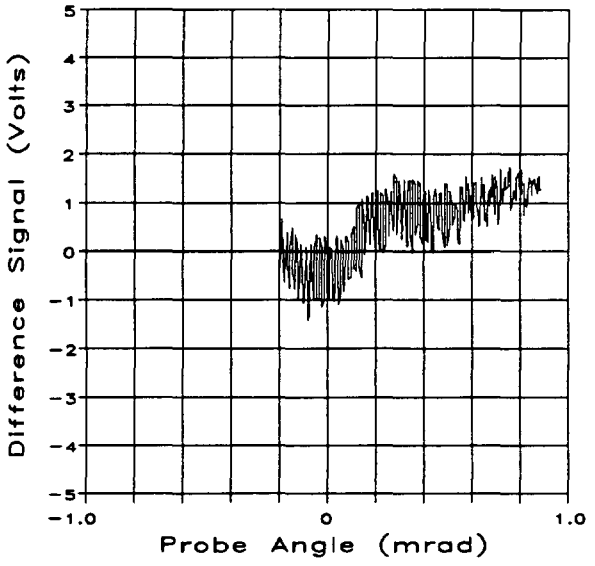


(a) Difference vs Probe Angle

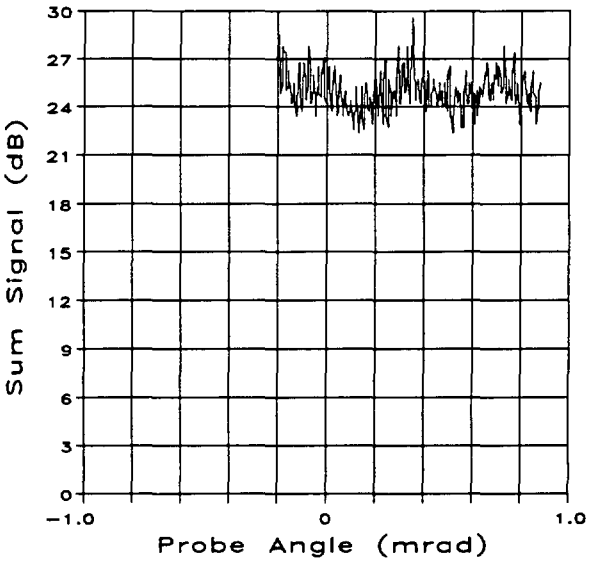


(b) Sum Signal vs Probe Angle

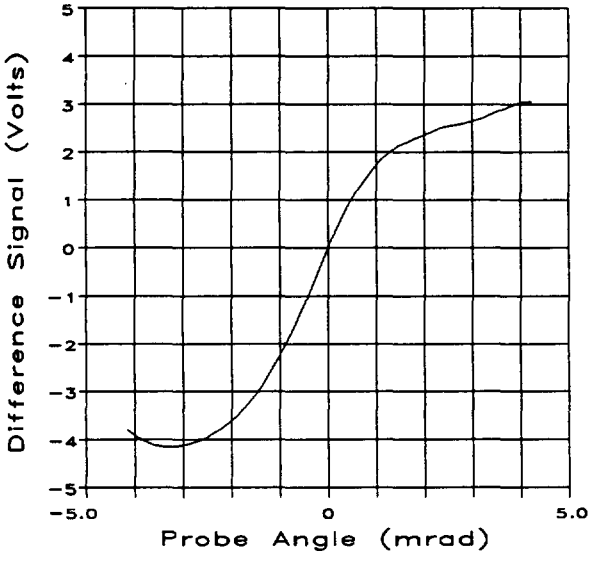


(c) Calibration Diff. vs Probe Angle

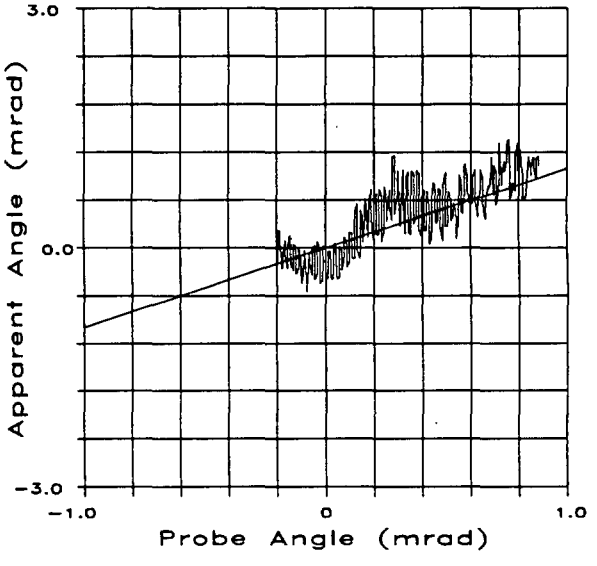


(d) Apparent Angle vs Probe Angle

Figure A-9. Trial 3, 2.8 km.

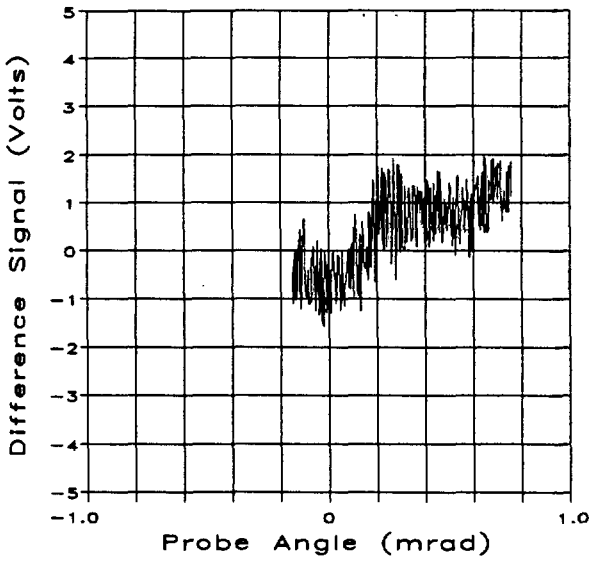


(a) Difference vs Probe Angle

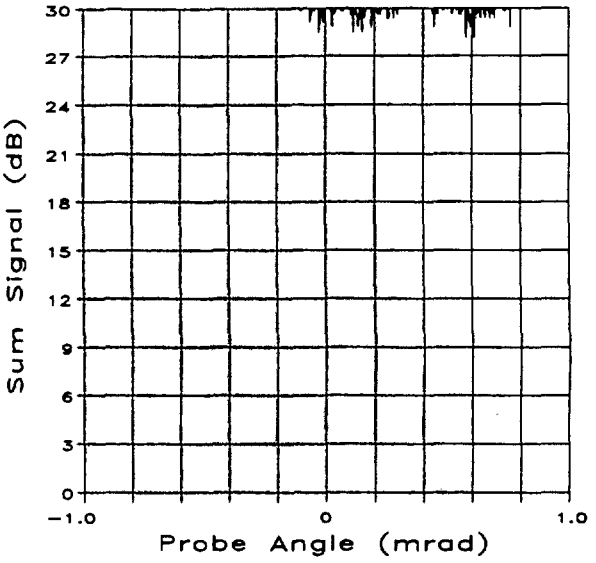


(b) Sum Signal vs Probe Angle

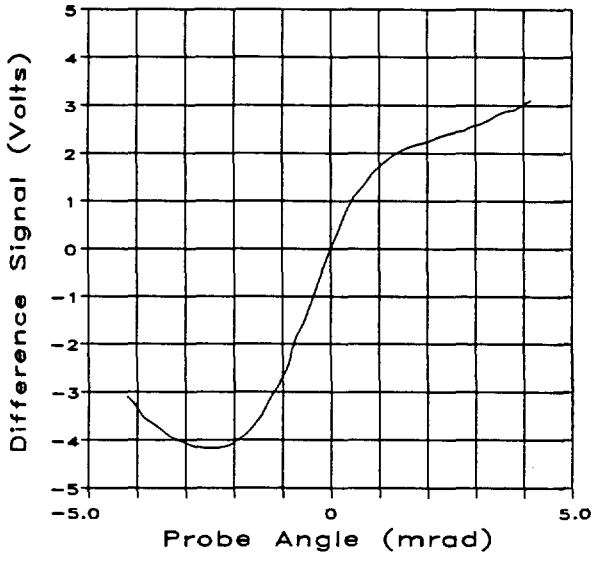


(c) Calibration Diff. vs Probe Angle

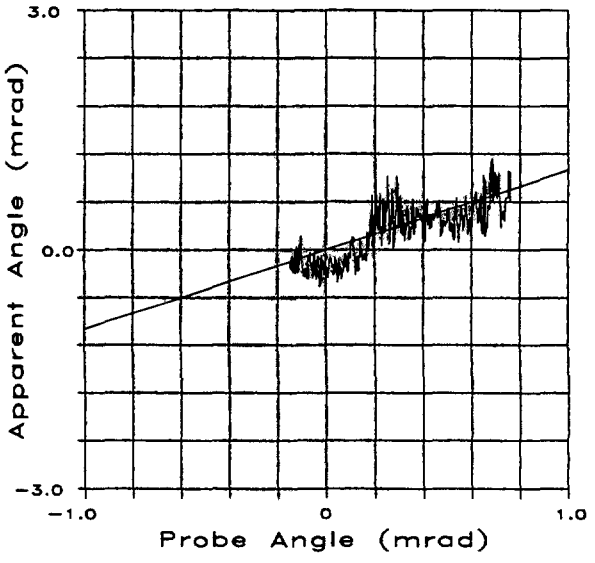


(d) Apparent Angle vs Probe Angle

Figure A-10. Trial 6, 2.8 km.

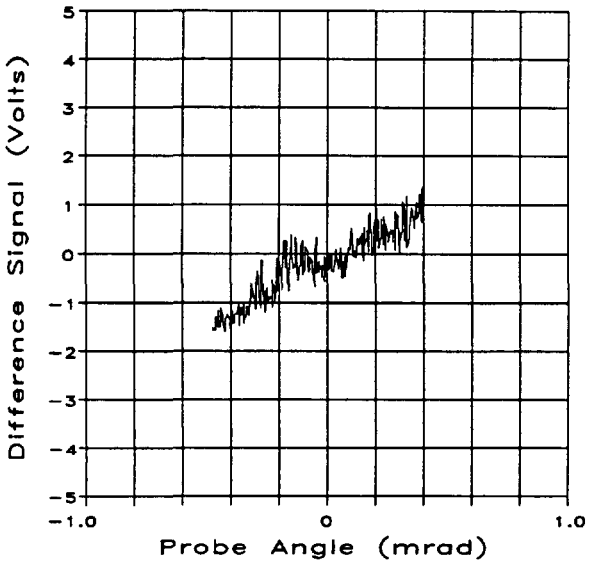


(a) Difference vs Probe Angle

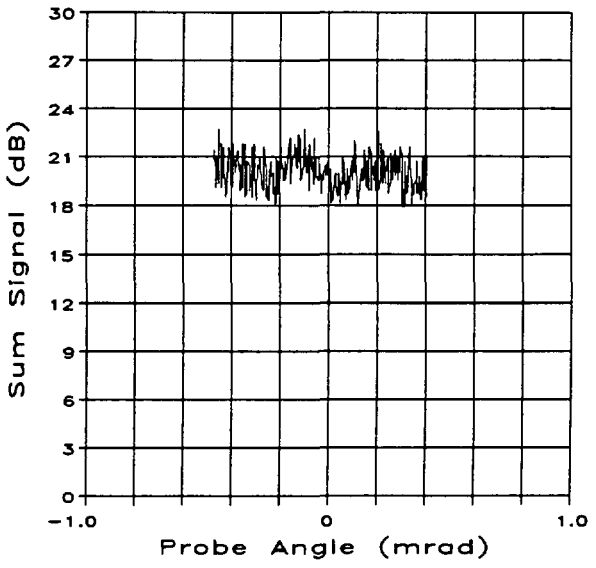


(b) Sum Signal vs Probe Angle

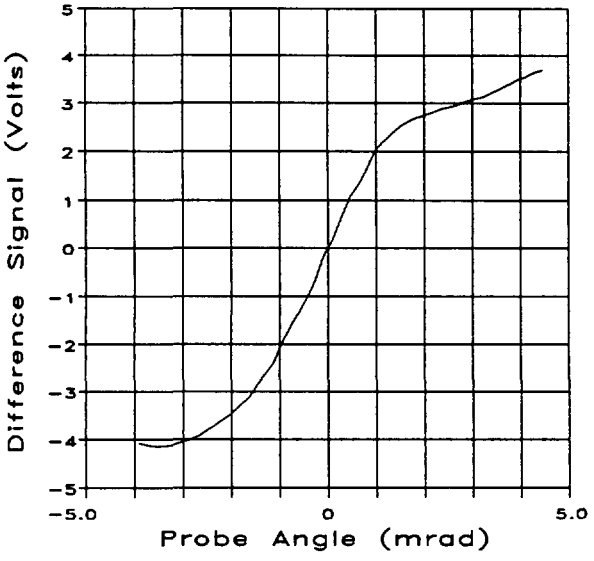


(c) Calibration Diff. vs Probe Angle

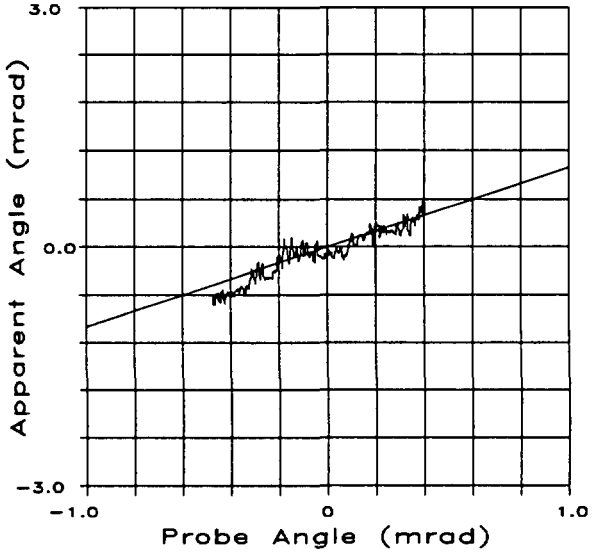


(d) Apparent Angle vs Probe Angle

Figure A-11. Trial 32, 2.8 km.

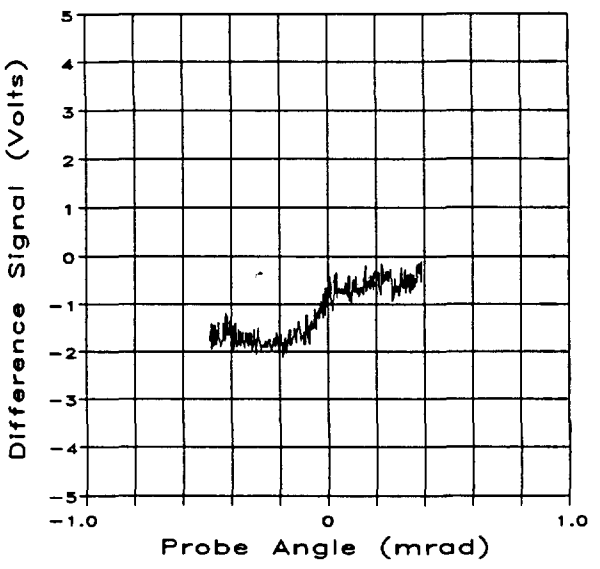


(a) Difference vs Probe Angle

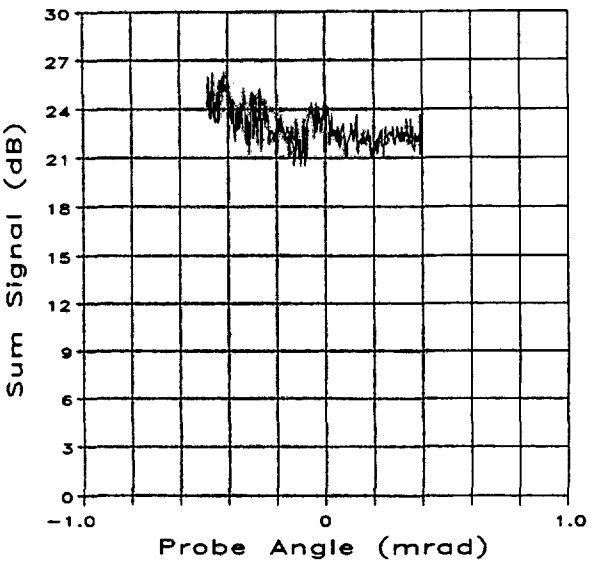


(b) Sum Signal vs Probe Angle

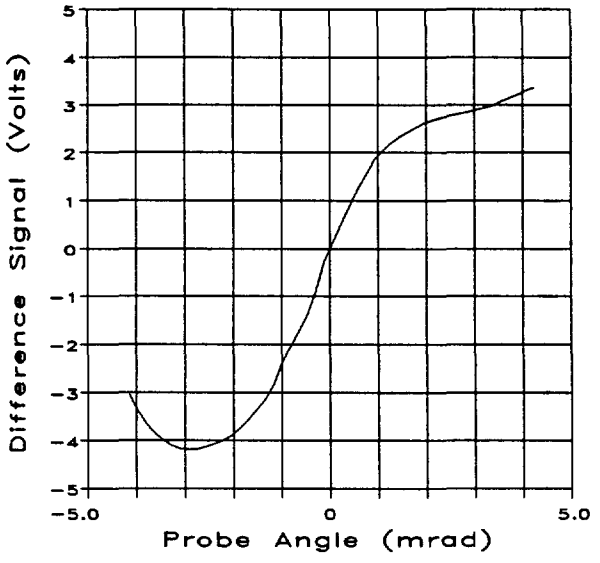


(c) Calibration Diff. vs Probe Angle

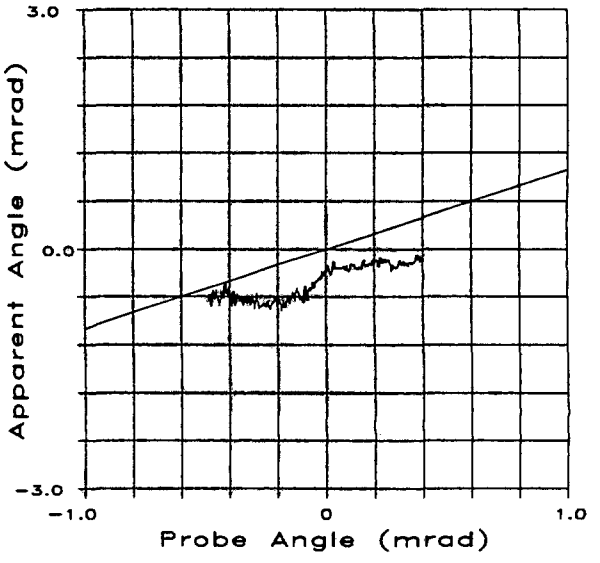


(d) Apparent Angle vs Probe Angle

Figure A-12. Trial 36, 2.8 km.

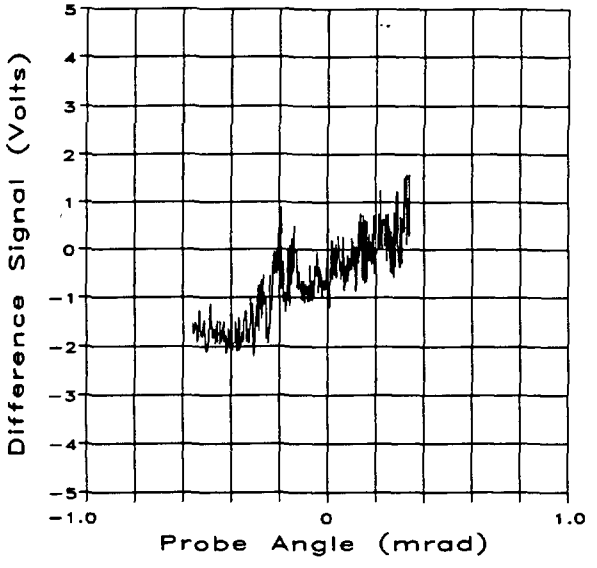


(a) Difference vs Probe Angle

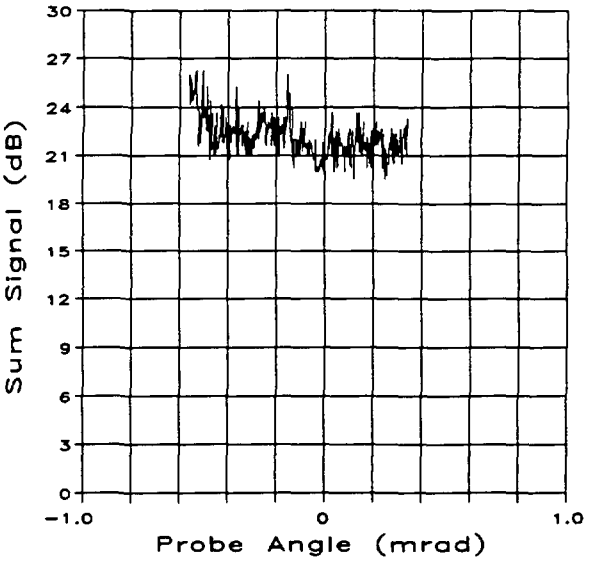


(b) Sum Signal vs Probe Angle

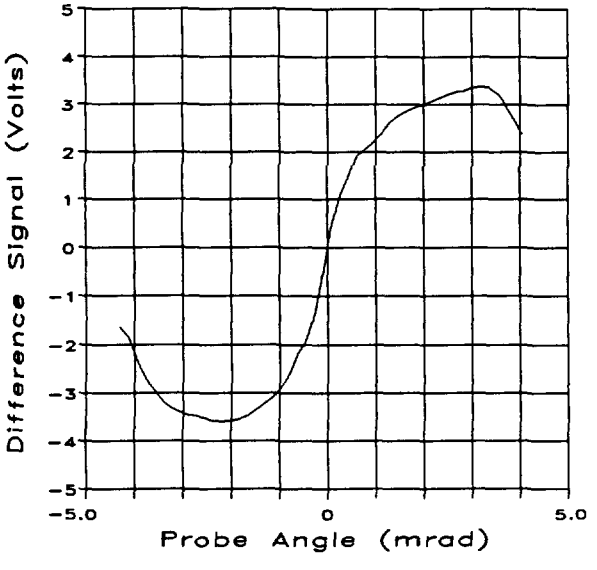


(c) Calibration Diff. vs Probe Angle

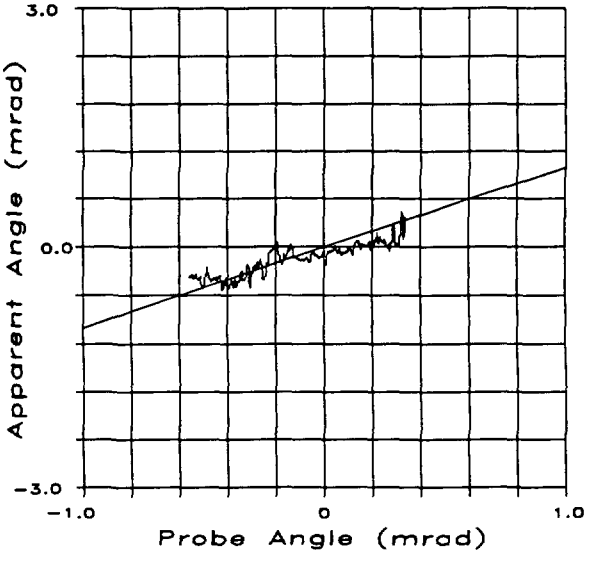


(d) Apparent Angle vs Probe Angle

Figure A-13. Trial 44, 2.8 km.

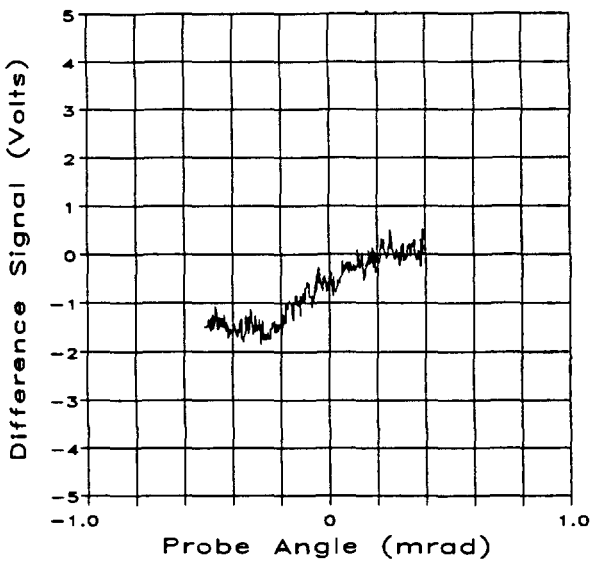


(a) Difference vs Probe Angle

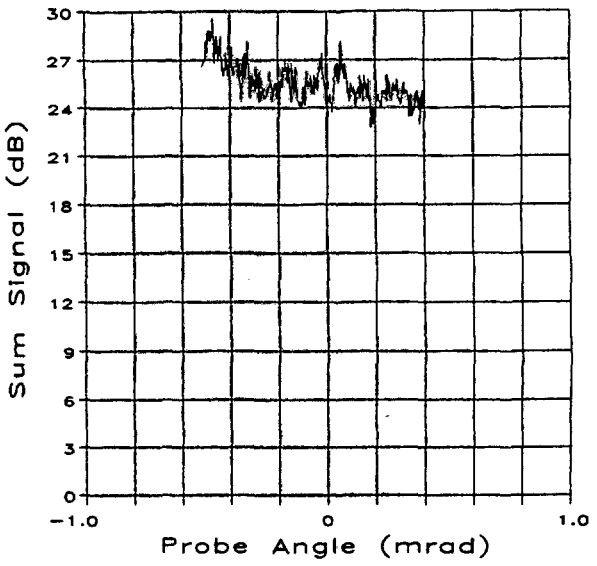


(b) Sum Signal vs Probe Angle

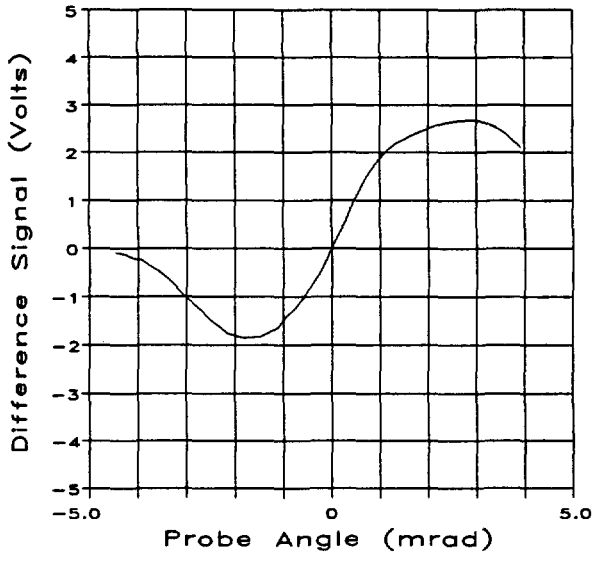


(c) Calibration Diff. vs Probe Angle

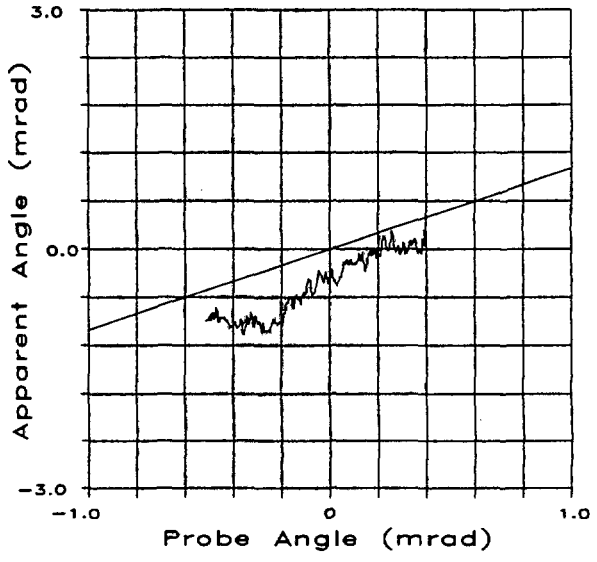


(d) Apparent Angle vs Probe Angle

Figure A-14. Trial 47, 2.8 km.

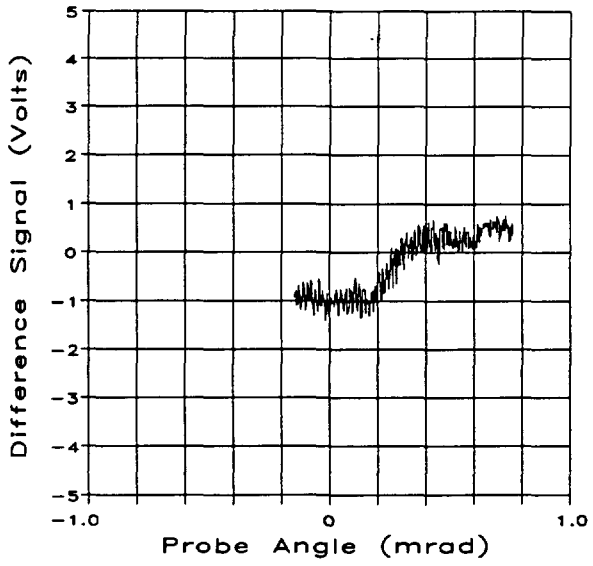


(a) Difference vs Probe Angle

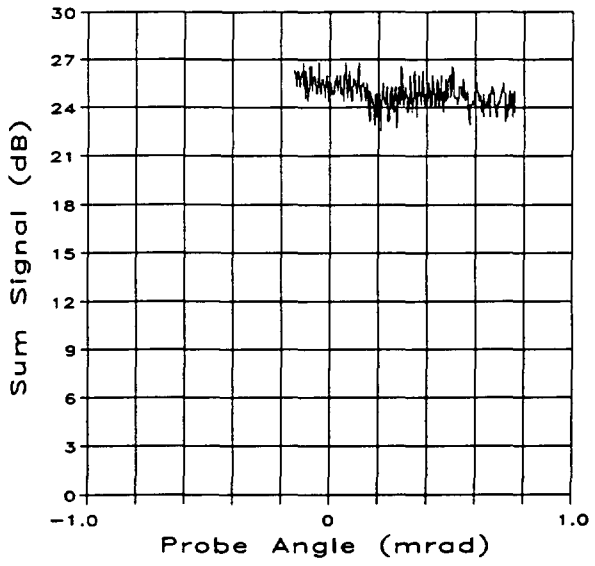


(b) Sum Signal vs Probe Angle

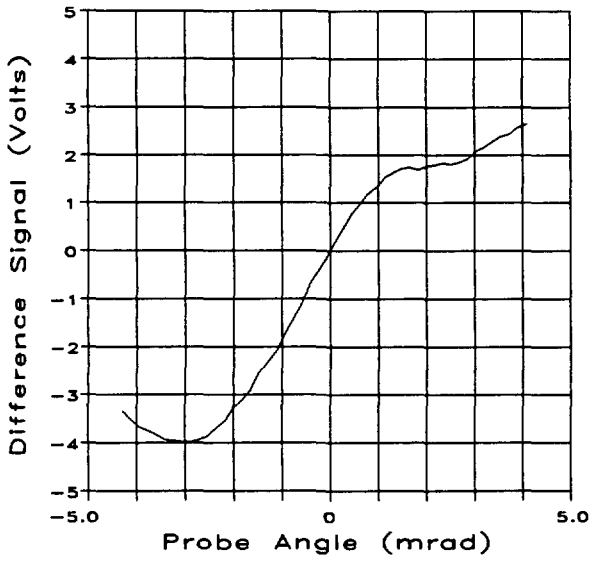


(c) Calibration Diff. vs Probe Angle

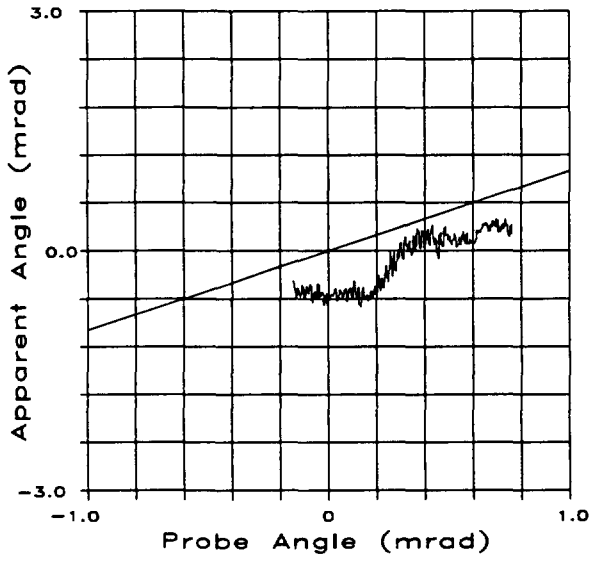


(d) Apparent Angle vs Probe Angle

Figure A-15. Trial 11, 2.8 km.

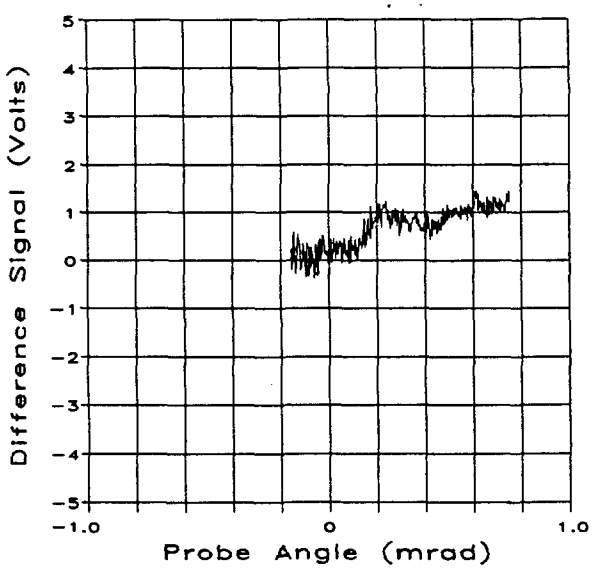


(a) Difference vs Probe Angle

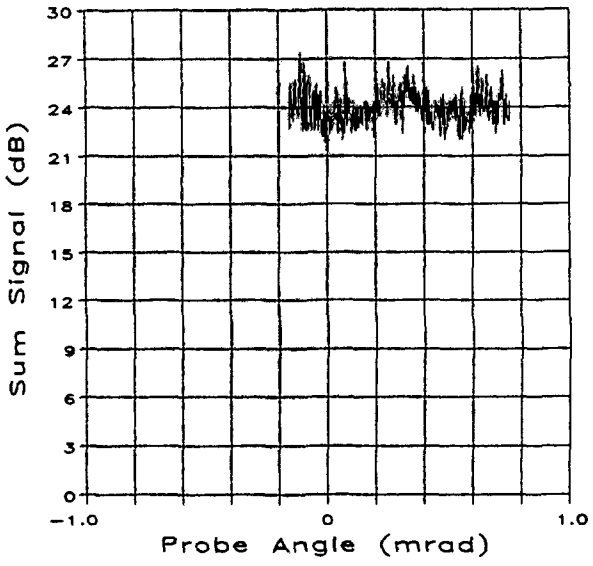


(b) Sum Signal vs Probe Angle

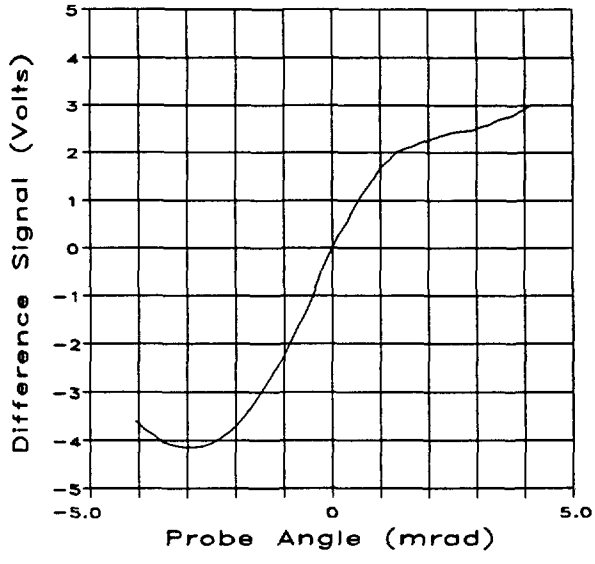


(c) Calibration Diff. vs Probe Angle

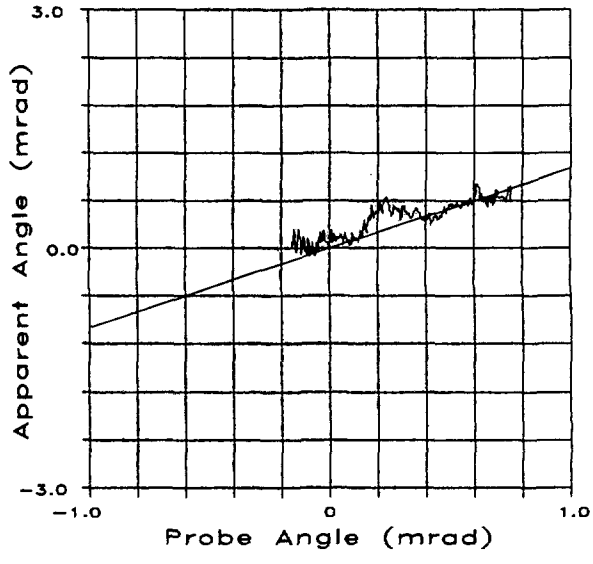


(d) Apparent Angle vs Probe Angle

Figure A-16. Trial 14, 2.8 km.

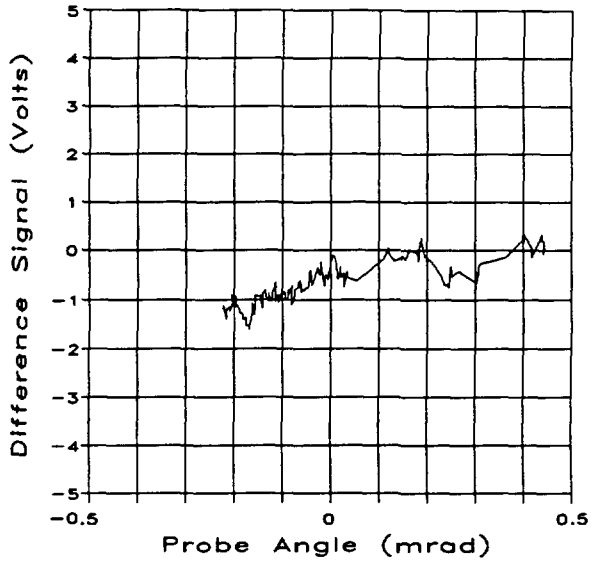


(a) Difference vs Probe Angle

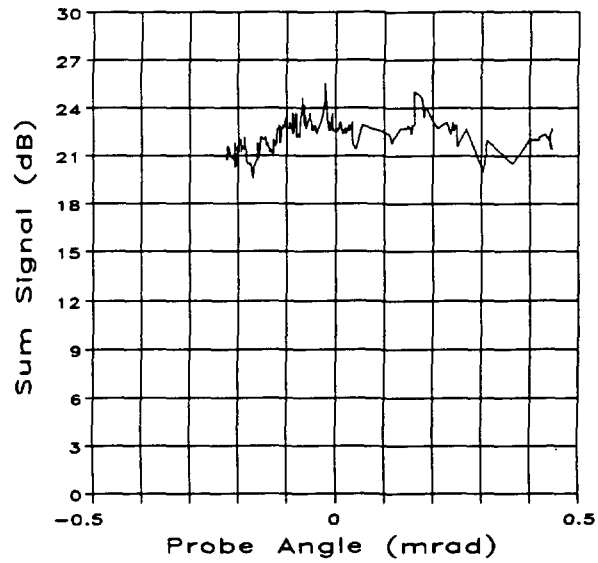


(b) Sum Signal vs Probe Angle

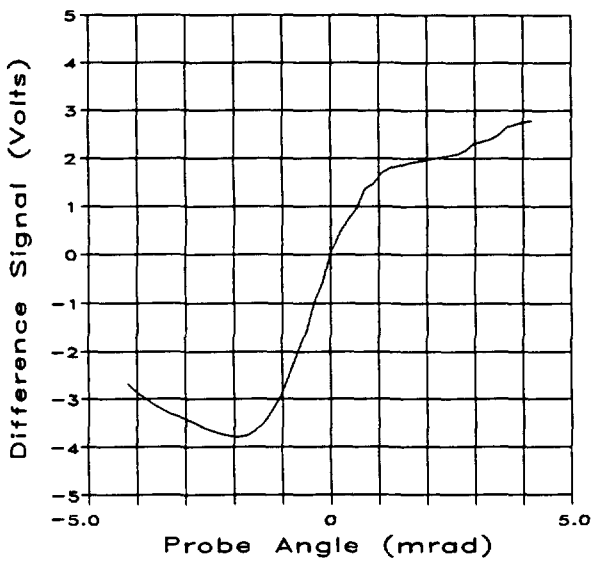


(c) Calibration Diff. vs Probe Angle

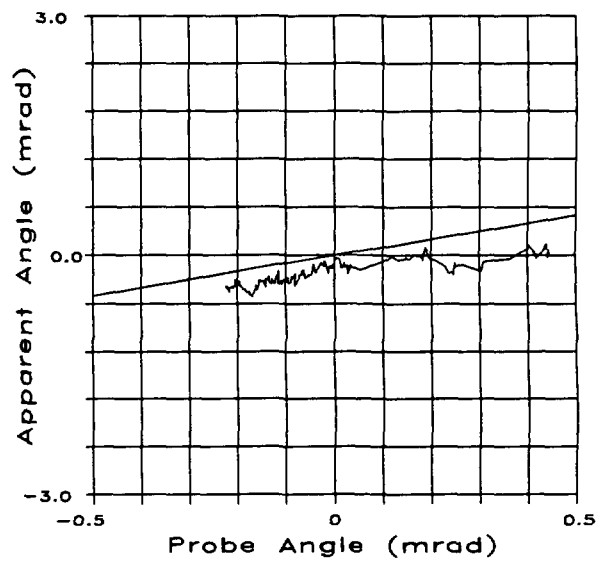


(d) Apparent Angle vs Probe Angle

Figure A-17. Trial 39, 3.8 km.

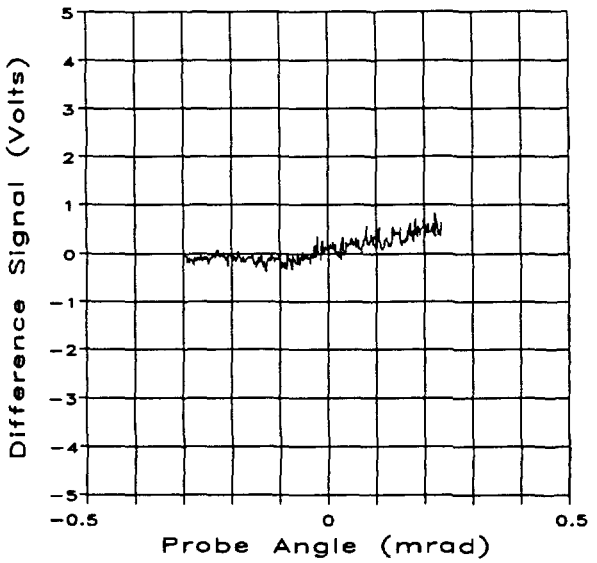


(a) Difference vs Probe Angle

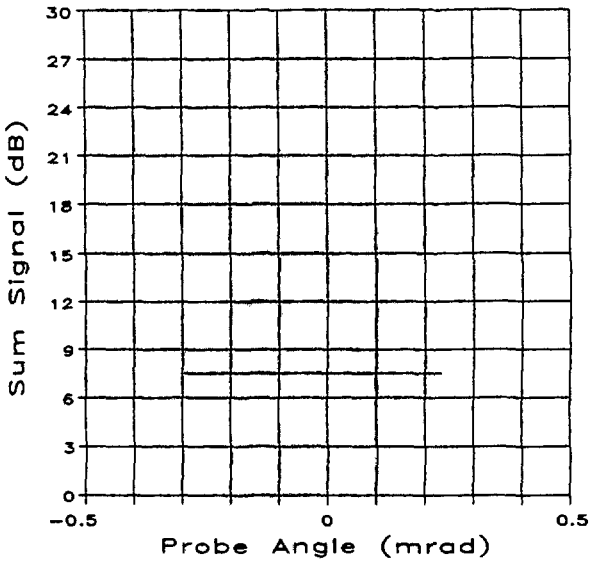


(b) Sum Signal vs Probe Angle

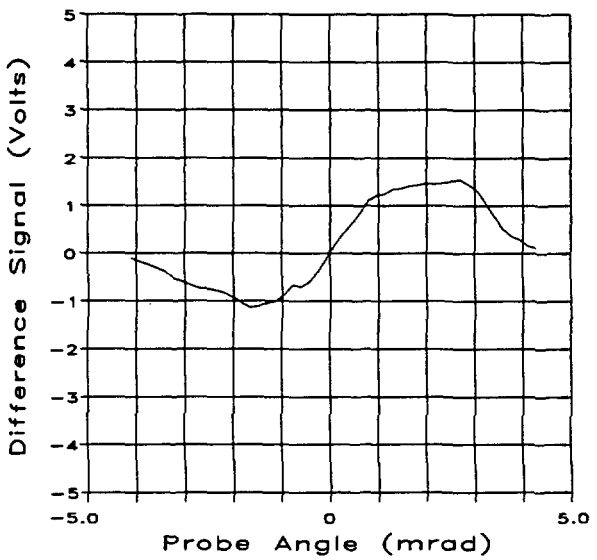


(c) Calibration Diff. vs Probe Angle

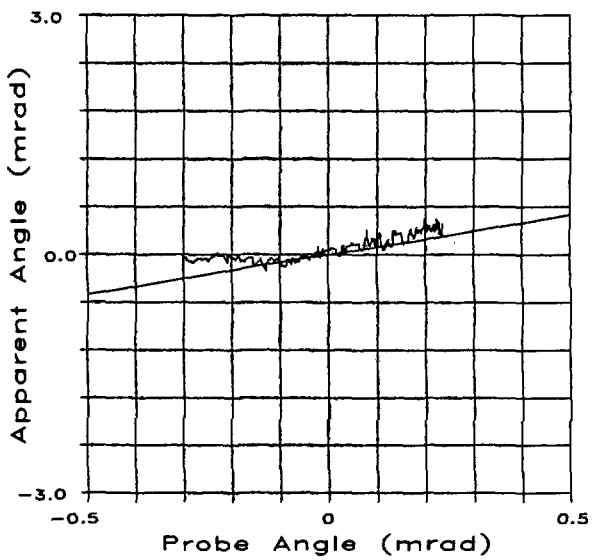


(d) Apparent Angle vs Probe Angle

Figure A-18. Trial 42, 4.8 km.

# APPENDIX B:

# NOISE MEASUREMENTS

INTENTIONALLY LEFT BLANK.

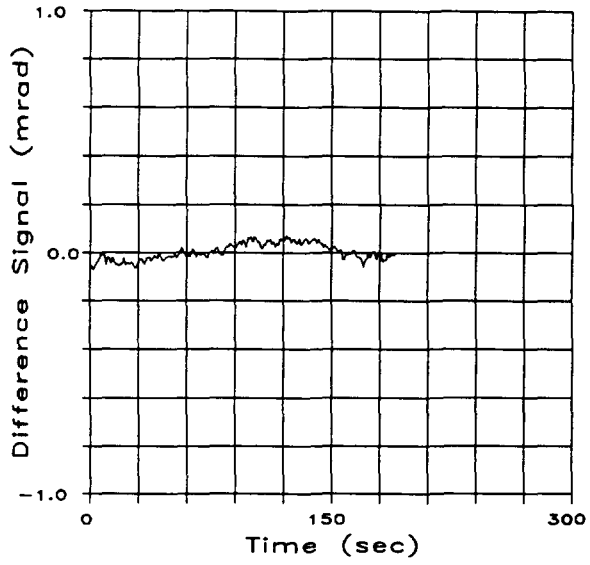


TR5, 11Sep91, 0850 hours

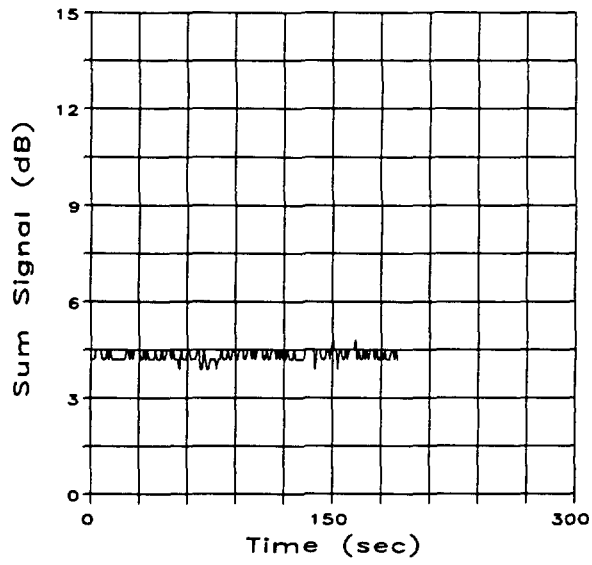


TR5, 11Sep91, 0850 hours

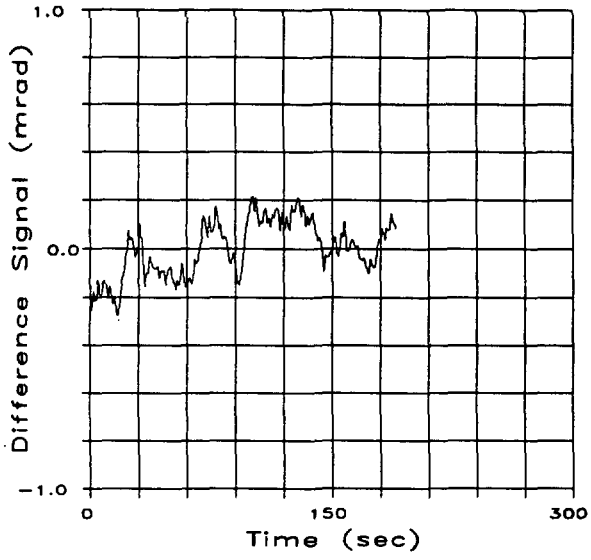


TR4, 11Sep91, 0830 hours

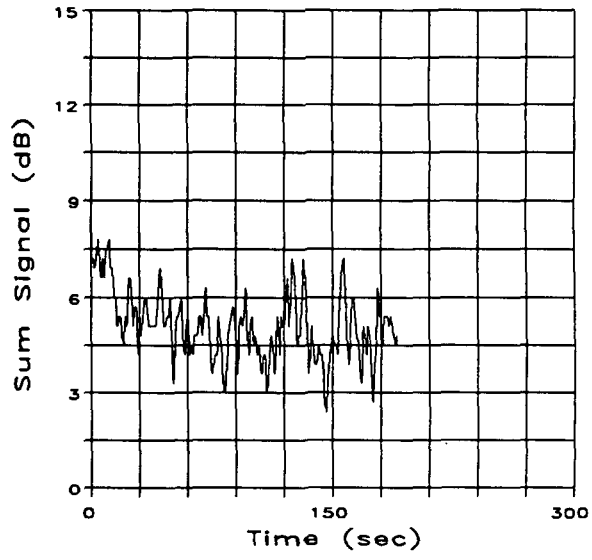


TR4, 11Sep91, 0830 hours

Figure B-1. Noise measurement at 0.4 km and 3 km, Trials 5 and 4.

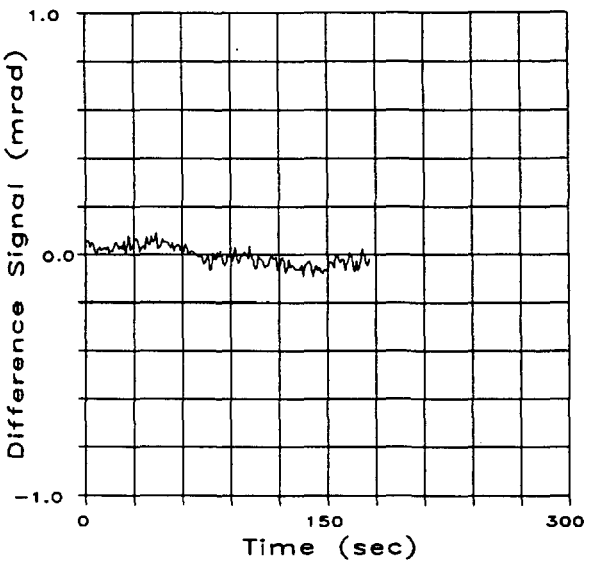


TR8, 11Sep91, 1445 hours

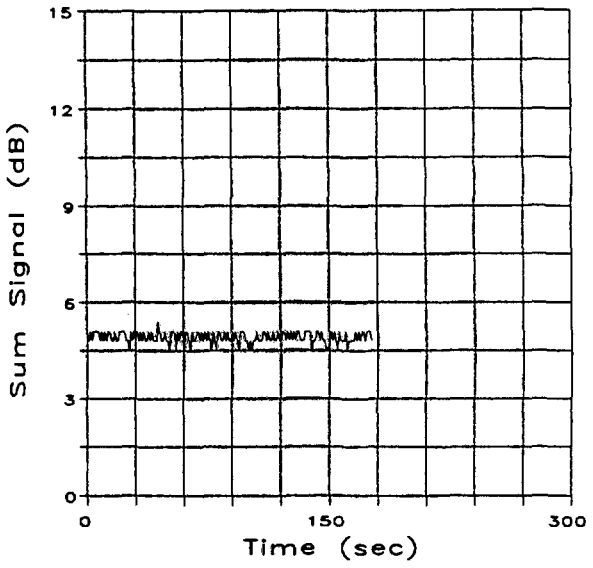


TR8, 11Sep91, 1445 hours

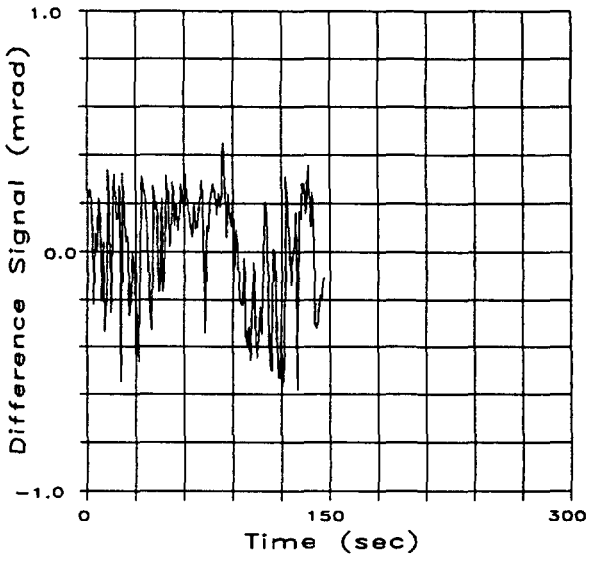


TR7, 11Sep91, 1400 hours

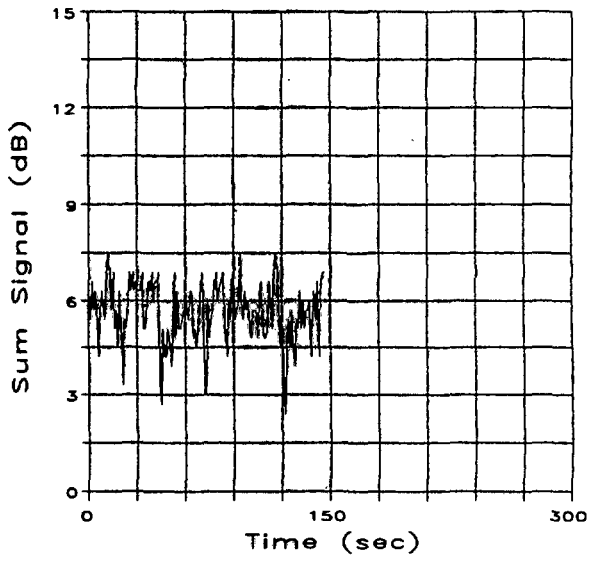


TR7, 11Sep91, 1400 hours

Figure B-2. Noise measurement at 0.4 km and 3 km, Trials 8 and 7.

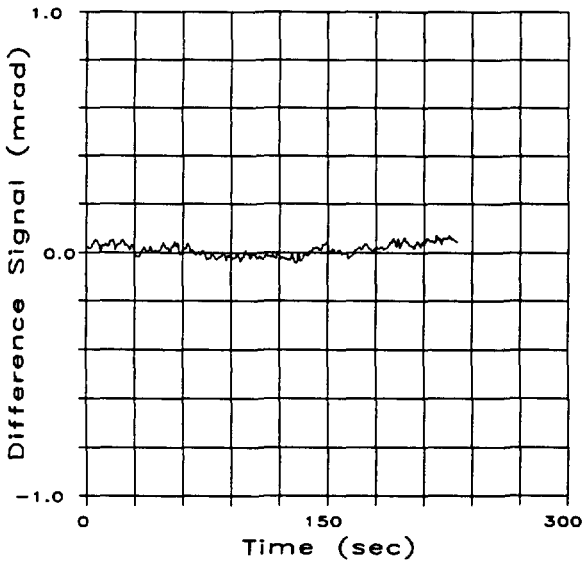


TR9, 12Sep91, 0817 hours

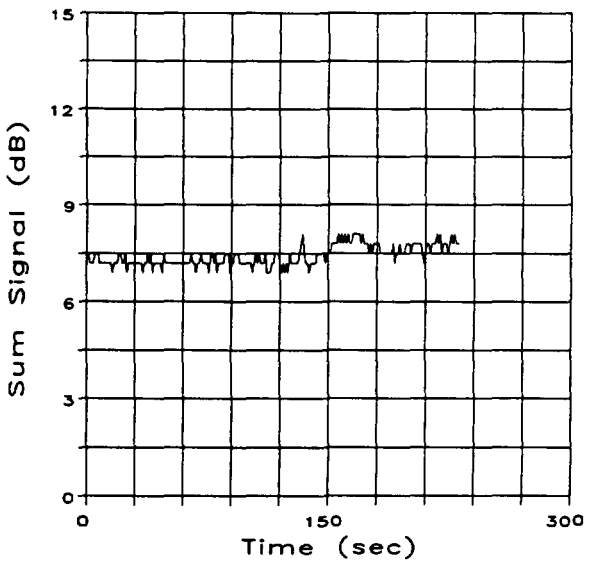


TR9, 12Sep91, 0817 hours

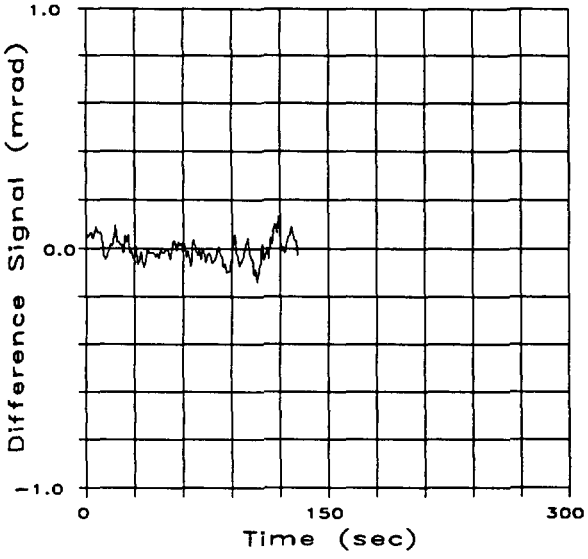


TR10, 12Sep91, 0830 hours

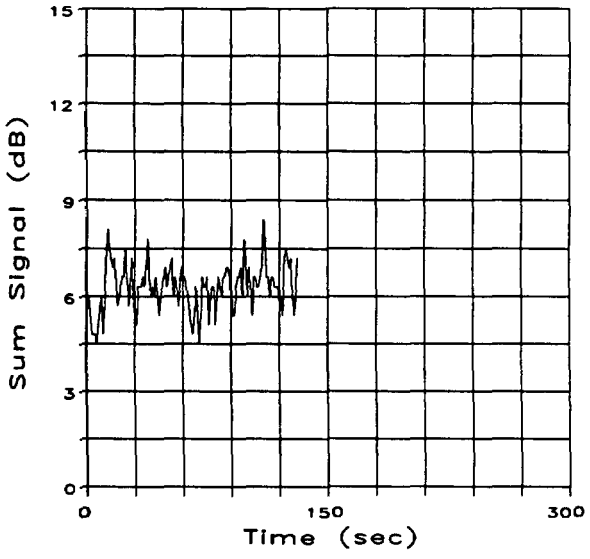


TR10, 12Sep91, 0830 hours

Figure B-3. Noise measurement at 0.4 km and 3 km, Trials 9 and 10.

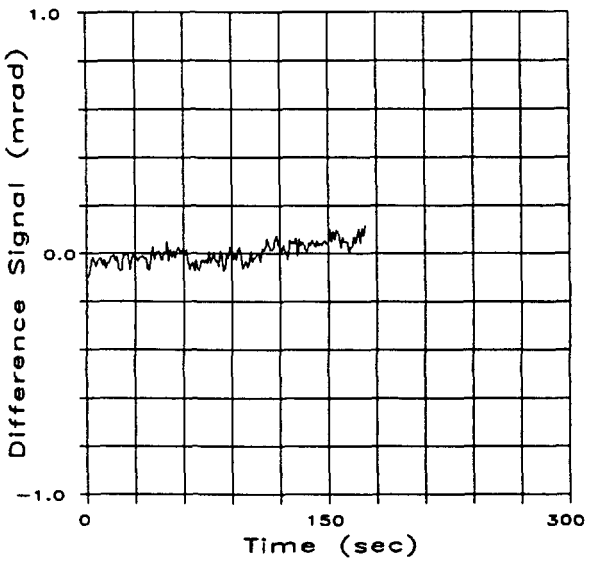


TR12, 12Sep91, 1207 hours

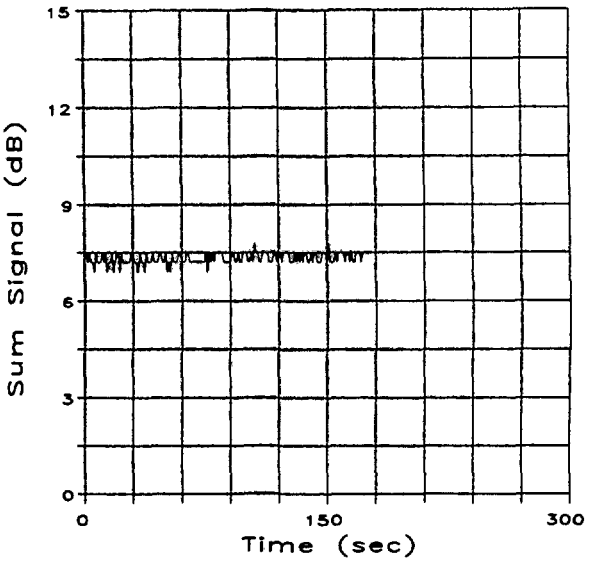


TR12, 12Sep91, 1207 hours

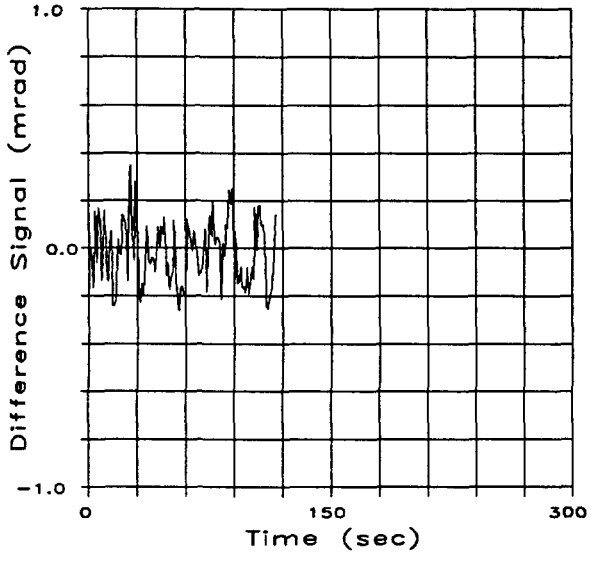


TR13, 12Sep91, 1220 hours

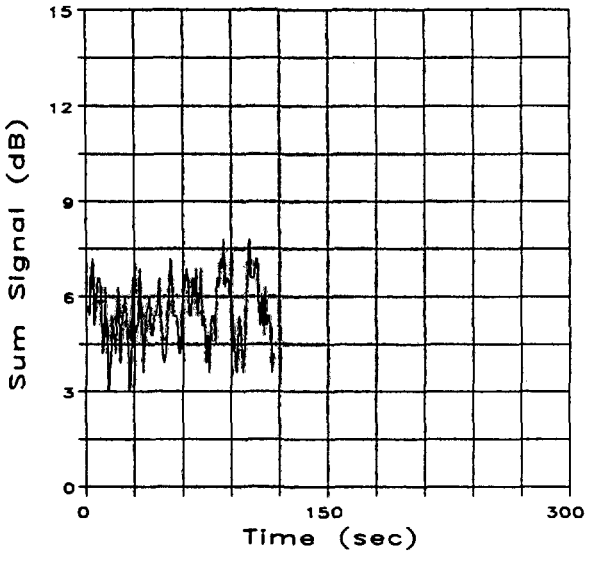


TR13, 12Sep91, 1220 hours

Figure B-4. Noise measurement at 0.4 km and 3 km, Trials 12 and 13.

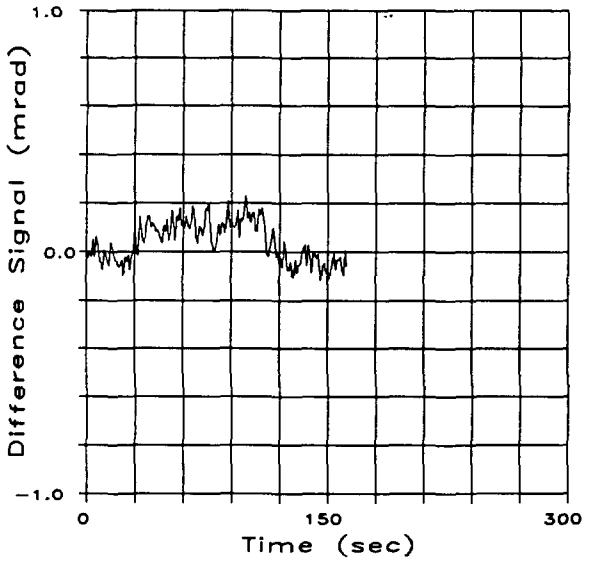


TR15, 12Sep91, 1425 hours

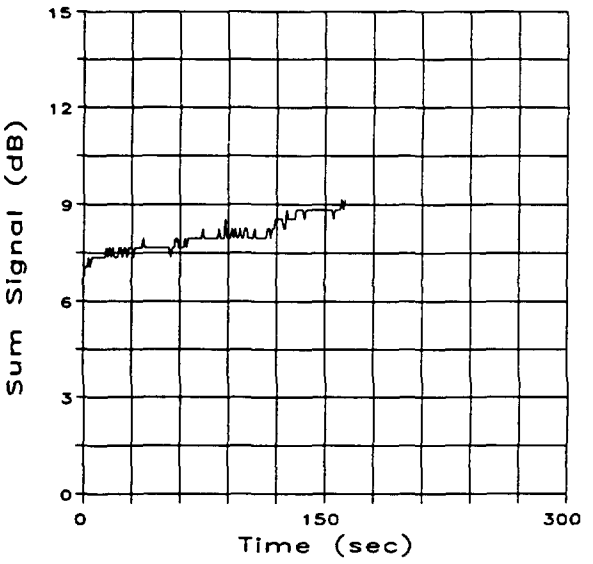


TR15, 12Sep91, 1425 hours

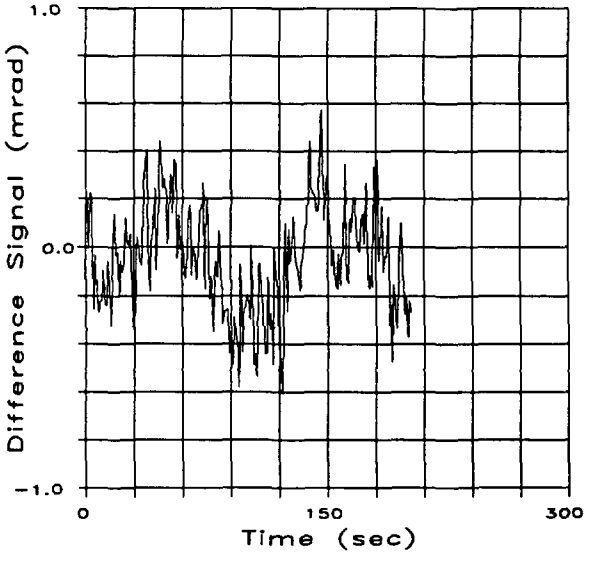


TR16, 12Sep91, 1430 hours

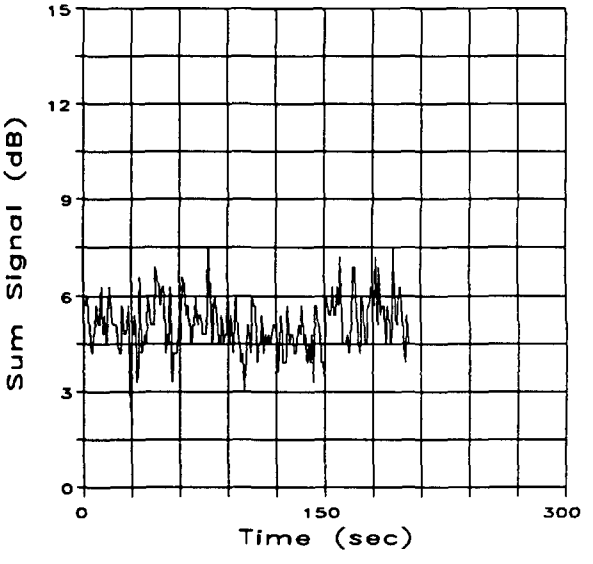


TR16, 12Sep91, 1430 hours

Figure B-5. Noise measurement at 0.4 km and 2 km, Trials 15 and 16.

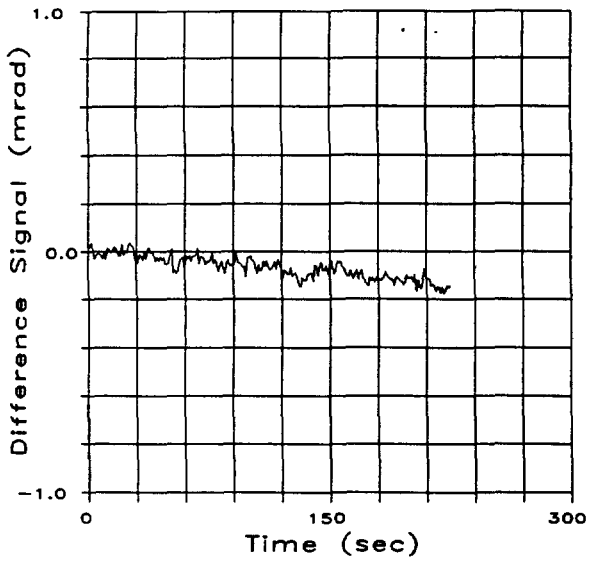


TR18, 13Sep91, 0828 hours

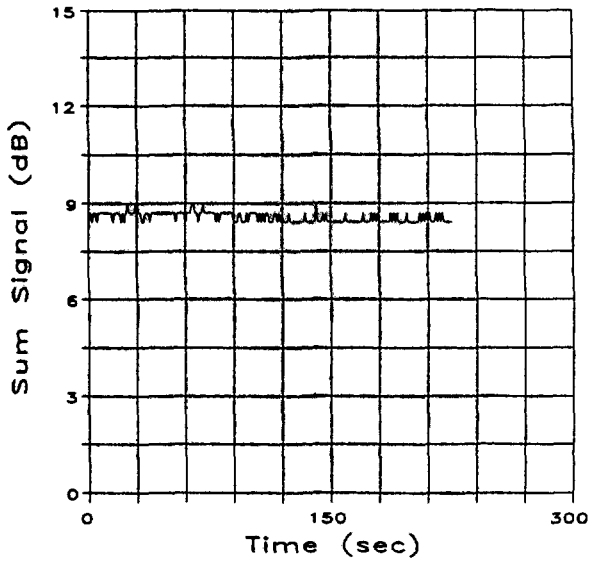


TR18, 13Sep91, 0828 hours

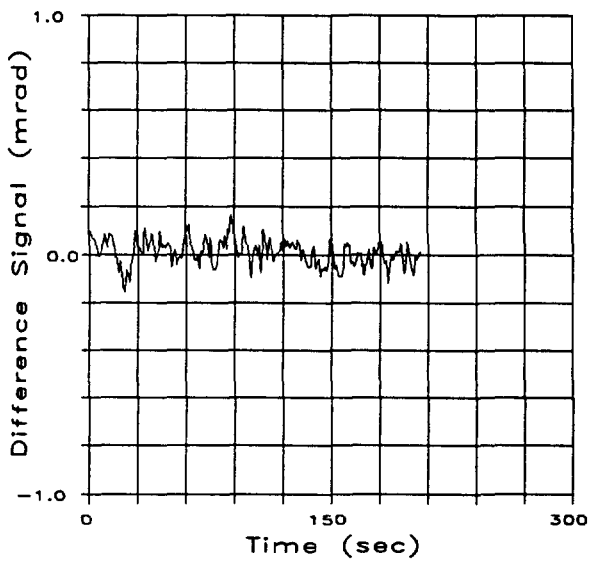


TR19, 13Sep91, 0840 hours

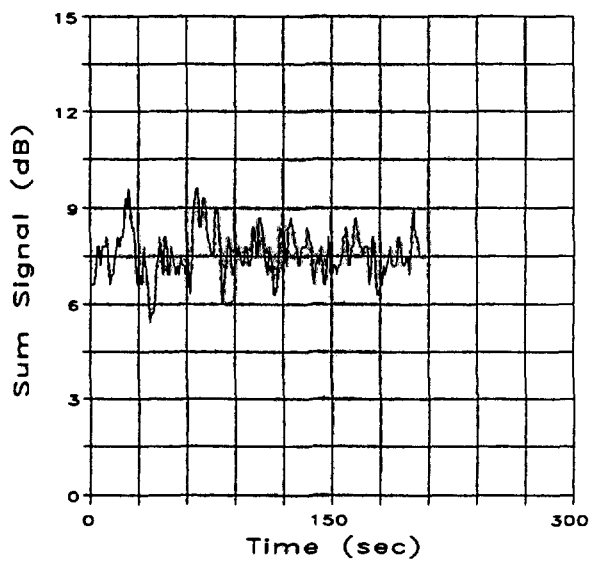


TR19, 13Sep91, 0840 hours

Figure B-6. Noise measurement at 0.4 km and 2 km, Trials 18 and 19.

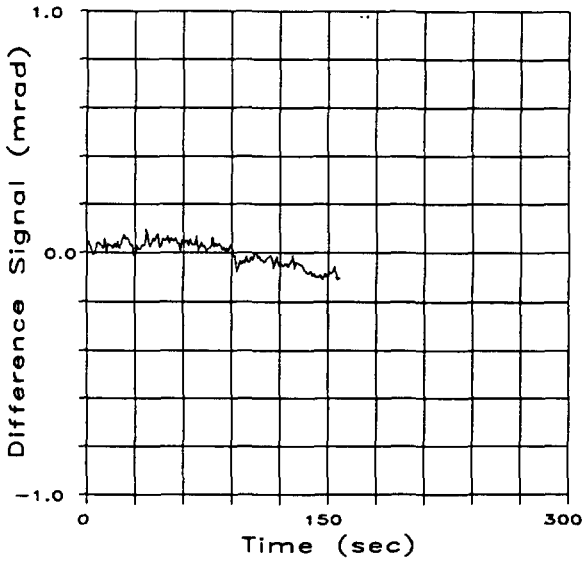


TR22, 13Sep91, 1054 hours

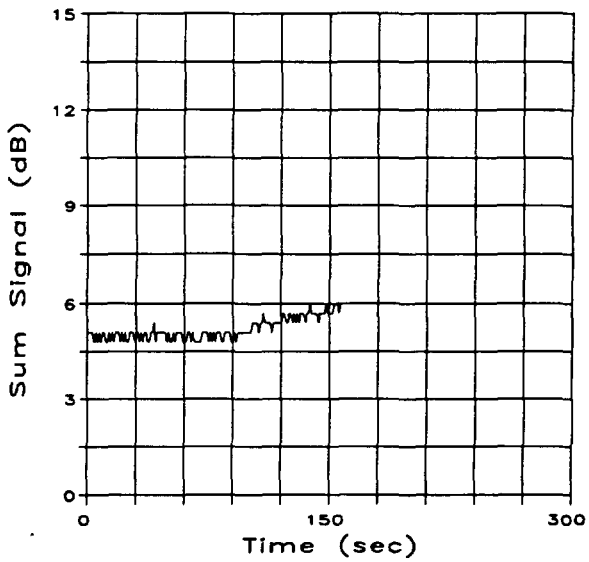


TR22, 13Sep91, 1054 hours

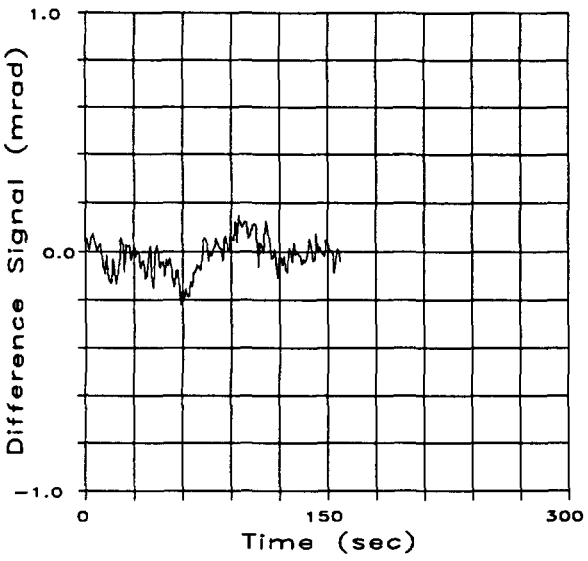


TR23, 13Sep91, 1110 hours

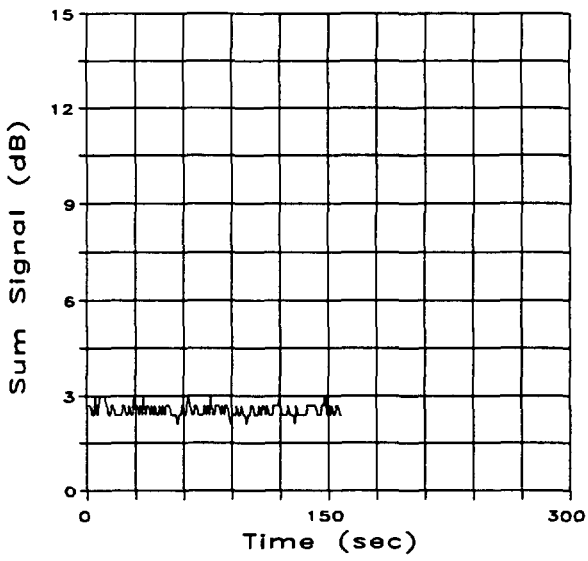


TR23, 13Sep91, 1110 hours

Figure B-7. Noise measurement at 0.4 km and 1 km, Trials 22 and 23.

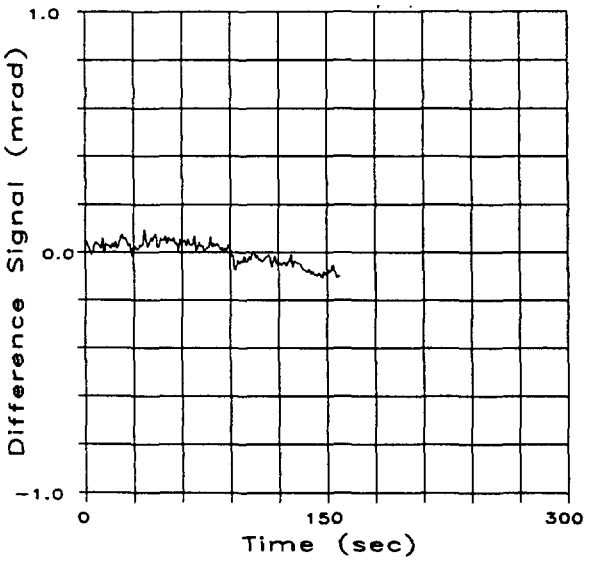


TR22, 13Sep91, 1054 hours

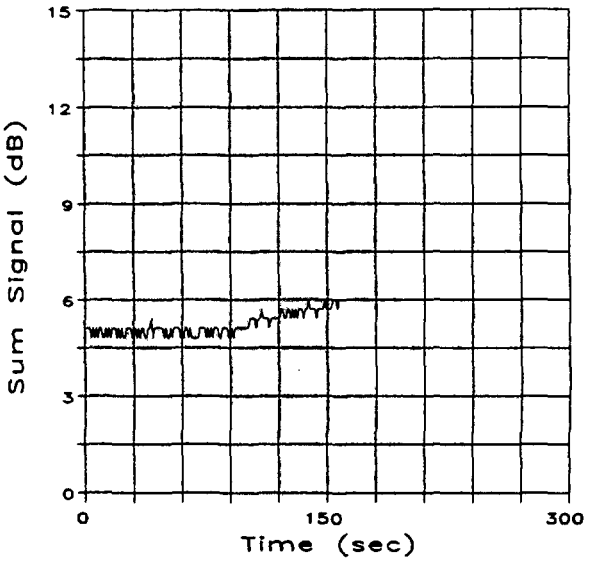


TR22, 13Sep91, 1054 hours

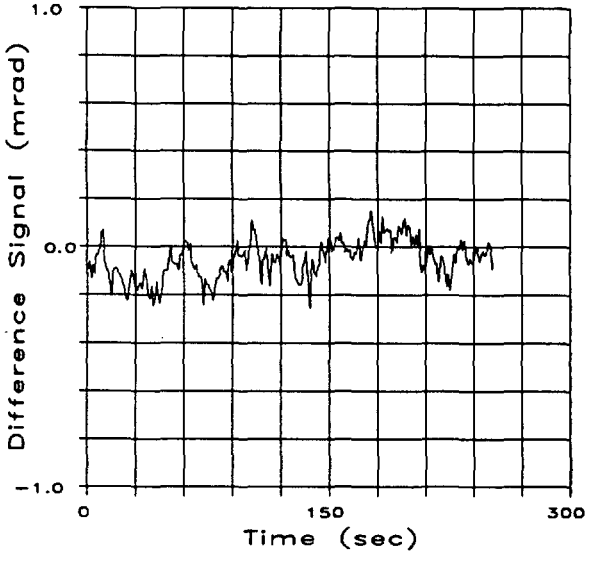


TR26, 13Sep91, 1505 hours

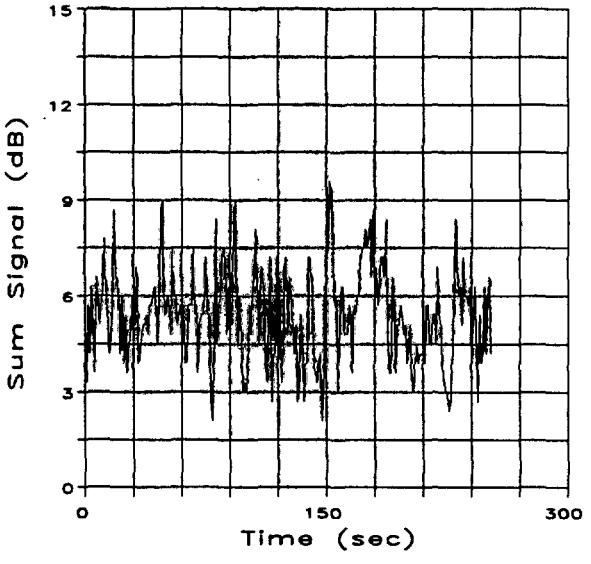


TR26, 13Sep91, 1505 hours

Figure B-8. Noise measurement at 0.4 km and 5 km, Trials 22 and 26.

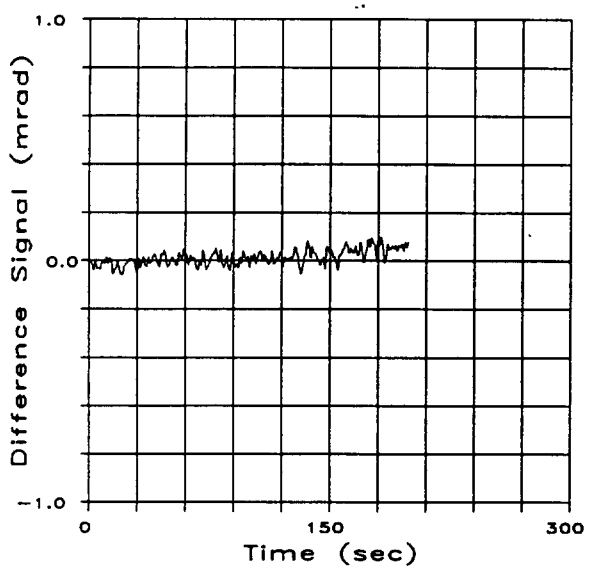


TR27, 16Sep91, 1129 hours

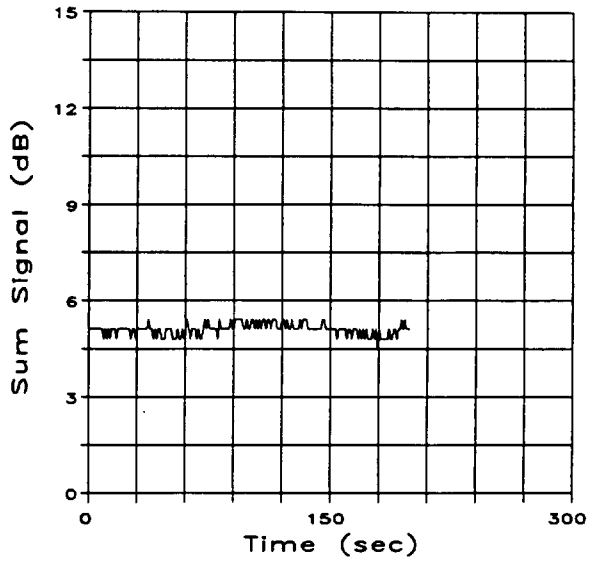


TR27, 16Sep91, 1129 hours

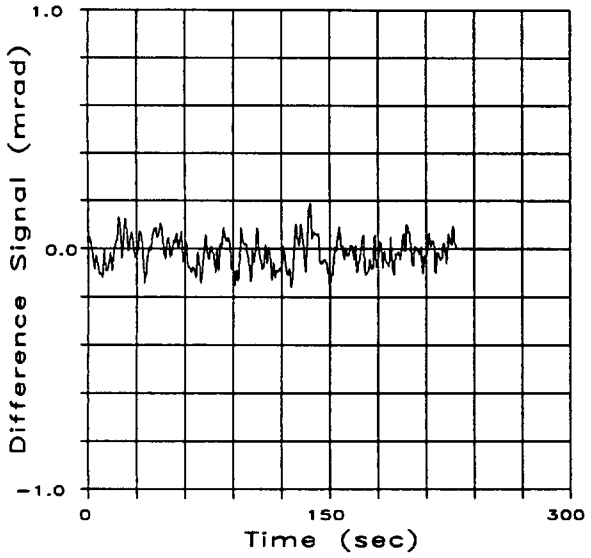


TR28, 16Sep91, 1142 hours

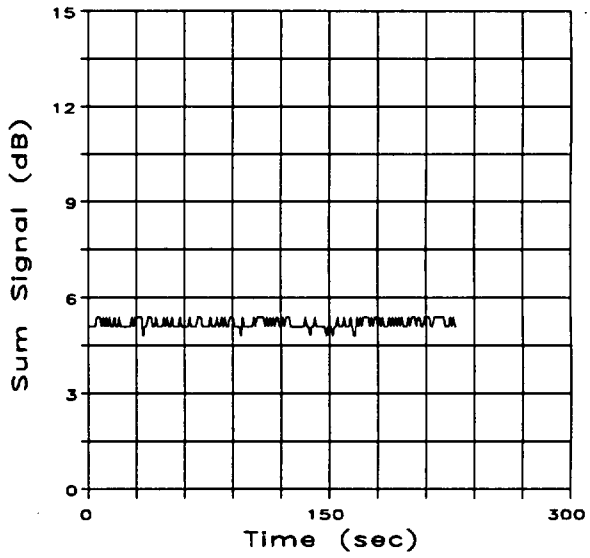


TR28, 16Sep91, 1142 hours

Figure B-9. Noise measurement at 0.4 km and 1 km, Trials 27 and 28.

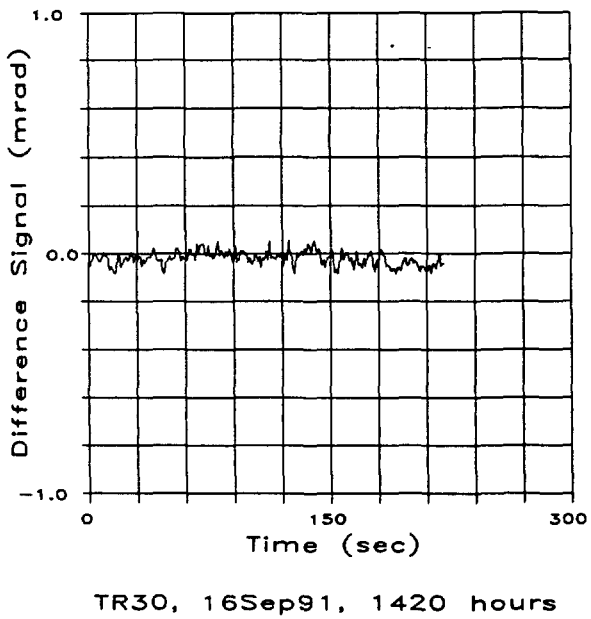


TR30, 16Sep91, 1420 hours

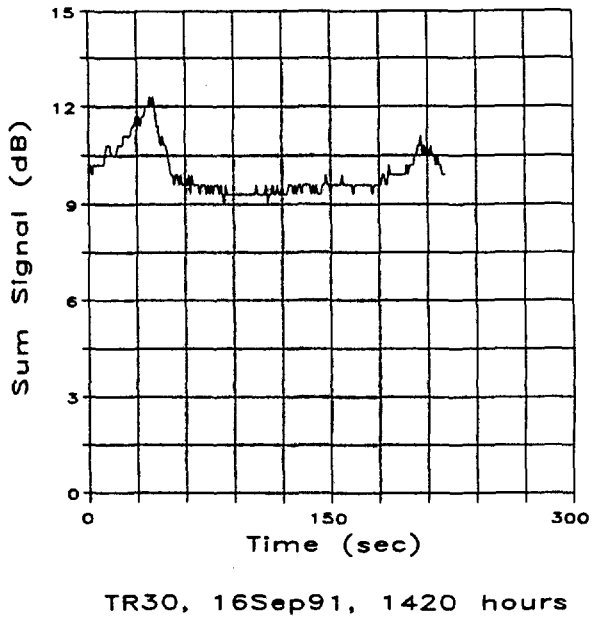


TR30, 16Sep91, 1420 hours

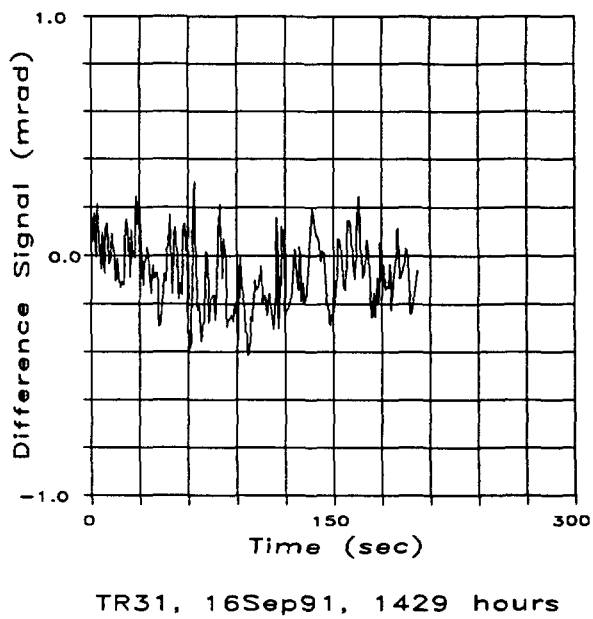


TR31, 16Sep91, 1429 hours

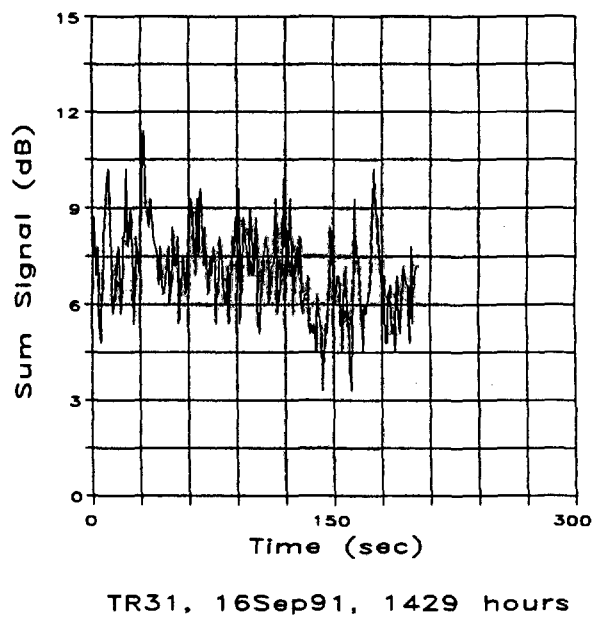


TR31, 16Sep91, 1429 hours

Figure B-10. Noise measurement at 0.4 km and 3 km, Trials 30 and 31.

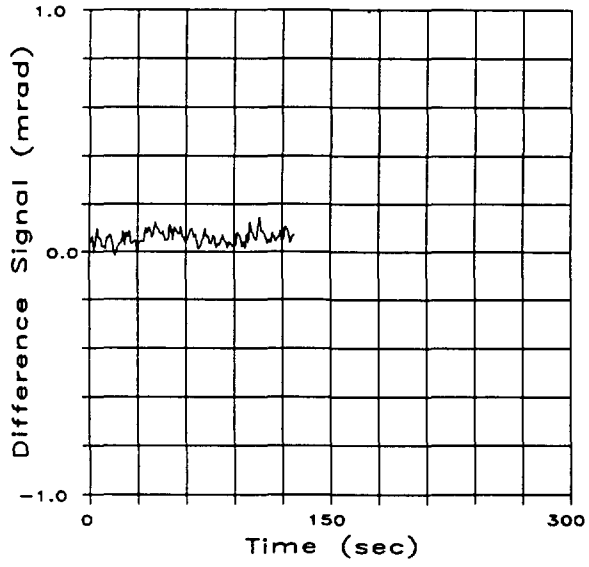


TR34, 17Sep91, 0843 hours

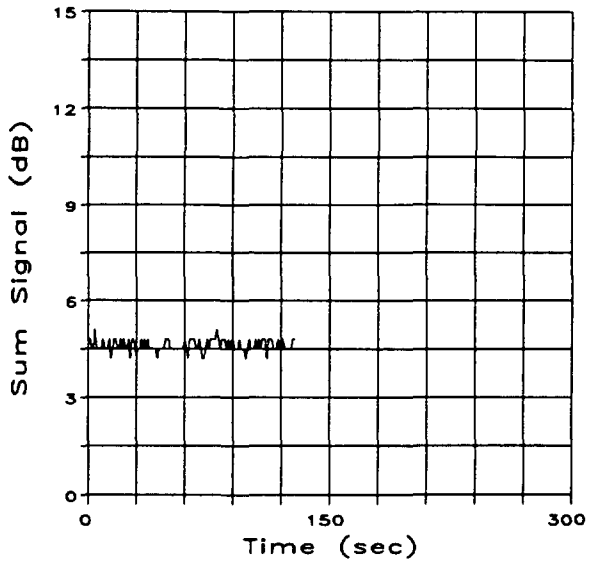


TR34, 17Sep91, 0843 hours

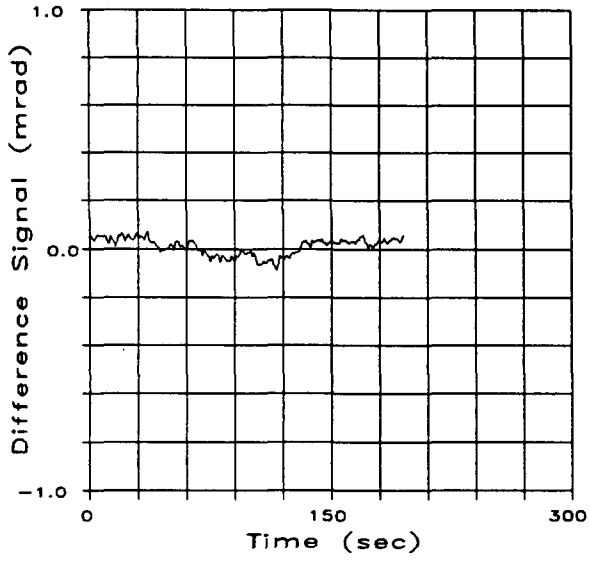


TR33, 17Sep91, 0710 hours

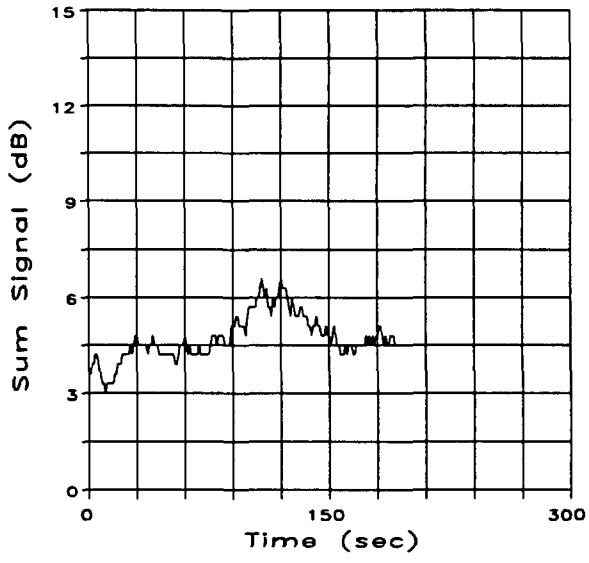


TR33, 17Sep91, 0710 hours

Figure B-11. Noise measurement at 0.4 km and 3 km, Trials 34 and 33.

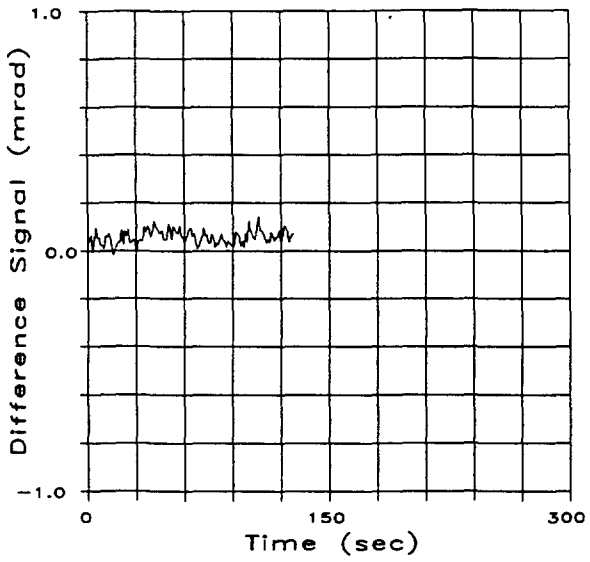


TR34, 17Sep91, 0843 hours

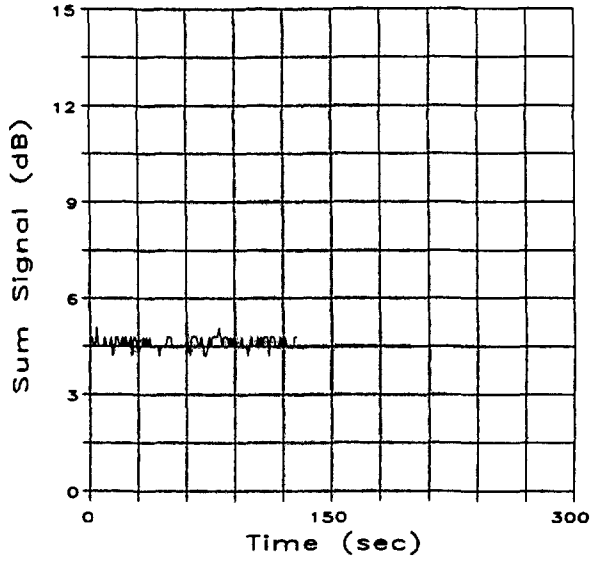


TR34, 17Sep91, 0843 hours

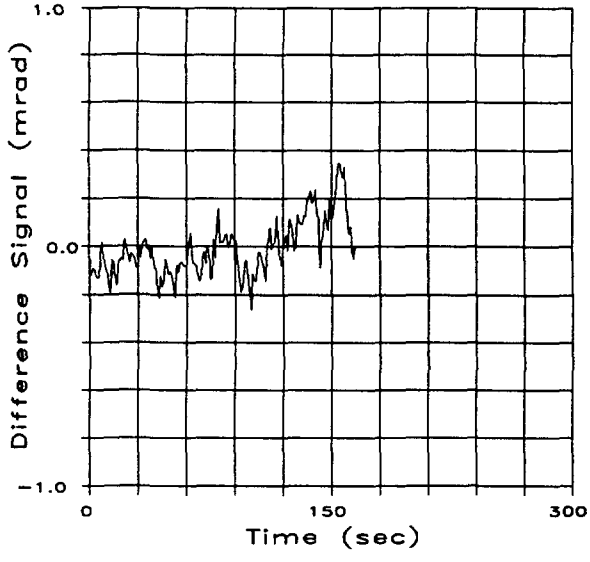


TR35, 17Sep91, 0854 hours

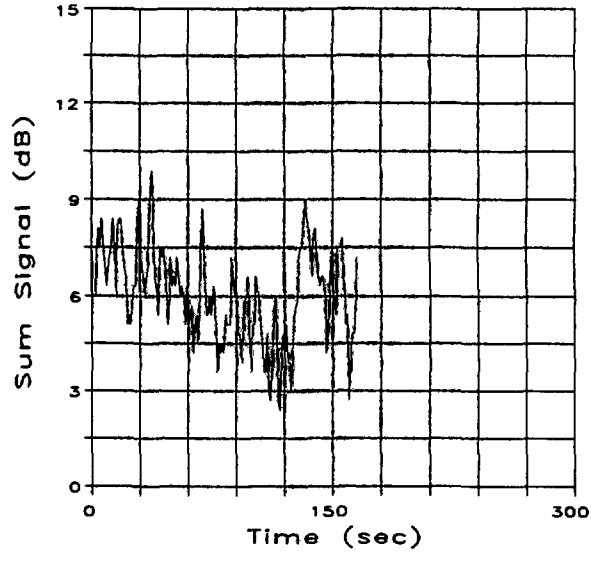


TR35, 17Sep91, 0854 hours

Figure B-12. Noise measurement at 0.4 km and 3 km, Trials 34 and 35.

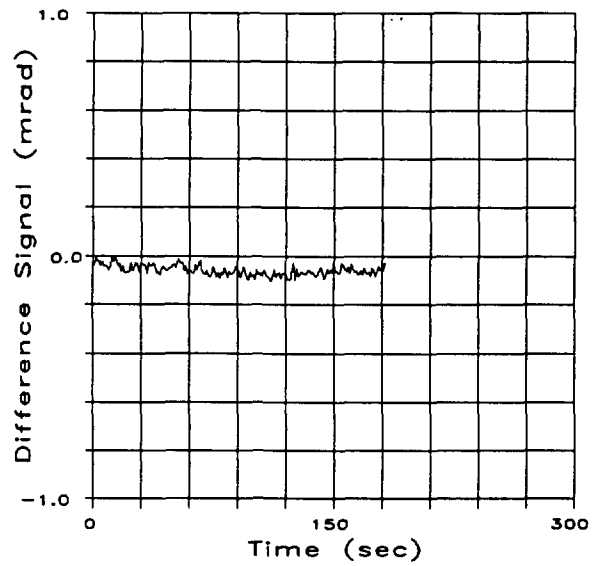


TR37, 17Sep91, 1059 hours

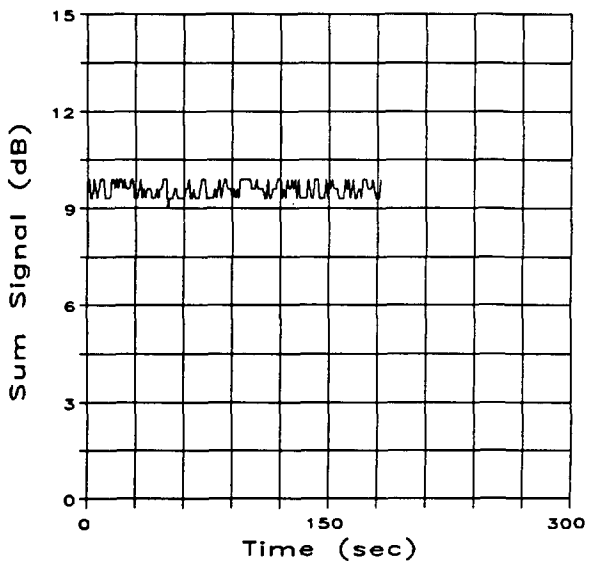


TR37, 17Sep91, 1059 hours

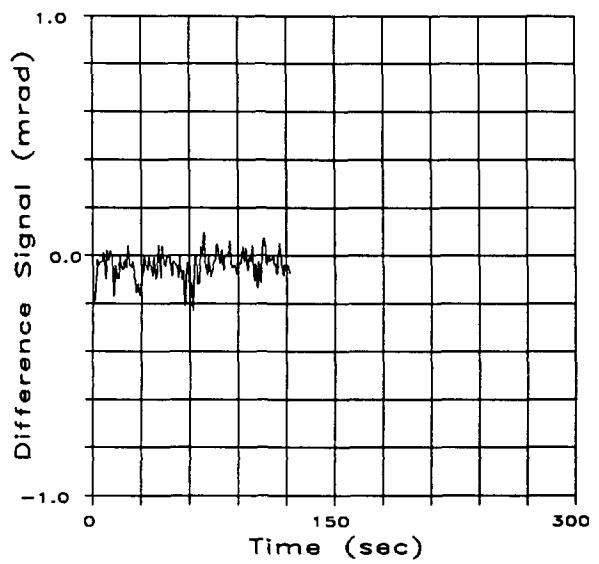


TR38, 17Sep91, 1130 hours

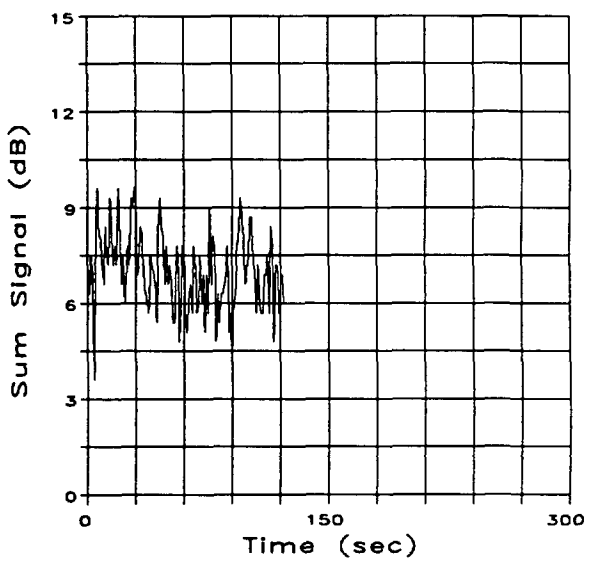


TR38, 17Sep91, 1130 hours

Figure B-13. Noise measurement at 0.4 km and 4 km, Trials 37 and 38.

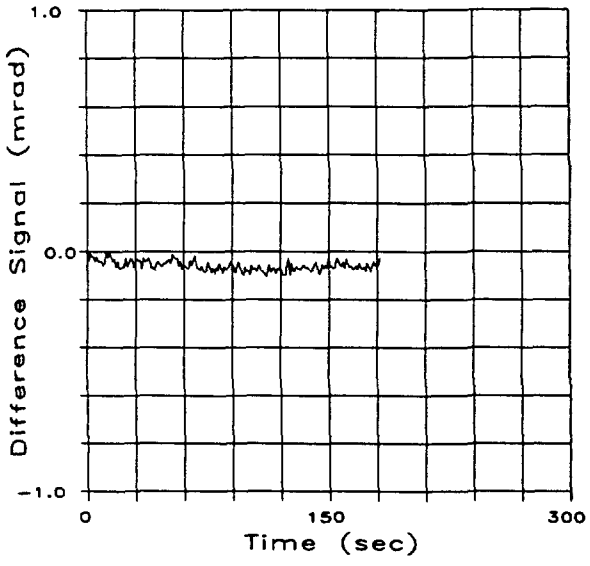


TR37, 17Sep91, 1059 hours

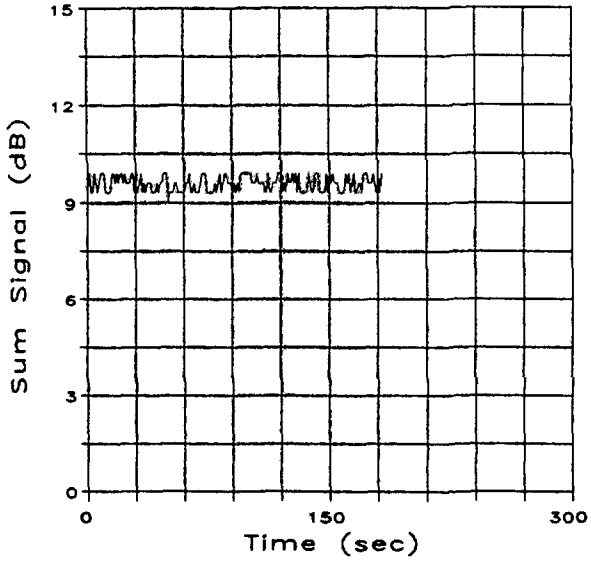


TR37, 17Sep91, 1059 hours

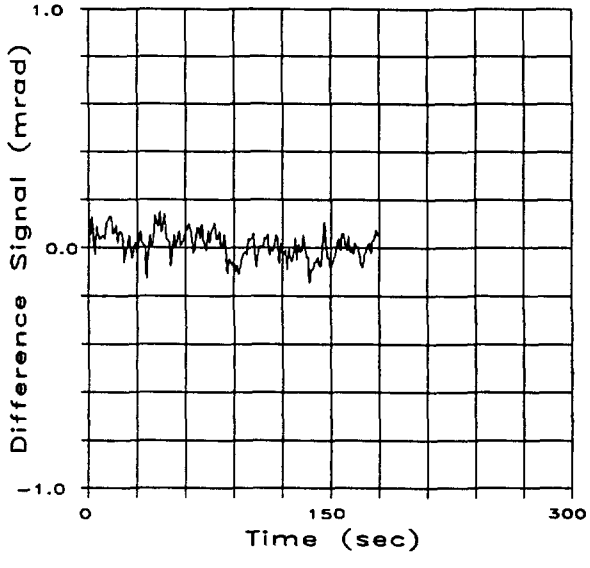


TR40, 17Sep91, 1301 hours

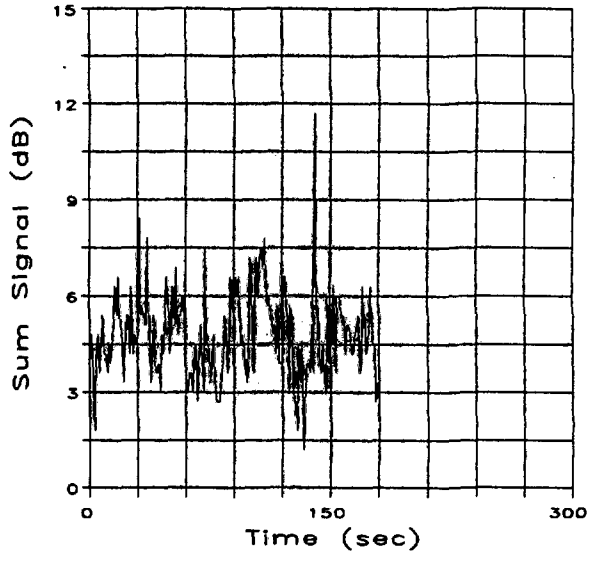


TR40, 17Sep91, 1301 hours

Figure B-14. Noise measurement at 0.4 km and 5 km, Trials 37 and 40.

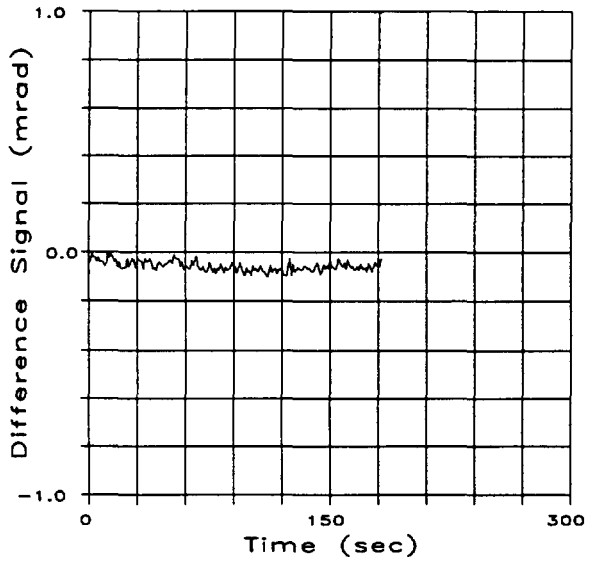


TR37, 17Sep91, 1059 hours

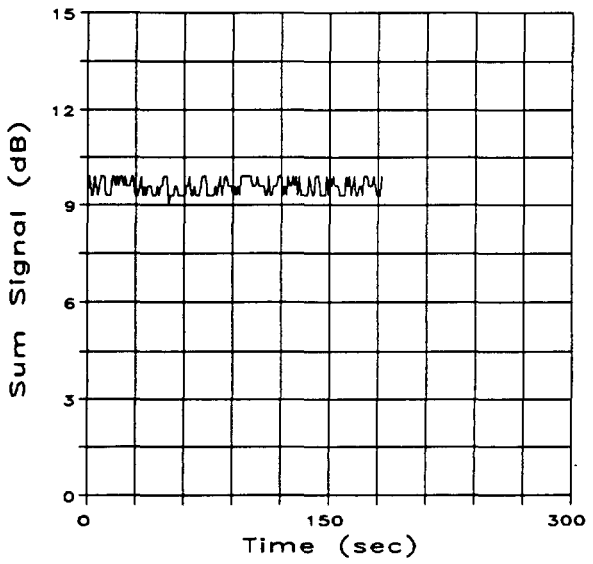


TR37, 17Sep91, 1059 hours

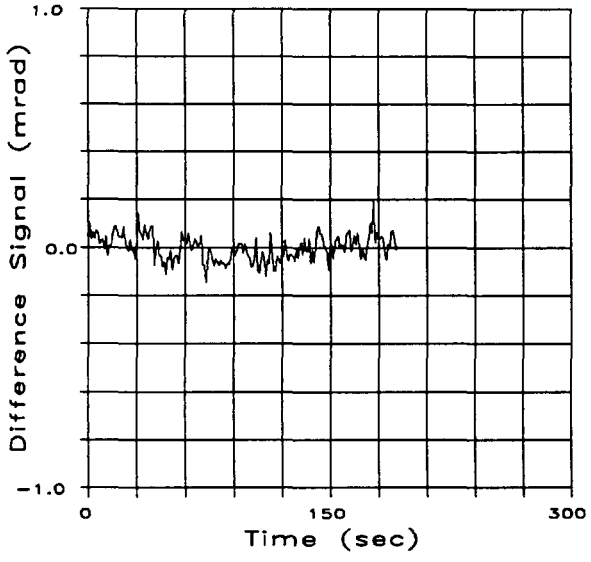


TR41, 17Sep91, 1401 hours

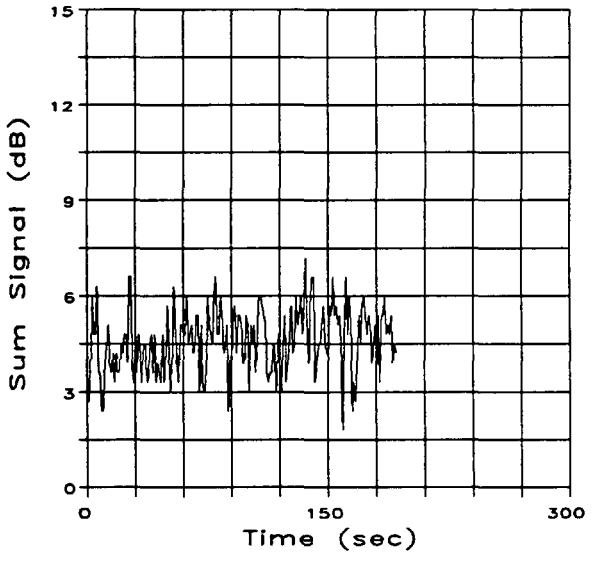


TR41, 17Sep91, 1401 hours

Figure B-15. Noise measurement at 0.4 km and 5 km, Trials 37 and 41.

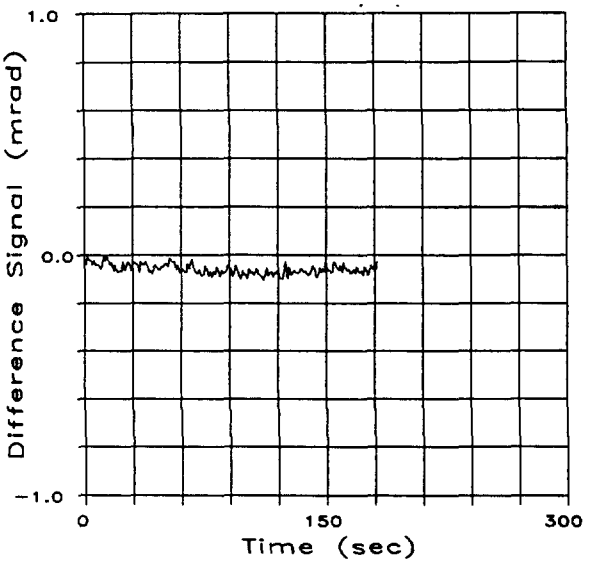


TR37, 17Sep91, 1059 hours

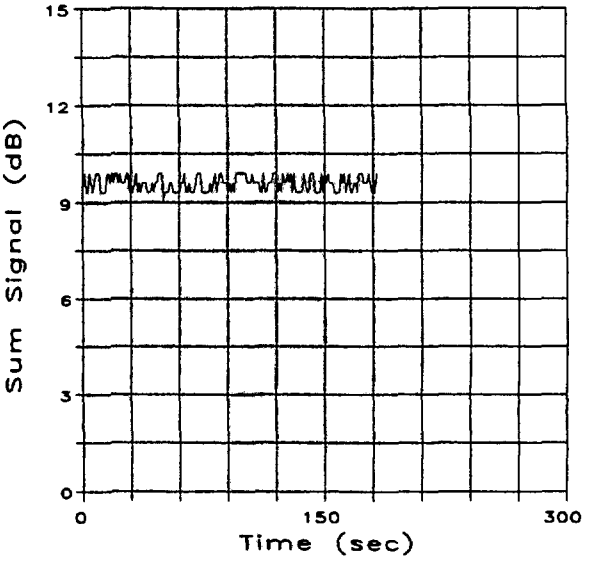


TR37, 17Sep91, 1059 hours

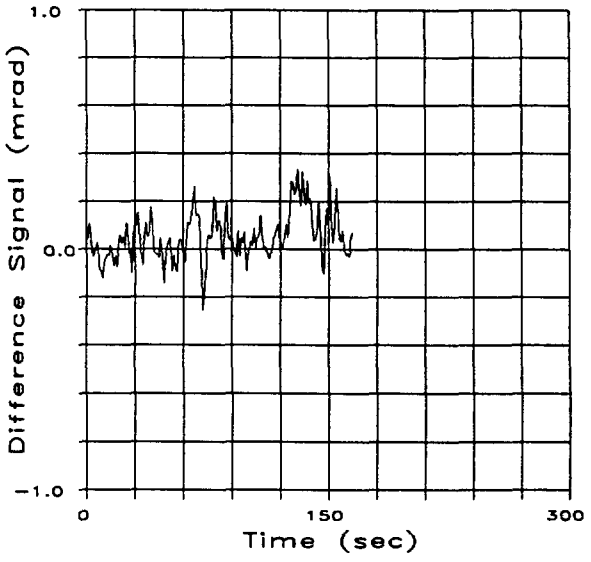


TR43, 17Sep91, 1511 hours

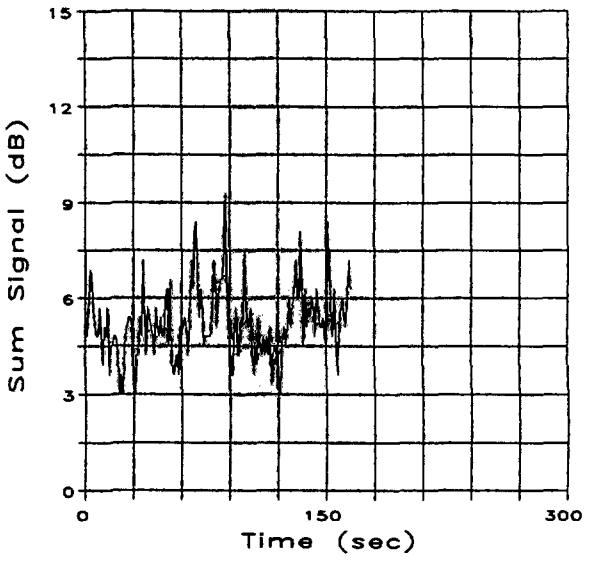


TR43, 17Sep91, 1511 hours

Figure B-16. Noise measurement at 0.4 km and 3 km, Trials 37 and 43.

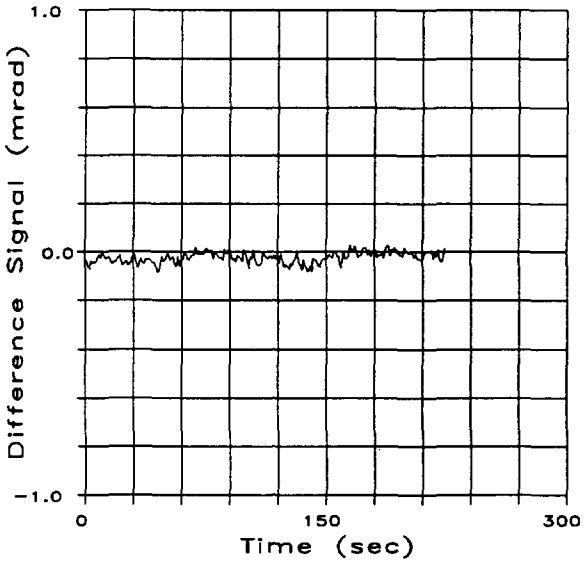


TR45, 18Sep91, 0853 hours

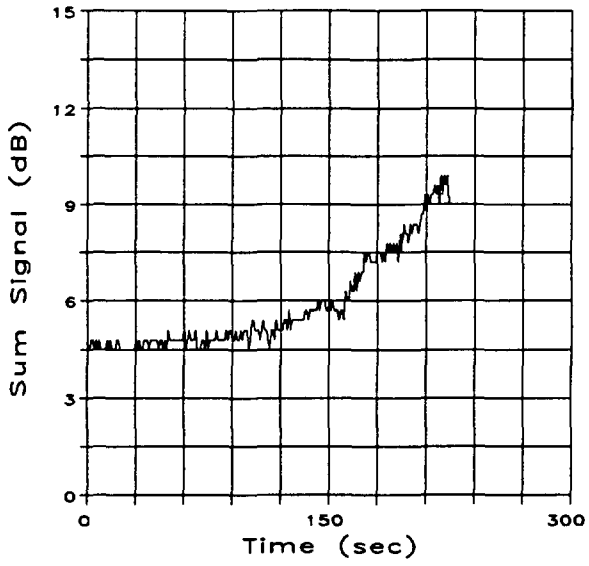


TR45, 18Sep91, 0853 hours

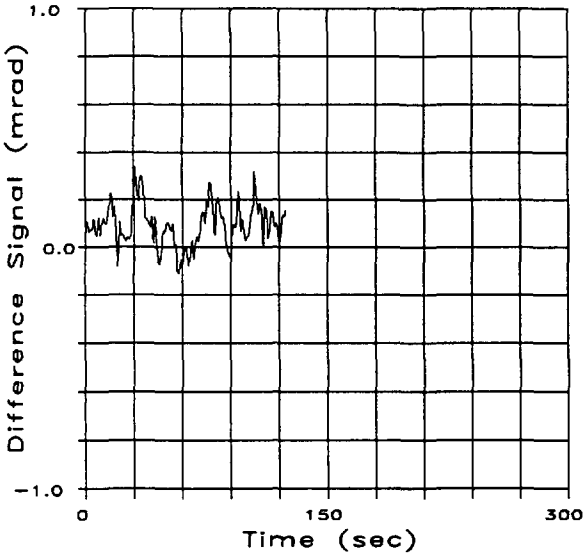


TR46, 18Sep91, 0903 hours

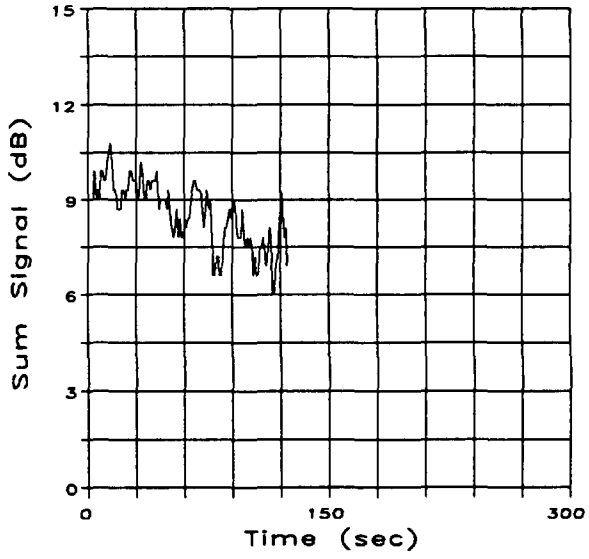


TR46, 18Sep91, 0903 hours

Figure B-17. Noise measurement at 0.4 km and 3 km, Trials 45 and 46.

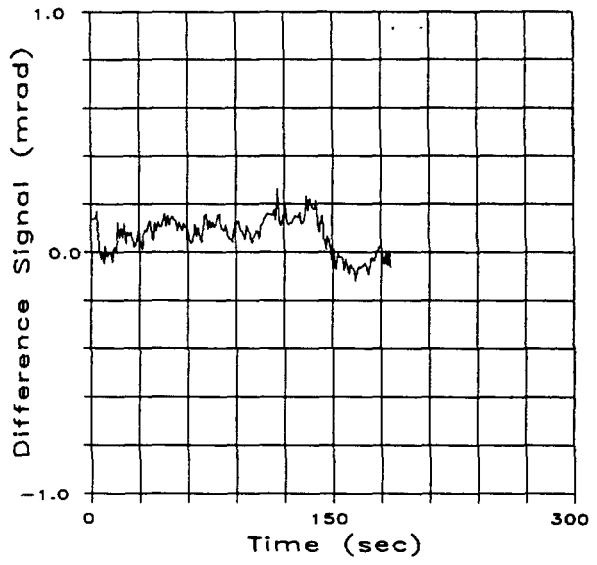


TR48, 18Sep91, 1000 hours

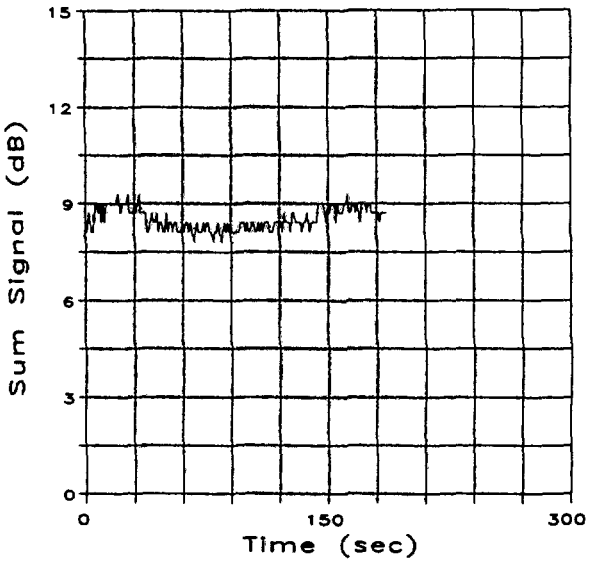


TR48, 18Sep91, 1000 hours

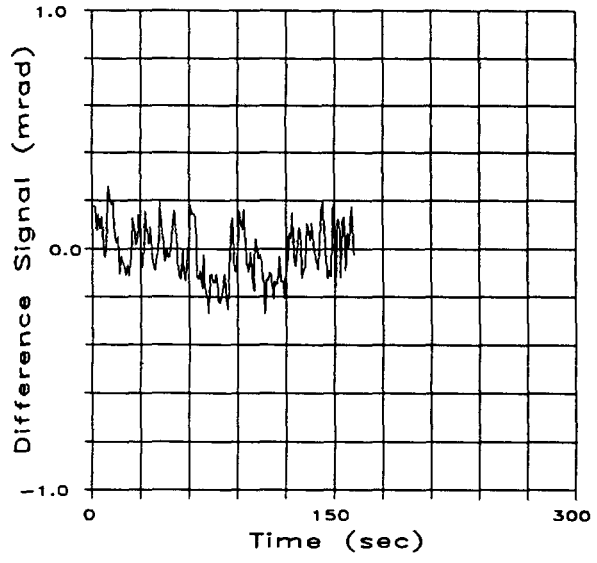


TR49, 18Sep91, 1011 hours

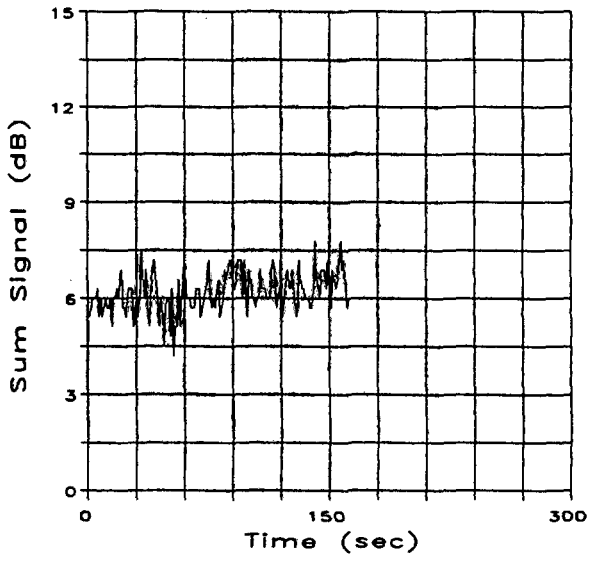


TR49, 18Sep91, 1011 hours

Figure B-18. Noise measurement at 0.4 km and 3 km, Trials 48 and 49.

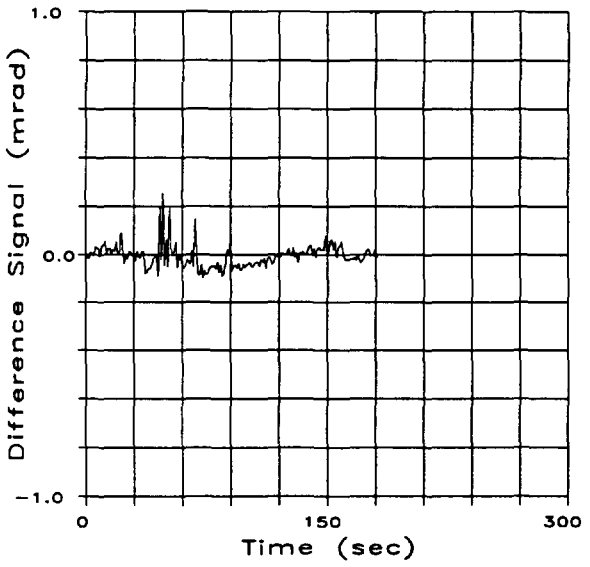


TR51, 18Sep91, 1418 hours

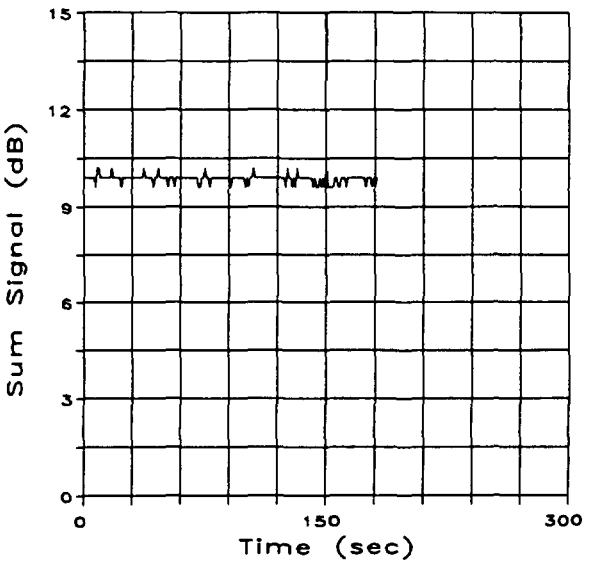


TR51, 18Sep91, 1418 hours

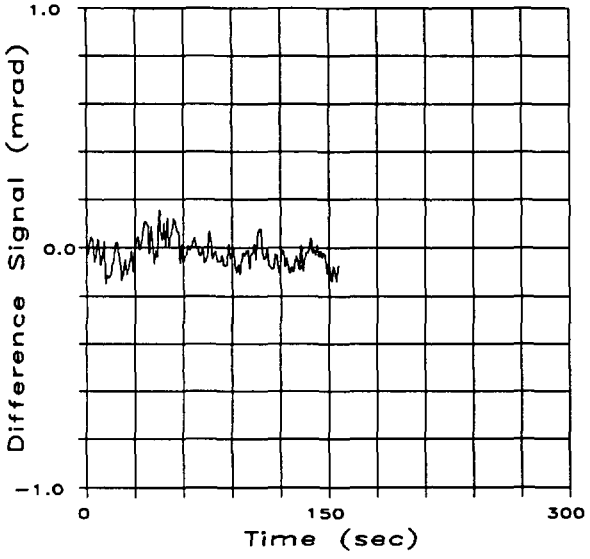


TR52, 18Sep91, 1430 hours

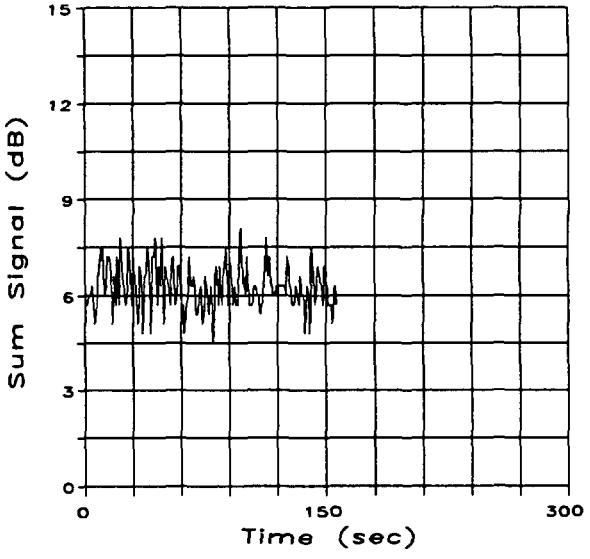


TR52, 18Sep91, 1430 hours

Figure B-19. Noise measurement at 0.4 km and 2 km, Trials 51 and 52.

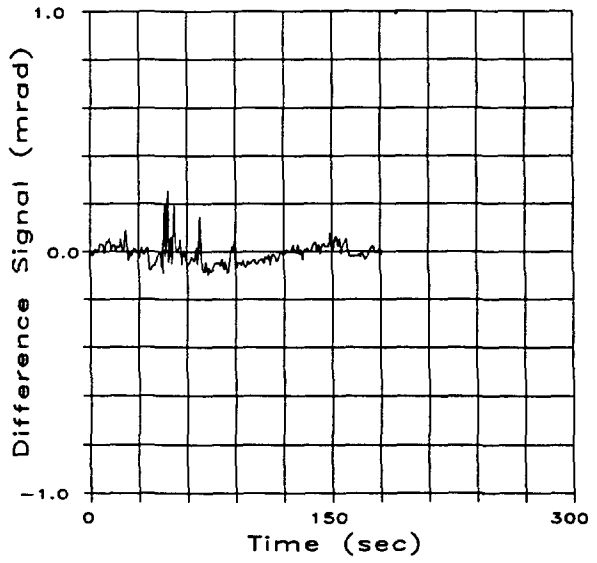


TR51, 18Sep91, 1418 hours

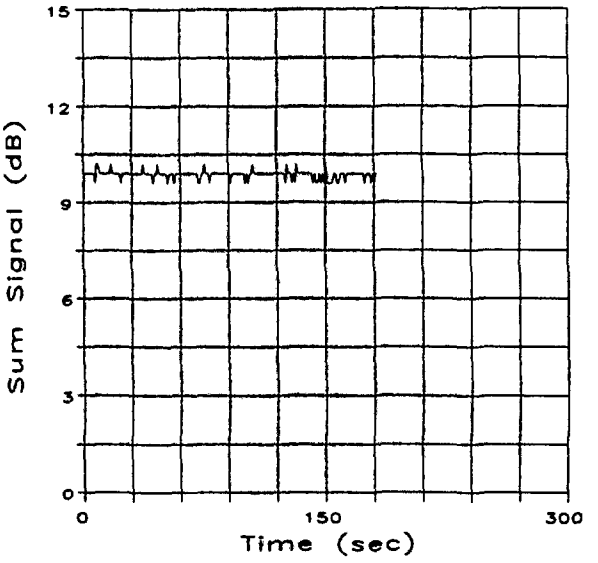


TR51, 18Sep91, 1418 hours

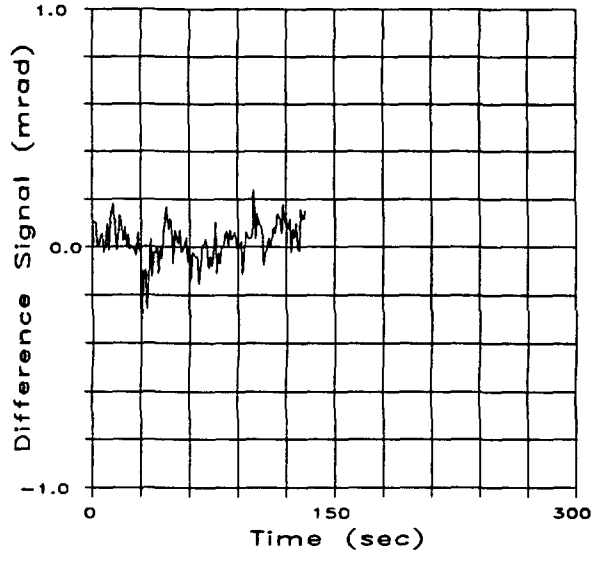


TR55, 18Sep91, 1536 hours

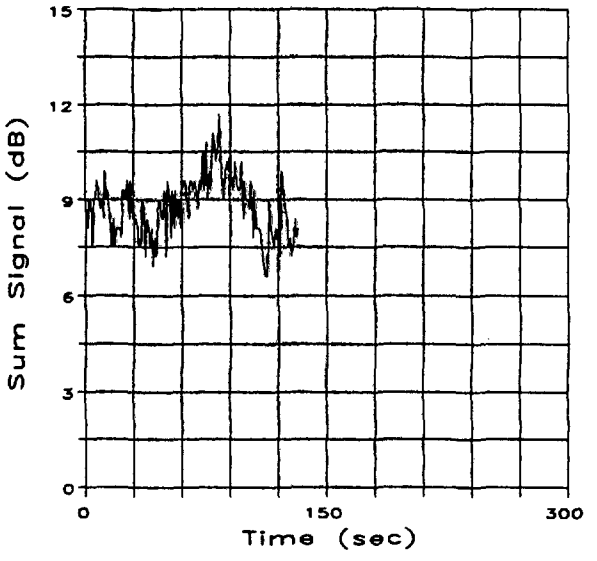


TR55, 18Sep91, 1536 hours

Figure B-20. Noise measurement at 0.4 km and 2 km, Trials 51 and 55.

# APPENDIX C:

# METEOROLOGICAL DATA

INTENTIONALLY LEFT BLANK.

Table C-1. Meteorological Data Recorded at 2-km Mark of Test Area 3

| Date | Time (hr) | Visibility (mi) | Temp. (°F) | Rel. Hum. (%) | Water Vapor Density ($g/m^3$) |
|---|---|---|---|---|---|
| 11 Sep | 0745 | 2.4 | 68.2 | 89 | 0.1549 |
| | 0800 | 4.0 | 69.6 | 89 | 0.1620 |
| | 0815 | 4.2 | 71.5 | 88 | 0.1703 |
| | 0830 | 4.2 | 73.0 | 86 | 0.1746 |
| | 0845 | 5.1 | 73.7 | 83 | 0.1723 |
| | 0900 | 6.3 | 74.7 | 81 | 0.1735 |
| | 0915 | 8.3 | 75.3 | 78 | 0.1703 |
| | 1330 | 11.7 | 91.7 | 54 | 0.1941 |
| | 1345 | 12.0 | 90.7 | 55 | 0.1920 |
| | 1400 | 12.6 | 91.7 | 53 | 0.1905 |
| | 1415 | 13.1 | 91.8 | 52 | 0.1875 |
| | 1430 | 13.5 | 92.6 | 50 | 0.1845 |
| | 1445 | 13.6 | 92.1 | 50 | 0.1818 |
| | 1500 | 13.3 | 92.2 | 50 | 0.1824 |
| 12 Sep | 0800 | 2.9 | 75.4 | 88 | 0.1927 |
| | 0815 | 4.3 | 77.1 | 86 | 0.1987 |
| | 0830 | 4.8 | 78.3 | 82 | 0.1966 |
| | 0845 | 5.7 | 79.9 | 79 | 0.1990 |
| | 0900 | 7.2 | 81.4 | 76 | 0.2005 |
| | 1200 | 15.0 | 90.4 | 61 | 0.2110 |
| | 1215 | 13.0 | 91.3 | 59 | 0.2096 |
| | 1230 | 13.8 | 90.9 | 59 | 0.2071 |
| | 1245 | 13.4 | 91.3 | 59 | 0.2096 |
| | 1300 | 12.9 | 93.4 | 55 | 0.2078 |
| | 1400 | 14.4 | 93.0 | 54 | 0.2016 |
| | 1415 | 14.8 | 94.7 | 50 | 0.1961 |
| | 1430 | 14.1 | 94.7 | 50 | 0.1961 |
| | 1445 | 15.4 | 95.1 | 48 | 0.1905 |
| | 1500 | 12.7 | 96.5 | 46 | 0.1901 |

Table C-1. Meteorological Data Recorded at 2-km Mark of Test Area 3 (continued)

| Date | Time (hr) | Visibility (mi) | Temp. (°F) | Rel. Hum. (%) | Water Vapor Density ($g/m^3$) |
|---|---|---|---|---|---|
| 13 Sep | 0800 | 2.7 | 75.1 | 88 | 0.1909 |
| | 0815 | 4.2 | 77.6 | 87 | 0.2041 |
| | 0830 | 4.6 | 79.9 | 83 | 0.2091 |
| | 0845 | 5.4 | 81.2 | 79 | 0.2072 |
| | 0900 | 7.0 | 83.8 | 75 | 0.2129 |
| | 0915 | 8.2 | 85.1 | 71 | 0.2097 |
| | 0930 | 7.6 | 85.6 | 70 | 0.2099 |
| | 1030 | 12.9 | 88.9 | 62 | 0.2052 |
| | 1045 | 13.2 | 89.9 | 60 | 0.2045 |
| | 1100 | 9.3 | 90.8 | 58 | 0.2030 |
| | 1115 | 10.4 | 91.8 | 57 | 0.2055 |
| | 1130 | 11.9 | 92.3 | 55 | 0.2012 |
| | 1145 | 14.3 | 92.2 | 54 | 0.1970 |
| | 1500 | 9.9 | 95.6 | 41 | 0.1651 |
| | 1515 | 12.9 | 95.7 | 41 | 0.1655 |
| 16 Sep | 1115 | 7.6 | 93.2 | 52 | 0.1953 |
| | 1130 | 7.2 | 93.4 | 52 | 0.1964 |
| | 1145 | 7.8 | 93.5 | 51 | 0.1932 |
| | 1200 | 7.7 | 92.7 | 51 | 0.1888 |
| | 1415 | 9.5 | 96.2 | 41 | 0.1679 |
| | 1430 | 9.9 | 96.4 | 40 | 0.1648 |
| | 1445 | 10.0 | 96.4 | 40 | 0.1648 |

Table C-1. Meteorological Data Recorded at 2-km Mark of Test Area 3 (continued)

| Date | Time (hr) | Visibility (mi) | Temp. (°F) | Rel. Hum. (%) | Water Vapor Density ($g/m^3$) |
|---|---|---|---|---|---|
| 17 Sep | 0700 | 0.1 | 69.5 | 89 | 0.1615 |
| | 0715 | 2.1 | 70.2 | 89 | 0.1652 |
| | 0730 | 1.0 | 71.0 | 89 | 0.1695 |
| | 0830 | 2.7 | 78.7 | 83 | 0.2015 |
| | 0845 | 3.0 | 80.0 | 79 | 0.1997 |
| | 0900 | 5.1 | 81.1 | 75 | 0.1961 |
| | 0915 | 4.8 | 71.8 | 44 | 0.0860 |
| | 1045 | 8.8 | 87.6 | 48 | 0.1528 |
| | 1100 | 8.6 | 88.3 | 46 | 0.1495 |
| | 1115 | 10.3 | 89.1 | 45 | 0.1498 |
| | 1130 | 10.1 | 89.3 | 44 | 0.1473 |
| | 1145 | 9.6 | 90.5 | 42 | 0.1457 |
| | 1300 | 10.8 | 93.5 | 36 | 0.1364 |
| | 1400 | 11.0 | 94.7 | 33 | 0.1294 |
| | 1415 | 11.3 | 93.8 | 33 | 0.1261 |
| | 1500 | 11.0 | 94.1 | 31 | 0.1195 |
| | 1515 | 10.8 | 93.8 | 30 | 0.1146 |
| | 1530 | 11.6 | 94.1 | 27 | 0.1041 |
| 18 Sep | 0845 | 5.8 | 76.6 | 75 | 0.1706 |
| | 9000 | 6.7 | 78.2 | 70 | 0.1673 |
| | 0915 | 7.1 | 79.7 | 67 | 0.1678 |
| | 0930 | 7.6 | 80.9 | 64 | 0.1663 |
| | 0945 | 7.8 | 82.5 | 61 | 0.1665 |
| | 1000 | 8.1 | 84.2 | 58 | 0.1667 |
| | 1015 | 8.5 | 85.4 | 54 | 0.1609 |
| | 1030 | 9.2 | 87.0 | 51 | 0.1595 |
| | 1415 | 13.6 | 94.7 | 32 | 0.1255 |
| | 1430 | 14.6 | 95.4 | 31 | 0.1241 |
| | 1445 | 11.9 | 95.6 | 28 | 0.1127 |
| | 1500 | 15.6 | 95.3 | 28 | 0.1118 |
| | 1515 | 15.7 | 94.9 | 28 | 0.1105 |
| | 1530 | 15.8 | 94.8 | 28 | 0.1102 |
| | 1545 | 15.8 | 94.9 | 28 | 0.1105 |

Table C-2. Meteorological Data Recorded at 5-km Mark of Test Area 3

| Date | Time (hr) | Visibility (mi) | Temp. (°F) | Rel. Hum. (%) | Water Vapor Density ($g/m^3$) |
|---|---|---|---|---|---|
| 11 Sep | 0745 | N/A | 68.6 | 85 | 0.1498 |
| | 0800 | N/A | 69.6 | 85 | 0.1547 |
| | 0815 | N/A | 71.2 | 85 | 0.1629 |
| | 0830 | N/A | 72.2 | 84 | 0.1662 |
| | 0845 | N/A | 73.0 | 84 | 0.1705 |
| | 0900 | N/A | 74.0 | 83 | 0.1739 |
| | 0915 | N/A | 74.6 | 82 | 0.1751 |
| | 1330 | N/A | 90.7 | 55 | 0.1920 |
| | 1345 | N/A | 92.2 | 53 | 0.1933 |
| | 1400 | N/A | 92.2 | 53 | 0.1933 |
| | 1415 | N/A | 91.2 | 53 | 0.1877 |
| | 1430 | N/A | 92.0 | 51 | 0.1849 |
| | 1445 | N/A | 91.7 | 51 | 0.1833 |
| | 1500 | N/A | 91.4 | 51 | 0.1817 |
| 12 Sep | 0800 | N/A | 74.1 | 84 | 0.1766 |
| | 0815 | N/A | 76.2 | 83 | 0.1864 |
| | 0830 | N/A | 77.6 | 82 | 0.1924 |
| | 0845 | N/A | 79.4 | 81 | 0.2010 |
| | 0900 | N/A | 79.9 | 79 | 0.1991 |
| | 1200 | N/A | 91.2 | 59 | 0.2090 |
| | 1215 | N/A | 91.7 | 58 | 0.2085 |
| | 1230 | N/A | 91.6 | 58 | 0.2079 |
| | 1245 | N/A | 92.1 | 57 | 0.2073 |
| | 1300 | N/A | 93.7 | 55 | 0.2096 |
| | 1400 | N/A | 92.8 | 54 | 0.2004 |
| | 1415 | N/A | 93.5 | 52 | 0.1970 |
| | 1430 | N/A | 94.2 | 51 | 0.1972 |
| | 1445 | N/A | 95.0 | 49 | 0.1939 |
| | 1500 | N/A | 95.2 | 48 | 0.1910 |
| 13 Sep | 0800 | N/A | 74.6 | 84 | 0.1794 |
| | 0815 | N/A | 76.1 | 83 | 0.1858 |
| | 0830 | N/A | 78.1 | 82 | 0.1954 |
| | 0845 | N/A | 79.6 | 82 | 0.2047 |
| | 0900 | N/A | 81.4 | 79 | 0.2085 |
| | 0915 | N/A | 83.1 | 77 | 0.2140 |
| | 0930 | N/A | 84.9 | 74 | 0.2172 |

Table C-2. Meteorological Data Recorded at 5-km Mark of Test Area 3 (continued)

| Date | Time (hr) | Visibility (mi) | Temp. (°F) | Rel. Hum. (%) | Water Vapor Density ($g/m^3$) |
|---|---|---|---|---|---|
| 13 Sep (continued) | 1030 | N/A | 88.4 | 62 | 0.2021 |
| | 1045 | N/A | 89.5 | 60 | 0.2021 |
| | 1100 | N/A | 90.2 | 59 | 0.2029 |
| | 1115 | N/A | 91.1 | 57 | 0.2013 |
| | 1130 | N/A | 92.0 | 55 | 0.1994 |
| | 1145 | N/A | 92.3 | 54 | 0.1975 |
| | 1500 | N/A | 96.1 | 41 | 0.1675 |
| | 1515 | N/A | 97.3 | 39 | 0.1649 |
| 16 Sep | 1115 | N/A | 91.9 | 55 | 0.1988 |
| | 1130 | N/A | 92.5 | 54 | 0.1987 |
| | 1145 | N/A | 92.2 | 54 | 0.1970 |
| | 1200 | N/A | 92.3 | 54 | 0.1975 |
| | 1415 | N/A | 95.6 | 44 | 0.1771 |
| | 1430 | N/A | 96.9 | 41 | 0.1714 |
| | 1445 | N/A | 96.8 | 40 | 0.1667 |
| 17 Sep | ---------- N/A ---------- | | | | |
| 18 Sep | ---------- N/A ---------- | | | | |

INTENTIONALLY LEFT BLANK.

| No. of Copies | Organization |
|---|---|
| 2 | Administrator<br>Defense Technical Info Center<br>ATTN: DTIC-DDA<br>Cameron Station<br>Alexandria, VA 22304-6145 |
| 1 | Commander<br>U.S. Army Materiel Command<br>ATTN: AMCAM<br>5001 Eisenhower Ave.<br>Alexandria, VA 22333-0001 |
| 1 | Director<br>U.S. Army Research Laboratory<br>ATTN: AMSRL-OP-CI-AD,<br>Tech Publishing<br>2800 Powder Mill Rd.<br>Adelphi, MD 20783-1145 |
| 1 | Director<br>U.S. Army Research Laboratory<br>ATTN: AMSRL-OP-CI-AD,<br>Records Management<br>2800 Powder Mill Rd.<br>Adelphi, MD 20783-1145 |
| 2 | Commander<br>U.S. Army Armament Research,<br>Development, and Engineering Center<br>ATTN: SMCAR-TDC<br>Picatinny Arsenal, NJ 07806-5000 |
| 1 | Director<br>Benet Weapons Laboratory<br>U.S. Army Armament Research,<br>Development, and Engineering Center<br>ATTN: SMCAR-CCB-TL<br>Watervliet, NY 12189-4050 |
| 1 | Director<br>U.S. Army Advanced Systems Research<br>and Analysis Office (ATCOM)<br>ATTN: AMSAT-R-NR, M/S 219-1<br>Ames Research Center<br>Moffett Field, CA 94035-1000 |

| No. of Copies | Organization |
|---|---|
| 1 | Commander<br>U.S. Army Missile Command<br>ATTN: AMSMI-RD-CS-R (DOC)<br>Redstone Arsenal, AL 35898-5010 |
| 1 | Commander<br>U.S. Army Tank-Automotive Command<br>ATTN: AMSTA-JSK (Armor Eng. Br.)<br>Warren, MI 48397-5000 |
| 1 | Director<br>U.S. Army TRADOC Analysis Command<br>ATTN: ATRC-WSR<br>White Sands Missile Range, NM 88002-5502 |
| (Class. only) 1 | Commandant<br>U.S. Army Infantry School<br>ATTN: ATSH-CD (Security Mgr.)<br>Fort Benning, GA 31905-5660 |
| (Unclass. only) 1 | Commandant<br>U.S. Army Infantry School<br>ATTN: ATSH-WCB-O<br>Fort Benning, GA 31905-5000 |
| 1 | WL/MNOI<br>Eglin AFB, FL 32542-5000 |
| | Aberdeen Proving Ground |
| 2 | Dir, USAMSAA<br>ATTN: AMXSY-D<br>AMXSY-MP, H. Cohen |
| 1 | Cdr, USATECOM<br>ATTN: AMSTE-TC |
| 1 | Dir, USAERDEC<br>ATTN: SCBRD-RT |
| 1 | Cdr, USACBDCOM<br>ATTN: AMSCB-CII |
| 1 | Dir, USARL<br>ATTN: AMSRL-SL-I |
| 5 | Dir, USARL<br>ATTN: AMSRL-OP-AP-L |

| No. of Copies | Organization |
|---|---|
| 2 | Commander<br>U.S. Army Missile Command<br>ATTN: AMSMI-RD-AS-MM, Mike Christian<br>Redstone Arsenal, AL 35898-5253 |
| 1 | Commander<br>U.S. Army Armament Research, Development, and Engineering Center<br>ATTN: SMCAR-FSP-AI, Murray Rosenbluth<br>Bldg 353N<br>Picatinny, NJ 07806-5000 |
| 1 | Commander<br>U.S. Army Armament Research, Development, and Engineering Center<br>ATTN: SMCAR-FSP-BD, Larry Yung<br>Bldg 353N<br>Picatinny, NJ 07806-5000 |
| 1 | Commander<br>U.S. Army Communications and Electronics Command<br>ATTN: Scott Mollica<br>Fort Monmouth, NJ 07703 |
| 2 | Commander<br>Naval Surface Warfare Center<br>ATTN: Code F41,<br>Jim Morrissett<br>Douglas Marker<br>Dalhgren, VA 22448-5000 |
| 1 | Commander<br>U.S. Army Test and Evaluation Command<br>ATTN: STEDP-MT-DA-0, Dennis Bodrero<br>Dugway Proving Ground, UT 84022-5000 |
| 1 | Institute for Defense Analysis<br>Science and Technology Division<br>ATTN: Dr. James M. Ralston<br>1801 N. Beauregard Street<br>Alexandria, VA 22311-1772 |
| 1 | Georgia Tech Research Institute<br>Radar Systems Applications Laboratory<br>ATTN: Jay Saffold<br>Atlanta, GA 30332-0800 |

| No. of Copies | Organization |
|---|---|
| 2 | AAI Corporation<br>ATTN: David Cleveland, 100/444<br>Paul Shipley, 100/403<br>P.O. Box 126<br>Hunt Valley, MD 21030-0126 |
| 1 | MIT Lincoln Laboratory<br>ATTN: Pamela Reynolds<br>244 Wood St.<br>Room A082<br>Lexington, MA 02173 |
| 1 | MIT Lincoln Laboratory<br>ATTN: Jack Fleischman, B363<br>244 Wood St.<br>Lexington, MA 02173 |
| 1 | University of Nebraska<br>Electrical Engineering Dept.<br>ATTN: Ram Narayanan<br>Mail Stop 0511<br>Lincoln, NE 68588 |
| 2 | Rockwell International<br>MMW Radar Technology Dept.<br>Tactical Systems Division<br>ATTN: Keith Hull, MS-DC04<br>Roland H. Wright, MS-DD46<br>3370 Miraloma Ave<br>P.O.Box 3170<br>Anaheim, CA 92803-3170 |
| | Aberdeen Proving Ground |
| 1 | Dir, USAMSAA<br>ATTN: AMXSY-GA, Floyd Wofford |
| 11 | Dir, USARL<br>ATTN: AMSRL-SS-SD,<br>Donald Bauerle<br>Robert Bender<br>Suzanne Stratton (5 cp)<br>Bruce Wallace<br>Joseph Nemarich (ADELPHI)<br>AMSRL-WT-WB,<br>Victor Leitzke<br>Richard McGee |

## USER EVALUATION SHEET/CHANGE OF ADDRESS

This Laboratory undertakes a continuing effort to improve the quality of the reports it publishes. Your comments/answers to the items/questions below will aid us in our efforts.

1. ARL Report Number ARL-MR-140 Date of Report June 1994

2. Date Report Received _____

3. Does this report satisfy a need? (Comment on purpose, related project, or other area of interest for which the report will be used.) _____

4. Specifically, how is the report being used? (Information source, design data, procedure, source of ideas, etc.) _____

5. Has the information in this report led to any quantitative savings as far as man-hours or dollars saved, operating costs avoided, or efficiencies achieved, etc? If so, please elaborate. _____

6. General Comments. What do you think should be changed to improve future reports? (Indicate changes to organization, technical content, format, etc.) _____

CURRENT ADDRESS

_____
Organization

_____
Name

_____
Street or P.O. Box No.

_____
City, State, Zip Code

7. If indicating a Change of Address or Address Correction, please provide the Current or Correct address above and the Old or Incorrect address below.

OLD ADDRESS

_____
Organization

_____
Name

_____
Street or P.O. Box No.

_____
City, State, Zip Code

(Remove this sheet, fold as indicated, tape closed, and mail.)

**(DO NOT STAPLE)**

DEPARTMENT OF THE ARMY

OFFICIAL BUSINESS

**BUSINESS REPLY MAIL**
FIRST CLASS PERMIT No 0001, APG, MD

Postage will be paid by addressee.

Director
U.S. Army Research Laboratory
ATTN: AMSRL-OP-CI-B (Tech Lib)
Aberdeen Proving Ground, MD 21005-5066

NO POSTAGE
NECESSARY
IF MAILED
IN THE
UNITED STATE